A Study of the Quasielastic (e,e′p) Reaction in ^{16}O at High Recoil Momentum

Experiment Handbook Version 7.0

Kevin Fissum
Nuclear Interactions Group
Massachusetts Institute of Technology

October 6, 1997

Preface

The contents of this document are intended to serve as setup documentation for Jefferson Laboratory Hall A EXPINT experiment E89-003.

The following individuals have made valuable contributions to this work.

William Bertozzi, MIT
Brian Diederich, Old Dominion University
Juncai Gao, MIT
Shalev Gilad, MIT
Meihua Liang, Jefferson Lab
Nilanga Liyanage, MIT
Jeff Templon, University of Georgia
Arun Saha, Jefferson Lab
Adam Sarty, Florida State University
Paul Ulmer, Old Dominion University
Larry Weinstein, Old Dominion University
Jianguo Zhao, MIT

Questions or comments may be directed to:

K.G. Fissum
Room 16-125 Jefferson Laboratory
12000 Jefferson Avenue
Newport News, VA 23606 USA
phone: (757) 269 7325
fax: (757) 269 6273
pager: (757) 680 2036
email: fissum@cebaf.gov

Contents

List of Figures

List of Tables

Chapter 1

In the beginning...

1.1 Expint proposal

To: Nuclear Physics Experiment Scheduling Committee
From: W. Bertozzi, R. Lourie, A. Saha, L. Weinstein
(Spokespersons for Experiment 89-003)
Contact Person: A. Saha (TJNAF)
Re: Beam time request for Exp. 89-003

- **1. Interest in obtaining beamtime:**

  The Exp.89-003 collaboration is interested in obtaining beamtime for running the first phase of Exp.89-003, as part of the first approved experiment in Hall A. This is in accordance with the commissioning plan recommended by the Experiment Integration (EXPINT) Committee, and approved by the PAC and by the TJNAF Administration. The first commissioning experiment consists of the first phases of Exp.89-003 and Exp.89-033. The first phase of Exp.89-003 is expected to begin as soon as the coincidence operation of the HRS spectrometers is established (Projected date: March, 1997).

- **2. Proposed use of the beamtime:**

  Beamtime is requested to carry out part of the first approved experiment in Hall A and also continue in the development and checkout of the experimental equipment in the hall. In particular, Exp.89-003 will focus on establishing the reliable performance of all existing aspects of the electron and hadron spectrometers. While the spectrometers will presumably have been commissioned by this time, it will be the very first opportunity to take publishable data with them. In doing so, we will provide further checks on the reliablility of the entire Hall A instrumentation package, and in particular, conduct tests of the long-term performance aspects of the VDC detector package under experiment conditions.

- **3. Partial or complete experiment?**

  In accordance with the EXPINT plan, we should expect to complete only the low Q^2 $(0.8\ \mathrm{GeV/c})^2$ portion of Exp.89-003 during this first commissioning run. This constitutes approximately 58% of the total approved beamtime allocated for this experiment.

- **4. 100% efficient beam time and beam conditions requested:**

  During this first phase, we request two weeks of 100% efficient beam time. Polarized beam is not required. Currents of 50 μA (or more) are strongly preferred. Total missing mass resolution, including contributions from both the beam and the spectrometers, must be ≤ 0.7 MeV. Desired electron beam energies are nominally 2.4 GeV and 0.8 GeV. The 2.4 GeV requirement can be relaxed if absolutely necessary to a nominal beam energy of 1.6 GeV, but *only* if this is required by the energy resolution considerations presented above.

  To achieve the physics and development goals proposed to EXPINT and the PAC for this phase of the experiment, we *must* have the beam time and equipment capability to achieve the following:

  - a parallel kinematics measurement to separate the response functions R_L and R_T for 0 MeV/c $\leq p_{miss} \leq$ 100 MeV/c at both the stipulated beam energies.
  - a quasi-perpendicular kinematics measurement to separate the response functions $R_L + (q^2/2Q^2) \cdot R_{TT}$, R_T and R_{LT} for 50 MeV/c $\leq p_{miss} \leq$ 420 MeV/c at both the stipulated beam energies.
  - clean separation of the $1s_{1/2}$, $1p_{1/2}$ and $1p_{3/2}$ states, as well as part of the continuum, in the $^{16}O(e,e'p)$ coincidence spectra.

- **5. Readiness and resources:**

  This experiment requires that the coincidence operation of the HRS spectrometer pair in its "standard" operational configuration and instrumentation be established and that we have ≤ 0.7 MeV resolution. HRS_e commissioning has begun in August 1996, and HRS_h will be commissioned around December 1996. Coincidence operation is scheduled for February/March, 1997. Regardless of the beam energy employed, as it is expected that much of the data for the first part of Exp.89-033 will run in kinematics similar to those requested here, the coincidence resolution we obtain will provide valuable diagnostics for the subsequent measurement.

  The waterfall target from INFN must be installed and commissioned, and its ability to handle a 50 μA beam demonstrated. The inner region of this target, which contains the modified waterfall assembly required by experiments Exp.89-003 and Exp.89-033, must be fabricated and installed (by the INFN, Rome group). This waterfall target is presently onsite at

TJNAF and is scheduled for installation during September 1996. The target will be employed in many of the pre-commissioning activities this Fall and as such, its operating parameters will be well-understood by the time we wish to use it.

- **6. Scheduling constraints:**

  This part of the experiment will run subsequent to the completion of HRS coincidence commissioning. As it represents the top priority of many members of the collaboration, it will determine the schedule of their other activities, rather than vice-versa.

- **7. Plans for building up on-site collaboration:**

  Exp.89-003 is one of the original collaboration experiments approved to run in Hall A and as such is a full Hall A collaboration experiment. The members of this collaboration come from many institutions and have contributed in the development of all the equipment, detectors, beamline, targets etc. in Hall A, most of which will be useful in realizing this experiment. The primary institutions responsible for Exp.89-003 are MIT and TJNAF. The TJNAF committment to this experiment consists of all of the Hall A staff; they are fully committed to the smooth running of this experiment. They are already helping in every aspect of this experiment from designing and putting the equipment together and will continue to do so till the final analysis and dissemination of the results. The MIT committment to Exp.89-003 consists of a faculty member, a principal research scientist, four (soon to be five) postdocs, and two Ph.D. students. Of this group, one postdoc and the two students are permanently-based onsite at TJNAF, with a second postdoc to come in the near future. This group has been responsible for the construction and installation of the VDC instrumentation packages for the HRSs. It is expected that the on-site contingent will spend 100% of their time on this project once all VDC milestones are reached. The remaining offsite contingent pledges 50% of their time. Other institutions in the collaboration have been invited to participate in the experiment and to identify Ph. D. thesis projects associated with it. Committments should be in place this Fall.

- **8. EH&S reviews and documentation:**

  Since the TSOP's associated with the pre-commissioning period will need to be replaced with the permanent EH&S documentation prior to the running of Exp.89-003, we will continue to assist in the development of this documentation.

- **9. Radiation budget:**

  The radiation budget estimate has been prepared by G. Stapleton and is well within the normal operating average for the hall. It uses up only 2.5% of the total annual dose budget and is well within the limits for putting up any local shielding.

1.2 Conduct of Operations for E89-003

All experiment personnel must acknowledge their familiarity with this document as well as their intention to comply with all the conditions defined within on record by sending an email message to `saha@cebaf.gov` **before performing any shiftwork.**

1.2.1 Preface

Jefferson Laboratory is a single-purpose facility for basic research in nuclear physics. Its scientific mission is to explore the underlying structure of hadrons and nuclei using the electromagnetic probe. The central device is a superconducting electron accelerator with a nominal maximum energy of 4 GeV and a 100% duty cycle. The electron beam, with a maximum current of 200 μA, can be used simultaneously for electron scattering experiments in three experimental areas: Halls A, B and C.

As part of its mission, Jefferson Lab provides the resources necessary for international scientific collaborations to carry out basic research at the frontiers of the field of nuclear physics and related disciplines. This research must be conducted in a manner that ensures Environmental, Health and Safety (EH&S) concerns receive the highest consideration. At the same time, the program goals of the laboratory require that it produces the highest quality physics results efficiently.

Guidance on how to balance thoughtful, measured EH&S concerns with efficient operation has been taken from the Department of Energy (DOE) Order 5480.10, "Conduct of Operations", the Jefferson Lab EH&S Committee, the *Jefferson Lab EH&S Manual*, and the Jefferson Lab Director's Office. A graded approach is followed in which the measures taken are matched to the scale, the cost complexity and the hazards of the operation.

The Hall A Collaboration firmly supports the concept that quality physics research is compatible with the safe operation of the Jefferson Lab facilities. This document serves as a summary definition of how the Hall A Collaboration intends to conduct its operations in a safe and efficient manner. It must be read, understood, and followed by all members of the Collaboration.

1.2.2 Introduction

General Hall A Considerations

This experiment uses the standard apparatus in Hall A at Jefferson Lab, which includes the beam transport system, the beam dump, the two high resolution magnetic spectrometer systems in standard configuration, the Hall A electronics and data acquisition system, and the scattering chamber and target systems. Since all of the required equipment for the execution of the experiment is part of the "base" equipment in the Hall, all of the procedures appropriate for the operation of the equipment that will be used during the course of the experiment are contained in the following documents:

- *Conduct of Operations for Jefferson Lab Hall A Experiment E89-003* (this document);
- *Hall A Basic Experimental Equipment Operations Manual* (a basic operations manual for the Hall which includes discussions of the following subjects and provides cross references to other appropriate documentation);
  1. *Procedures for Experiments*;
  2. *Experimental Equipment Operation*;
  3. *Safety Assessment Document for Hall A Equipment*;
  4. *Personnel Allowed to Operate Hall A Equipment.*

Reference copies of these documents will be available at all times in the Hall A Counting House for the duration of the experiment.

Description of E89-003

The primary physics goal of this experiment is to perform separations of the structure functions R_l, R_t, R_{lt}, and R_{l+tt} for quasi-elastic ^{16}O(e,e′p) over a large range of missing energy and missing momentum. A complete description of the physics motivation and the general plan for carrying out the experiment can be found at the E89-003 website `http://marie.mit.edu/~kgf/16Oeep.html`. This experiment is part of the Hall A EXPINT program and is designated a "commissioning" experiment for the base equipment. As such, it is a considered a Hall A Collaboration experiment.

1.2.3 Operations, Organization and Administration

The functional organization of the experiment is shown in Fig.1.1.

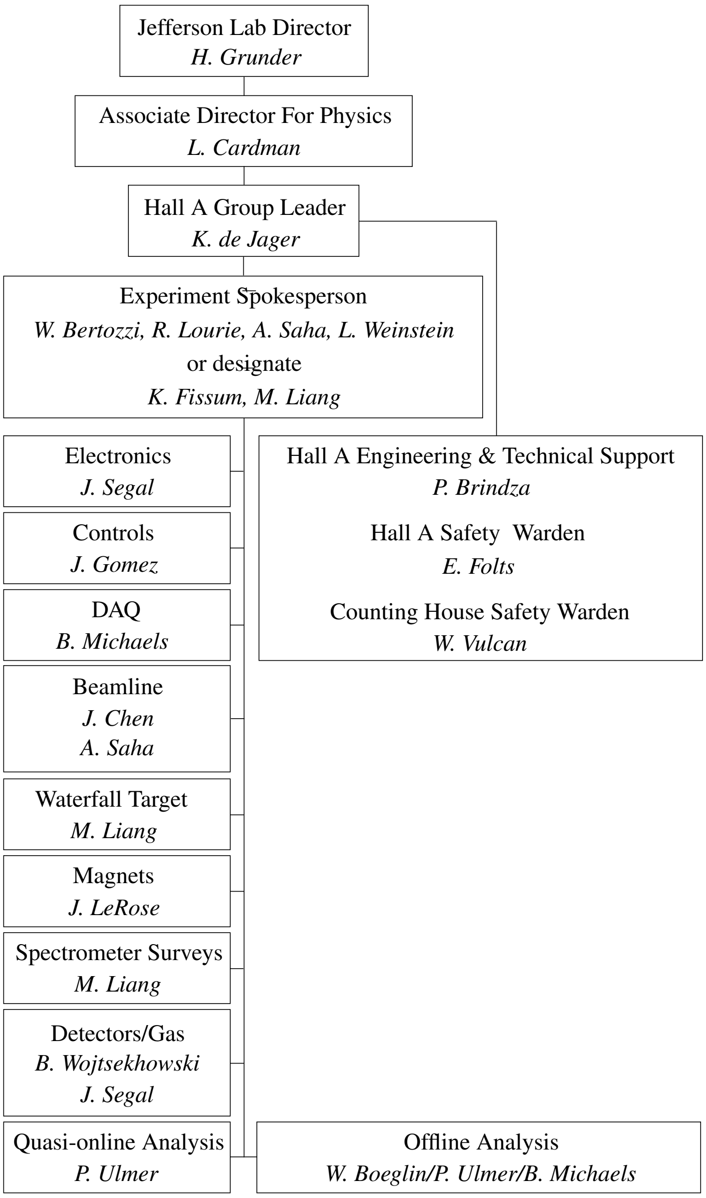

Figure 1.1: Functional organization of E89-003.

The operational organization of the experiment is directed by the *Spokespersons* and the *Hall A Group Leader*. The immediate on-site management of the experiment will be the responsibility of the experiment spokespersons or their designate. The person in this position at any given time shall be referred to as the *Run Coordinator*. The Run Coordinator will be in residence in the local Jefferson Lab area at all times during a running period. The functions of the Run Coordinator are:

- to manage the daily operation of the experiment, including the safe operation of the experiment;
- to coordinate interactions between Jefferson Lab and the experiment;
- to represent the experiment at the weekly accelerator scheduling meeting (Wednesdays at 13:30 in the MCC Conference Room) one week before the run period, one week after the run period, and during the run period itself;
- to set and post goals for each shift and evaluate the progress of the experiment;
- to ensure the Hall A Group Leader and the Spokespersons are aware of all necessary issues;
- to oversee and verify that the equipment is operated properly and in accordance with the *Hall A Basic Experimental Equipment Operations Manual*;
- to define the data quality measures appropriate for the goals of each shift;
- to ensure sufficient overlap and transfer of information between Shift Leaders.

1.2.4 Shift Routines and Operating Procedures

There are two types of shifts for the time when the experiment is designated as occupying Hall A: *standby* and *operating*. Operating shifts are the normal status when beam is available for the experiment. Standby shifts are periods designated by the spokepersons or their designated alternates when beam is not available in the Hall and none of the equipment that is operating requires continuous monitoring. Standby status may result from normal operational planning or from abnormal conditions such as a major down time for the accelerator due to equipment failure.

Standby Shifts

During standby shifts, the shift personnel are not required to be on site at Jefferson Lab, but must be available via telephone contact to arrive at the Hall in an expeditious manner in the event of a problem with the equipment that is their responsibility. The Run Coordinator will ensure that the shift checklist (see Table 1.1) is executed at least once every 24 hours. Any access to the Hall will require a minimum of two persons.

Operating Shifts

During operating shifts, 24-hour occupation of the Hall A Counting House area will be maintained by crews of at least three people, in 8-hour shifts. One person per shift will be designated the *Shift Leader*. This person has the following authority and responsibilities:

- primary responsibility for carrying out the scientific program planned for the shift by the Run Coordinator;
- overall responsibility for the proper operation of the Hall A equipment during the shift;
- primary responsibility for coordinating the response of the shift crew to emergency situations, including the notification of appropriate individuals as outlined in the *Jefferson Lab Emergency Response Plan* and the *Hall A Emergency Checklist*;
- primary responsibility for monitoring the operation of the Hall A equipment and for the coordination of the response to and the reporting of all abnormal/unusual occurrences. Reporting shall include entering the relevant information in the Log Book, notifying the Hall A responsible staff member for the relevant equipment, and notifying the Accelerator Crew Chief and/or other Accelerator Division personnel as appropriate for the system that had the occurrence;
- acting as primary experiment contact between the Machine Control Center (MCC) and experiment personnel. This includes the authority to request entries into the Hall;
- primary responsibility for keeping accurate records of the operation of the accelerator, experiment equipment and simultaneous availability of beam (standard forms exist) for use in evaluating the operational responsibility for reconciliation of the Hall A records on beam availability with those kept by the Accelerator Crew Chief at the end of the shift;
- can authorize qualified personnel to make modifications in the experiment configuration within the allowed parameters;
- primary responsibility for the actions of shift crews under their leadership;
- primary responsibility for the orderly transition of crews at shift change and the writing of the *End-of-Shift Summary*. This summary shall include pointing out the existence of any new documents pertaining to the experiment;
- primary responsibility for the Log Book containing a complete and accurate description of the events and actions of the shift;

- primary responsibility for ensuring that the shift check list is performed and that the equipment is operating within expected normal operating parameters;

- authority to limit the number of people in the Hall A Counting House or the Hall itself as necessary to effectively and safely carry out the experiment;

- authority to limit access to the Hall A acquisition computers if required to effectively and safely carry out the experiment;

- primary responsibility to ensure that malfunctioning equipment is properly labeled, that the existence of the malfunction is reported both to shift personnel and the individual(s) responsible for the operation and maintenance of the equipment, and whenever necessary, to ensure the equipment is locked-out by a trained and responsible individual.

The number of persons assigned to a shift will nominally be four - the previously-discussed Shift Leader, two experienced operators, and a novice operator. The shift schedule for each run period will be clearly posted in the Hall A Counting House, listing the times of each shift, the names of the personnel on shift, and the Shift Leader for each shift. The shift schedule for each run period will also be available from the E89-003 website. Also posted will be the name of the Run Coordinator, as well as phone numbers for support staff. Secondary teams for such tasks as data analysis and spectrometer surveying will be recognized by the Run Coordinator, will be under the control of the Shift Leader, and will have a designated secondary leader (see Fig. 1.1).

The responsibilities of each shift member are to:

- carry out the scientific goals of the shift in a safe and efficient manner under the direction of the Shift Leader;

- read the Log Book to be aware of changes in goals, operating parameters and new documentation;

- monitor the operation of all equipment for departures from normal operations;

- maintain adequate records of the progress of the shift;

- be present in a timely fashion before the start of each shift so that a smooth, coordinated transition between shifts may be accomplished.

In addition, each shift member is responsible for carrying out their work in a safe and efficient manner, according to the rules and procedures documented in the *Jefferson Lab EH&S Manual* and in the documents listed in Section 1.2.2.

Shift Personnel Training

All personnel on shift are required to have successfully completed and be current in the following Jefferson Lab safety training programs:

- EH&S Orientation;
- Radiation Worker Training;
- Oxygen Deficiency Hazard Training.

In addition, all shift personnel will be trained in the safety procedures to be followed for access to Hall A and its close-up prior to beam delivery. This training will include a brief discussion of the purpose and operation of the Personnel Safety Sytem (PSS) for the Hall, a trained escort for the individual the first time they enter Hall A on a controlled access, and an escorted General Hazard Awareness Walk-Through of Hall A.

Individuals within the Collaboration may be required to have other equipment or procedure-specific training as their responsibilities demand. The need for such training shall be determined by the Spokespersons or their designate in consulation with the Hall A Group Leader and Physics Division EH&S personnel.

All commissioning activity personnel are also required to have read and to be familiar with the documents listed in Section 1.2.2. Reference copies of these documents will be kept in the Hall A Counting House.

In addition, experiment personnel should familiarize themselves with the section of the Jefferson Lab EH&S Manual relevant to their work in the Hall. A reference copy of this document is available in the main hallway of the Counting House or from `http://www.cebaf.gov/services/ehsinfo/ehsman.html`.

Finally, Jefferson Lab *Lock and Tag Training* is required for all staff/users who will be performing maintenance on electrical or mechanical equipment which cannot be physically and continuously isolated from an energy source.

All experiment personnel are required to have radiation badges in their possession during their shifts. The *two-person rule* is in strict enforcement for all entries into the Hall. It is strongly recommended that hard hats are worn during access.

1.2.5 Control of Equipment and System Status

The operation of the Hall A Experiment Equipment is discussed in the *Hall A Basic Experimental Equipment Operations Manual.* This document includes information on the normal response to alarms and equipment malfunctions; however, in general, during this phase of Hall A operations, the basic emergency response is to bring the situation to the attention of the expert for the system in question after taking immediate response measures as such common sense as well as those which Jefferson Lab policies and procedures dictate.

During Hall A EXPINT activities, the only individuals authorized to make **significant** modifications, repairs and/or changes to the operating status of equipment are the resident "experts" or persons under their direct supervision. Significant changes to the operating status of equipment include *any* changes within the stated safe parameters of operation in the operating procedures that are beyond those described in the *Hall A Basic Experimental Equipment Operations Manual* as routine. Shift personnel will make routine changes in operating conditions as specified in the operating procedures. Authorized subsystem experts are also listed. This list may be amended as necessary to reflect personnel and training changes with the signed and written authorization of **both** an expert for that subsystem **and** the Hall A Leader or his authorized designate. A copy of these amendments will be maintained in the Hall A Counting House attached to the reference copy of the *Hall A Basic Experimental Equipment Operations Manual*.

Access to the Hall will be governed as described in the *Jefferson Lab Beam Containment Policy and Implementation* document and by the *General Access Radiation Work Permit (RWP) for Hall A*. This RWP is kept in the Hall A Counting House. All personnel must read the RWP and sign the log indicating that they have done so prior to entering the Hall. A sign-up log is also kept at the PSS gate in Hall A for convenience. Work in designated radiation areas will be governed by the *Jefferson Lab RadCon Manual*. In particular, no material may be removed from the Hall after beam delivery to the Hall without proper approval from an Assigned Radiation Monitor responsible for the Hall or from the RADCON Group, as appropriate.

All general equipment installation, maintenance and testing activities shall be carried out in accordance with the *Jefferson Lab EH&S Manual*.

1.2.6 Independent Verification

The basic checklist given in Table 1.1 will be performed once per shift during operating shifts and once per day during standby shifts. Additional items may be added to the list at the discretion of the Run Coordinator.

Bookkeeping	Date and Time Shift Checklist Recorder
HRS_e	Magnet Currents Magnet Fields Cryogenic Fill Levels Drift Chamber Gas (Gas Shed) Drift Chamber HV, Current Pb-glass HV Cherenkov Gas/Pressure Cherenkov HV Hodoscope HV angle
HRS_h	Magnet Currents Magnet Fields Cryogenic Fill Levels Drift Chamber Gas (Gas Shed) Drift Chamber HV, Current Pb-glass HV Cherenkov Gas/Pressure Cherenkov HV Hodoscope HV angle
Vacuum	Scattering Chamber HRS_e HRS_h
Electronics	Status Visual Survey of CH
CODA	Status
Target	position angle
Beam and Beamline	Energy Current Rastering Duty Factor Special Conditions Switchyard Magnet Currents

Table 1.1: Items to be included in the shift checklist as appropriate for the current apparatus configuration.

The Run Coordinator will define a set of quality measures for the data and communicate these to the shift crews. These measures may change over the course of the experiment. The *Hall A Basic Experimental Equipment Operations Manual* provides a more general checklist for closing the Hall, and for situations where the Hall is used as an accelerator dump.

1.2.7 Logkeeping

A single series of hard-bound Log Books will serve as the record of the experiment. All relevant activities are to be recorded in these books, including all changes of experiment conditions and equipment failures. The quality of the information recorded in the Log Book is often critical to the ability of the Collaboration to ultimately "make sense" of the data, through a careful correlation of events in the written history of the experiment with the apparent changes in the experimental conditions inferred from changes in the data stream.

The Log Book will also serve as the primary reference for the determination of the operational efficiency of the Hall A apparatus. As such, it is essential that it provide an accurate record of the capability of the equipment to carry out the intended research program. Finally, the Log Book is the place of record for all safety issues and for providing notification of all new or updated documentation and procedures.

All data recorded electronically will be referenced in the Log Book with the location of the appropriate files and media. The only exception to the Log Book as the place of record is the experiment checklist, which will be stored in binders in the Hall A Counting House. However, all deviations from normal operating parameters observed during the checklist evaluation procedure will be recorded in the Log Book. All Log Books will remain in the Hall A Counting House for the duration of the experiment (unless they are being copied). After the experiment has been completed, the Log Books will be archived at Jefferson Lab for future reference.

All entries in the Log Book shall be made in ink. All entries and corrections should contain a time, a date and the name of the person making the notation.

Chapter 2

Theoretical Aspects

2.1 Motivation

Most of our knowledge of the nuclear momentum distribution comes from (e,e′p) data. One framework for the (e,e′p) formalism is based on four assumptions:

- the same nucleon momentum distribution appears in all the response functions (factorization).
- Final State Interactions (FSI) such as distortion and absorption can be handled with (non-) relativistic optical potentials. For FSI to be correctly addressed, *the optical potential must be varied as a function of outgoing proton energy.*
- The one-body interaction can be successfully explained with an off-shell *ep* cross section using the free-space on-shell form factors. These form factors depend on momentum transfer.
- No medium modifications to the nucleon are required; these are effectively handled by the inclusion of Meson Exchange Currents (MEC) and isobar configurations (nucleon resonances.)

The behaviour expected of nucleon momentum distributions in the Independent Particle (IP) model can be deduced from two very simple arguments: the maximum momentum is related to the size of the nucleus, and the maximum missing energy (the energy of the unobserved A-1 system for (e,e′p) reactions) is related to the maximum binding energy of a nucleon. For all but the lightest nuclei, the values are roughly $p^{MAX} \approx 250$ MeV/c and $E^{MAX} \approx 40$ MeV. However, these general arguments break down if there are strong interactions between individual nucleons which approach each other closely. Such interactions introduce structure in the nuclear wavefunction at short distances, and these in turn introduce structure in the nucleon momentum distributions at momenta of approximately $\hbar$/d, where "d" is the separation between the pair. These large momenta involve large nucleon energies as well, and can thus generate large effective binding energies. Such interactions are generally called *short-range correlations* (SRC).

In general, proton momentum distributions in nuclei are only known to about 300 MeV/c. A very interesting question is: does the nucleon-meson framework for nuclear physics provide an adequate description of the interaction when the distance scale approaches that of a single nucleon (~ 1 fm)? By extending our knowledge of these momentum distributions to higher nucleon momenta, strict constraints may be imposed on nuclear structure models. A related question is: does the mean-field approximation of nuclear structure break down? And if so, how?

It is generally accepted that the nucleon momentum distribution must be at least somewhat modified by these effects, since the integrated momentum distributions over the range populated in the IP model are experimentally found to be roughly 30% too small. Non-nucleonic degrees-of-freedom provide competing effects which can also cause modification of the nuclear response at high E_m and $\vec{p}_m$. All of these concepts have been supported by theoretical model calculations, which predict nucleon momentum distributions with orders of magnitude more strength at high $\vec{p}_m$ than predicted by the Independent Particle Shell Model (IPSM). These calculations are supported by ^{3}He data taken at Saclay.

Several experiments at MIT-Bates and later at NIKHEF-K have measured large enhancements of the high-$\vec{p}_m$ momentum distribution for heavier nuclei (*e.g.* ^{12}C and ^{208}Pb). At moderate values of E_m, these results are in good agreement with the correlation models. At higher E_m, there is more strength measured than predicted. Most of this strength seems to reside at higher missing energy. FSI can only explain about 10% of this strength. Further, beginning at about 28 MeV (the threshold for two nucleon emission), while the structure function $\mathbf{R_l} \rightarrow 0$, $\mathbf{R_t}$ does not. More about the structure functions later.

The predominantly-transverse nature of this strength argues against an explanation in terms of correlations, which should show up equally well in both the longitudnal and transverse components of the cross section. The use of FSI as an explanation also meets this problem. Model calculations indicate that MEC and the Δ-resonance are not the culprits, although these processes are predominantly transverse in character. The data up until now seem to indicate that some unknown two-body current, primarily transverse in nature, causes large modifications to the momentum distributions at very high E_m.

Except in few-body systems, the distribution of the continuum strength over excitation energy is virtually unknown. Separation of the structure functions will constrain the possible contributing mechanisms. Furthermore, an investigation of the low-E_m nuclear structure at high Q^2 and initial momenta will tightly constrain the nuclear mean-field theory. In particular, a comparison of the single particle spin-orbit partner states such as $^1P_{3/2}$ and $^1P_{1/2}$ is of great interest because their respective properties allow for an explicit investigation of the Spin-Orbit (SO) force. This force arises from the $\vec{L} \cdot \vec{S}$ term in the NN interaction, which in turn arises from ρ and ω meson exchange in One Boson Exchange (OBE) models.

Finally, it should be noted that it would be very interesting to investigate the Q^2 dependences of these phenomena.

2.2 Framework

Consider the general formalism for the scattering of unpolarized electrons from an unpolarized target illustrated in Fig. 2.1. Note that the vectors in the drawing are not to scale.

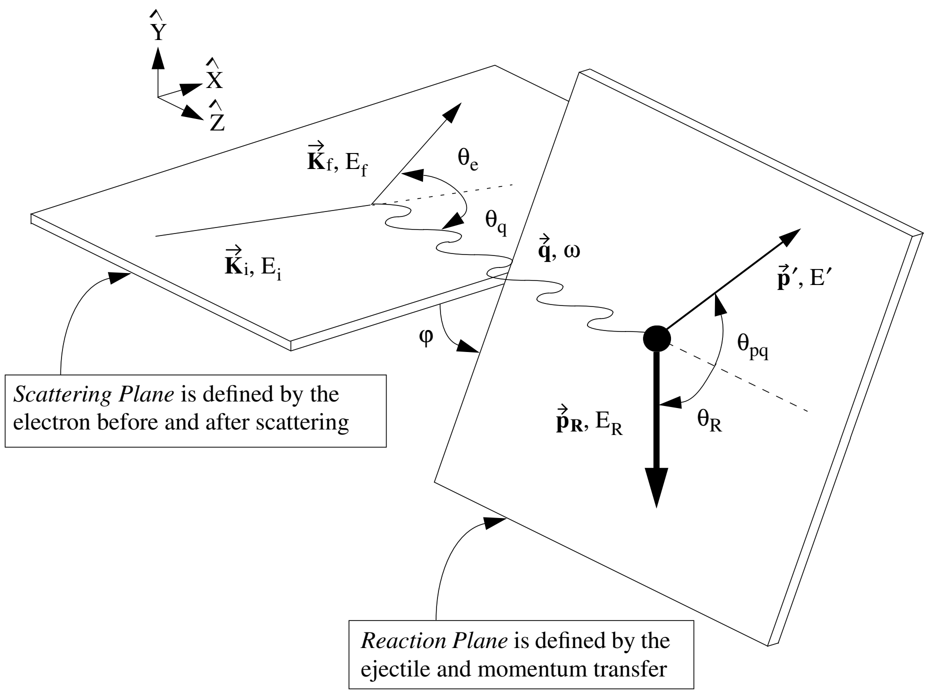

Figure 2.1: Unpolarized electron scattering.

In Hall A at Jefferson Lab (as at most other electron scattering facilities), the spectrometer which detects the ejected proton $\vec{p}\,'$ (here known as HRS_h) is in the plane defined by the beam $\vec{K}_i$ and the recoil electron $\vec{K}_f$. This results in a so-called *in-plane* experiment. There are a few facilities capable of performing out-of-plane experiments, the most notable of which is the OOPS Out-of-Plane Spectrometer project at MIT-Bates. Note also that Spectrometer B in the A1 Hall at MAMI (Mainz) and the SOS spectrometer in Hall C at Jefferson Lab both have marginal out-of-plane capabilities, and the large-acceptance non-magnetic detector HADRON-4 at NIKHEF-K has been used to access out-of-plane physics.

For the case of in-plane experiments, the rather complicated picture shown in Fig. 2.1 reduces to that shown in Fig. 2.2. Again, the vectors have not been drawn to scale.

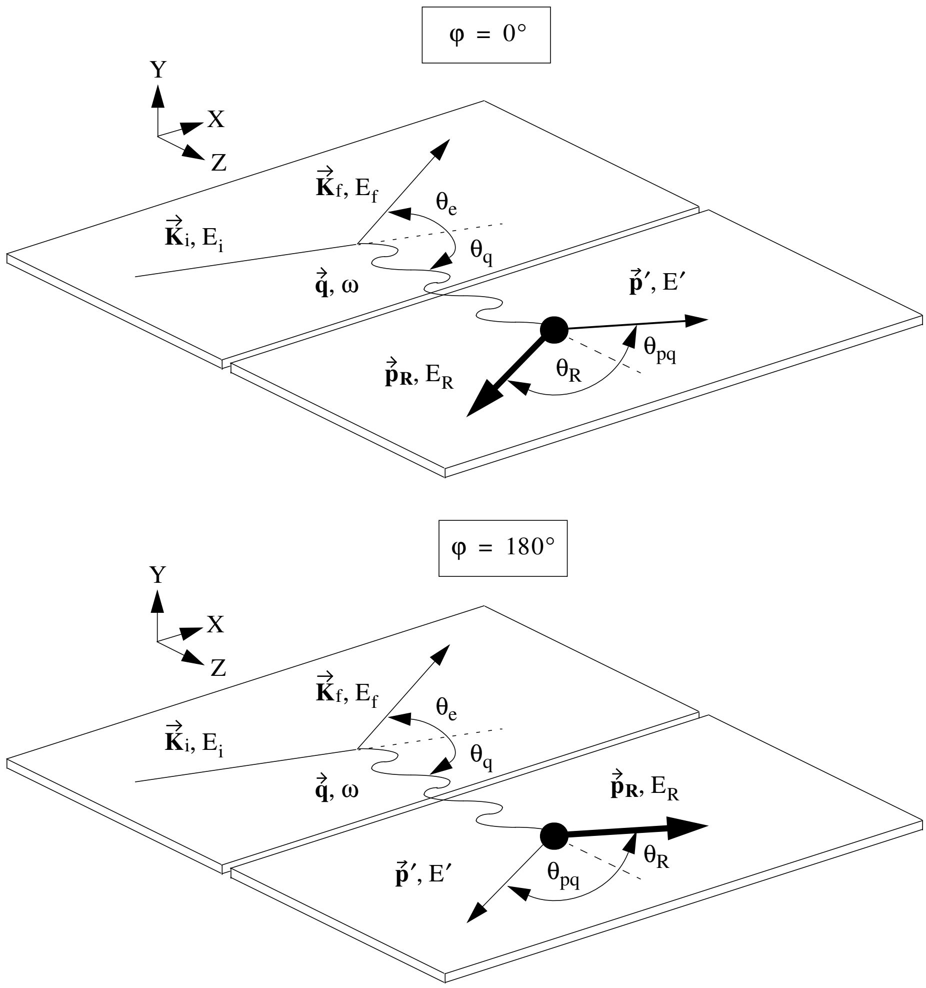

Figure 2.2: In-plane unpolarized electron scattering.

Note that for the case of in-plane scattering, there are two orientations of the vectors $\vec{p}_R$ and $\vec{p}\,'$, one corresponding to an angle $\phi = 0°$, and one corresponding to $\phi = 180°$. More about this later.

For the special case of in-plane kinematics, the electron scattering cross section from a nucleus may be expressed as the product of two terms: one due to the scattering of an electron from a stuctureless, spinless, infinitely-massive charge (the Mott cross section σ_M), and one due to the extended nature of the nucleus (the term in square brackets in 2.1). The expression for this scattering cross section is

$$\sigma = K\sigma_M[v_l\mathbf{R_l} + v_t\mathbf{R_t} + v_{lt}\mathbf{R_{lt}}cos(\phi) + v_{tt}\mathbf{R_{tt}}cos(2\phi)], \tag{2.1}$$

where the framework of [1] will be employed, and thus

$$\sigma = \frac{d^6\sigma}{d\Omega_e d\Omega_p dT_p d\omega}, \tag{2.2}$$

$$K = \frac{|\vec{p}'|E'}{(2\pi)^3}, \tag{2.3}$$

$$\sigma_M = [\frac{\alpha\cos(\theta_e/2)}{2E_i\sin^2(\theta_e/2)}]^2, \tag{2.4}$$

and

$$v_l = [\frac{Q^2}{q^2}]^2, \tag{2.5}$$

$$v_t = \frac{1}{2}[\frac{Q^2}{q^2}] + \tan^2(\theta_e/2), \tag{2.6}$$

$$v_{lt} = [\frac{Q^2}{q^2}]\sqrt{\frac{Q^2}{q^2} + \tan^2(\theta_e/2)}, \tag{2.7}$$

$$v_{tt} = \frac{1}{2}[\frac{Q^2}{q^2}], \tag{2.8}$$

are kinematical factors. The variables $\mathbf{R_l}$, $\mathbf{R_t}$, $\mathbf{R_{lt}}$, and $\mathbf{R_{tt}}$ are functions which contain all of the nuclear structure information.

In considering the formalism just outlined, two particularly useful sets of kinematics become immediately obvious: so-called *parallel* and *quasi-perpendicular* kinematics.

2.2.1 Parallel kinematics

Structure function separations

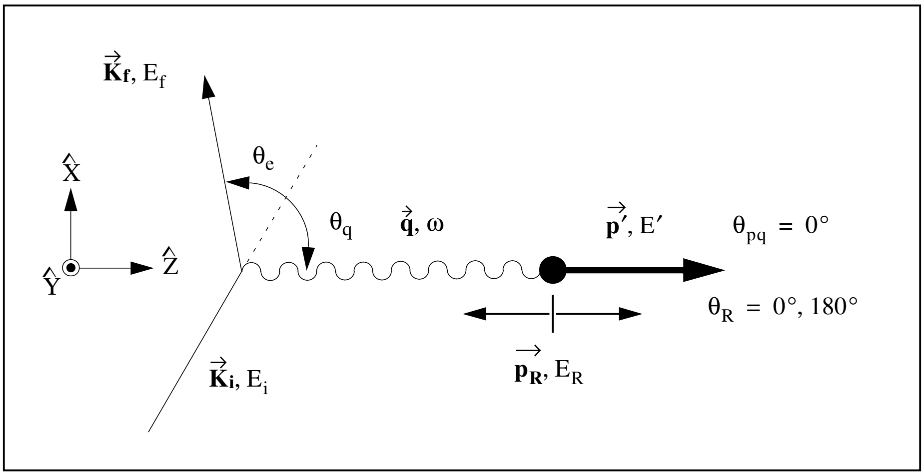

Figure 2.3: Parallel kinematics

In these kinematics, $\vec{p}\,' \parallel \vec{q}$ as shown in Fig. 2.3, so that ϕ is indeterminate. In detecting the ejected protons in the direction of the momentum transfer, the two periodic functions in 2.1 are integrated over, resulting in the expression for the differential cross section reducing to

$$\sigma = K\sigma_M[v_l\mathbf{R_l} + v_t\mathbf{R_t}] = 2Kv_t\sigma_M\sqrt{v_l}\left[\frac{\mathbf{R_t}}{2\sqrt{v_l}} + \epsilon\mathbf{R_l}\right], \tag{2.9}$$

where

$$\epsilon = \frac{\sqrt{v_l}}{2v_t} \tag{2.10}$$

is the virtual photon polarization.

In order to extract the structure functions $\mathbf{R_l}$ and $\mathbf{R_t}$, the cross section given in 2.9 must be measured at least twice, keeping Q^2, ω, E_m, and $\vec{p}_m$ fixed to ensure $\mathbf{R_l}$, $\mathbf{R_t}$ and v_l remain fixed. The remaining kinematical factor v_t is a strong function of θ_e, the scattered electron angle. Thus, so is ϵ, the so-called separation "lever arm". Clearly, it is desirable to vary ϵ as much as possible between the two measurements to ease the extraction of the structure functions. Thus, the measurement is best performed at two widely-separated electron angles, which translates into two dramatically different beam energies. This yields a second expression for the cross section given by

$$\sigma' = 2K'v_t'\sigma_M'\sqrt{v_l}\left[\frac{\mathbf{R_t}}{2\sqrt{v_l}} + \epsilon'\mathbf{R_l}\right]. \tag{2.11}$$

The simultaneous pair of equations 2.9 and 2.11 may then be solved for the structure functions

$$\mathbf{R_l} = \frac{1}{2\sqrt{v_l}(\epsilon' - \epsilon)} \left[\frac{\sigma'}{K' v_t' \sigma_M'} - \frac{\sigma}{K v_t \sigma_M} \right] \tag{2.12}$$

$$\mathbf{R_t} = \left(\frac{1}{1 - \epsilon'/\epsilon} \right) \left(\frac{\sigma'}{K' v_t' \sigma_M'} \right) + \left(\frac{1}{1 - \epsilon/\epsilon'} \right) \left(\frac{\sigma'}{K' v_t' \sigma_M'} \right). \tag{2.13}$$

The structure functions which will be extracted in this experiment from the measurements in parallel kinematics are given by 2.12 and 2.13. This technique is widely known as a *Rosenbluth separation*.

2.2.2 Quasi-perpendicular kinematics

Structure function separations

In these kinematics, $\pm\vec{p}_R \sim\perp \vec{q}$ (implying $\phi = 0°$ or $\phi = 180°$ depending upon the direction of the recoil momentum vector). A cartoon sketch of the situation is presented in Fig. 2.4.

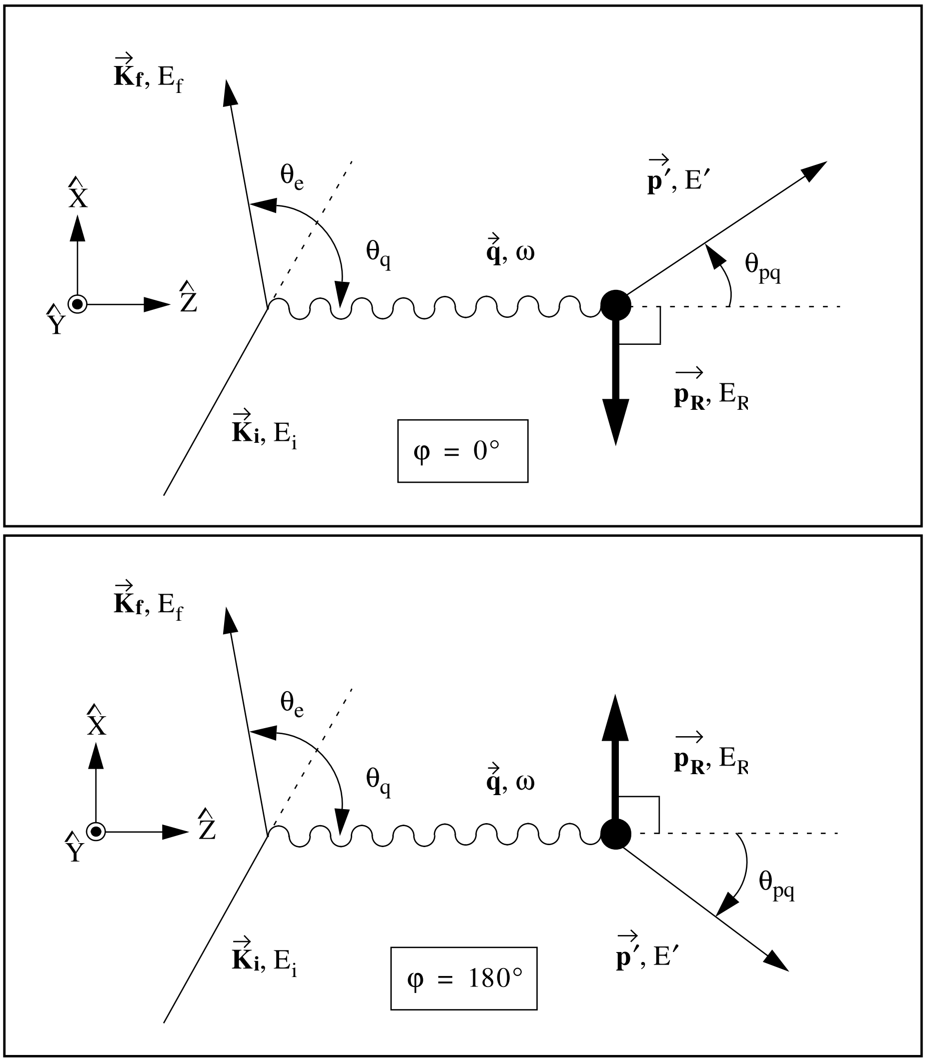

Figure 2.4: Quasi-perpendicular kinematics

This allows for further structure function separations to be performed by placing the HRS_h spectrometer at several values of $\pm\theta_{pq}$ symmetric about $\vec{q}$. Note that the angle at which the HRS_h spectrometer detects the ejected proton is given by

$$\theta_h = \theta_q \pm \theta_{pq}, \tag{2.14}$$

measured from the direction of the incident electron beam. Opposite sides of $\vec{q}$ result in $\phi = 0°$ or $180°$, which translates into two different expressions for the differential cross section

$$\sigma_0 = K\sigma_M[v_l\mathbf{R_l} + v_t\mathbf{R_t} + v_{lt}\mathbf{R_{lt}} + v_{tt}\mathbf{R_{tt}}]|_{\phi=0^\circ} \tag{2.15}$$

$$\sigma_{180} = K\sigma_M[v_l\mathbf{R_l} + v_t\mathbf{R_t} - v_{lt}\mathbf{R_{lt}} + v_{tt}\mathbf{R_{tt}}]|_{\phi=180^\circ}\ , \tag{2.16}$$

which may be combined to yield

$$\mathbf{R_{lt}} = \frac{1}{2v_{lt}K\sigma_M}[\sigma_0 - \sigma_{180}] \tag{2.17}$$

and

$$\frac{1}{2K\sigma_M v_l}[\sigma_0 + \sigma_{180}] = \mathbf{R_l} + \frac{v_t}{v_l}\mathbf{R_t} + \frac{v_{tt}}{v_l}\mathbf{R_{tt}}. \tag{2.18}$$

Thus, $\mathbf{R_{lt}}$ may be extracted according to 2.17 by measuring the cross section in quasi-perpendicular kinematics for a single value of θ_{pq} symmetric about $\vec{q}$ (that is, $\pm\theta_{pq}$), again keeping Q^2, ω, E_m, and $\vec{p}_m$ fixed. This procedure is known as an $\mathbf{R_{lt}}$ separation. The angles θ_{pq} are generally chosen such that there is a continuous variation in the acceptance of the proton spectrometer HRS$_h$ in recoil momentum space, and some overlap between adjacent angular settings is also desirable.

Furthermore, the idea behind the Rosenbluth technique may be applied, and a second quasi-perpendicular measurement at the same values of $\pm\theta_{pq}$ for a new combination of beam energy and electron scattering angle which preserves Q^2, ω, E_m, and $\vec{p}_m$ may be performed. This results in another pair of equations as before

$$\sigma'_0 = K'\sigma'_M[v_l\mathbf{R_l} + v'_t\mathbf{R_t} + v'_{lt}\mathbf{R_{lt}} + v_{tt}\mathbf{R_{tt}}]|_{\phi=0^\circ} \tag{2.19}$$

$$\sigma'_{180} = K'\sigma'_M[v_l\mathbf{R_l} + v'_t\mathbf{R_t} - v'_{lt}\mathbf{R_{lt}} + v_{tt}\mathbf{R_{tt}}]|_{\phi=180^\circ}\ . \tag{2.20}$$

However, because the required angle for the hadron spectrometer is very small for 2.19, it is spatially impossible at this facility to perform this measurement within our experimental constraints. Instead, for each value of $+\theta_{pq}$, the value for $\mathbf{R_{lt}}$ determined from 2.17 may be substituted into 2.20, and the result rewritten as

$$\frac{1}{v_l}(\frac{\sigma'_{180}}{K'\sigma'_M} + v'_{lt}\mathbf{R_{lt}}) = \mathbf{R_l} + \frac{v'_t}{v_l}\mathbf{R_t} + \frac{v_{tt}}{v_l}\mathbf{R_{tt}}. \tag{2.21}$$

Combining 2.21 with 2.18 allows for the extraction of

$$\mathbf{R_t} = \frac{1}{v_t - v'_t}\left[\frac{\sigma_0 + \sigma_{180}}{2K\sigma_M} - \frac{\sigma'_{180}}{K'\sigma'_M} - v'_{lt}\mathbf{R_{lt}}\right], \tag{2.22}$$

and produces another useful equation

$$\frac{\sigma_0 + \sigma_{180}}{2K\sigma_M v_l} + \frac{1}{v_l}\left(\frac{\sigma'_{180}}{K'\sigma'_M} + v'_{lt}\mathbf{R_{lt}}\right) = 2\mathbf{R_l} + \frac{\mathbf{R_t}}{v_l}(v_t + v'_t) + 2\frac{v_{tt}}{v_l}\mathbf{R_{tt}}. \tag{2.23}$$

Substitution of the value determined for $\mathbf{R_t}$ in 2.22 results in the last extractable combination of structure functions given our experimental constraints, namely

$$\mathbf{R_{l+tt}} = \frac{1}{2}\left[\frac{\sigma_0 + \sigma_{180}}{2K\sigma_M v_l} + \frac{1}{v_l}\left(\frac{\sigma'_{180}}{K'\sigma'_M} + v'_{lt}\mathbf{R_{lt}}\right) - \frac{\mathbf{R_t}}{v_l}(v_t + v'_t)\right], \tag{2.24}$$

where

$$\mathbf{R_{l+tt}} = \mathbf{R_l} + \frac{v_{tt}}{v_l}\mathbf{R_{tt}}. \tag{2.25}$$

Separation errors

As the intention in this experiment is to perform a series of structure function separations, it is very useful to estimate the uncertainty with which we can perform this task. To do this, the expressions for the structure functions and structure function combinations we intend to extract ($\mathbf{R_{lt}}$, $\mathbf{R_t}$, and $\mathbf{R_{l+tt}}$ given by equations 2.17, 2.22, and 2.24 respectively) must be modified so that they are functions of cross section only. Equation 2.17 requires no changes.

$$\mathbf{R_{lt}} = \frac{1}{2v_{lt}K\sigma_M}[\sigma_0 - \sigma_{180}]. \tag{2.26}$$

Substituting 2.17 into 2.22 and rewriting results in

$$\mathbf{R_t} = \frac{1}{v_t - v'_t}\left[\frac{1}{2K\sigma_M}\left\{\sigma_0(1 - \frac{v'_{lt}}{v_{lt}}) + \sigma_{180}(1 + \frac{v'_{lt}}{v_{lt}})\right\} - \frac{\sigma'_{180}}{K'\sigma'_M}\right]. \tag{2.27}$$

And finally, substituting 2.17 and 2.22 into 2.24 results in 2.28

$$\mathbf{R_{l+tt}} = \frac{1}{2K\sigma_M v_l}\left\{A \cdot \sigma_0 + B \cdot \sigma_{180}\right\} + \frac{1}{K'\sigma'_M v_l}\left\{C \cdot \sigma'_{180}\right\}, \tag{2.28}$$

where

$$A = \left(\frac{1}{v_t - v'_t}\right)\left(v_t\frac{v'_{lt}}{v_{lt}} - v'_t\right), \tag{2.29}$$

$$B = \left(\frac{1}{v_t - v'_t}\right)\left(-v'_t - v_t\frac{v'_{lt}}{v_{lt}}\right), \tag{2.30}$$

and

$$C = \frac{v_t}{v_t - v'_t}. \tag{2.31}$$

It is then a straightforward, albeit tedious, process to evaluate the errors in the extracted structure functions. They are given by

$$\frac{\delta\mathbf{R_{lt}}}{\mathbf{R_{lt}}} = \left(\frac{1}{\mathbf{R_{lt}}}\right)\frac{\sqrt{(\delta\sigma_0)^2 + (\delta\sigma_{180})^2}}{2v_{lt}K\sigma_M} \tag{2.32}$$

(where $\mathbf{R_{lt}}$ is defined in 2.17),

$$\frac{\delta\mathbf{R_t}}{\mathbf{R_t}} = \left(\frac{1}{\mathbf{R_t}}\right)\cdot\frac{\sqrt{\left(\frac{1-\frac{v'_{lt}}{v_{lt}}}{2K\sigma_M}\cdot\delta\sigma_0\right)^2 + \left(\frac{1+\frac{v'_{lt}}{v_{lt}}}{2K\sigma_M}\cdot\delta\sigma_{180}\right)^2 + \left(\frac{1}{K'\sigma'_M}\cdot\delta\sigma'_{180}\right)^2}}{(v_t - v'_t)} \tag{2.33}$$

(where $\mathbf{R_t}$ is defined in 2.27), and

$$\frac{\delta\mathbf{R_{l+tt}}}{\mathbf{R_{l+tt}}} = \left(\frac{1}{\mathbf{R_{l+tt}}}\right)\sqrt{(\frac{D}{2K\sigma_M v_l}\cdot\delta\sigma_0)^2 + (\frac{E}{2K\sigma_M v_l}\cdot\delta\sigma_{180})^2 + (\frac{F}{K'\sigma'_M v_l}\cdot\delta\sigma'_{180})^2}, \tag{2.34}$$

(where $\mathbf{R_{l+tt}}$ is defined in 2.28), and

$$D = \left(\frac{1}{v_t - v'_t}\right)\left(v_t\frac{v'_{lt}}{v_{lt}} - v'_t\right), \tag{2.35}$$

$$E = \left(\frac{1}{v_t - v'_t}\right)\left(-v'_t - v_t\frac{v'_{lt}}{v_{lt}}\right), \tag{2.36}$$

and

$$F = \left(\frac{v_t}{v_t - v'_t}\right). \tag{2.37}$$

Chapter 3

Apparatus

3.1 Beam

For this experiment, we have chosen to work at the top of the *quasi-elastic* (QE) peak. In this configuration, the interaction between the probe and the target nucleus is as one-body as possible, and thus all multi-body effects associated with the probe have been minimized. Since we intend to look for multi-body effects, this is desirable. The relative positioning of the QE peak as a function of energy transfer ω is shown in Fig. 3.1. This figure is drawn from inclusive electron scattering data.

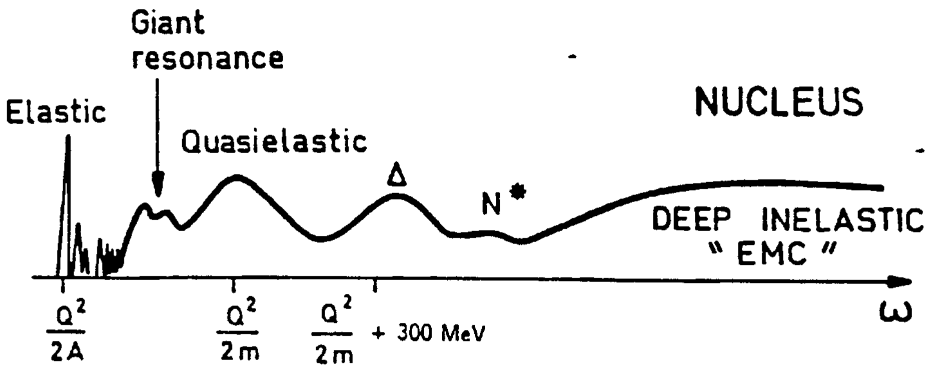

Figure 3.1: The quasi-elastic (QE) peak.

3.1.1 Q^2, ω, $\vec{q}$

We have chosen for this experiment to transfer a momentum $\vec{q} = 1.0$ GeV/c to our target nucleus. This momentum transfer corresponds to a virtual photon wavelength of a magnitude which reasonably ensures the probe interacts with a single nucleon in the target, further accentuating the one-body nature of the interaction.

Consider the general situation outlined in Fig. 3.2.

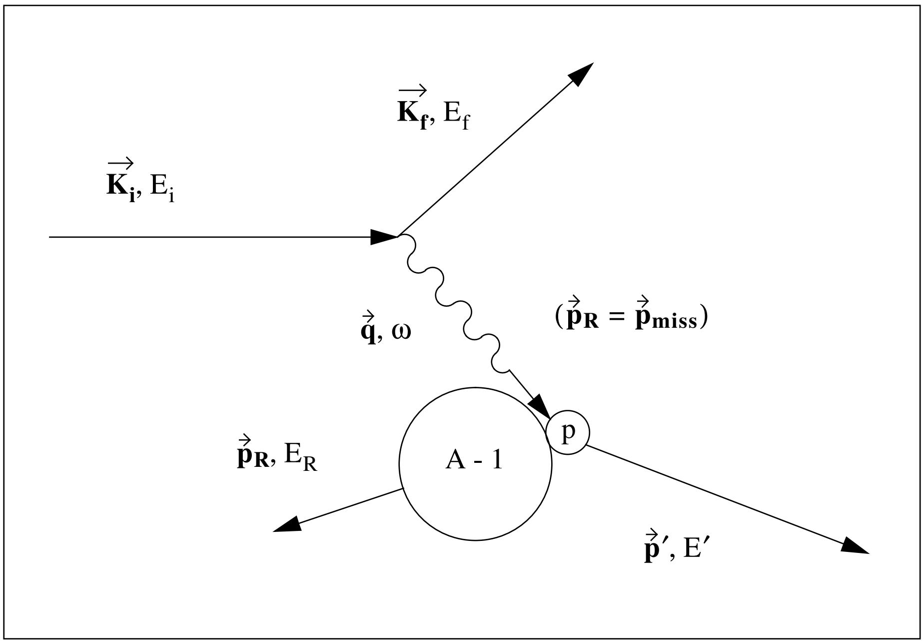

Figure 3.2: In-plane electron scattering.

The missing energy E_m is given by

$$E_m = \omega - T_p - T_b, \tag{3.1}$$

where ω is the energy transfer (the difference between the incident and scattered electron energies), T_p is the kinetic energy of the ejected proton, and T_b is the kinetic energy of the recoil nucleus. The missing momentum $\vec{p}_{miss}$ is given by

$$\vec{p}_{miss} = \vec{q} - \vec{p}\,'. \tag{3.2}$$

Consider the limiting case where the missing momentum $\vec{p}_m = \vec{0}$ ($T_b = 0$ GeV). Here, the momentum of the virtual photon $\vec{q}$ is completely transferred to the ejected proton so that its momentum $\vec{p}\,' = 1.0$ GeV/c, which corresponds to a kinetic energy $T_p = 0.433$ GeV.

Application of the conservation of energy to 3.1 results in

$$E_m = (m_p + M_b) - M_a, \tag{3.3}$$

where m_p is the mass of the proton (0.938 GeV/c^2), M_a is the mass of the target nucleus ^{16}O (14.895 GeV/c^2), and M_b is the mass of the recoil nucleus ^{15}N (13.969 GeV/c^2 for a ground state recoil). Thus, for our experiment, $E_m =$ 12.1 MeV and beyond. Further, assuming this limiting value of E_m, the limiting value of $\omega = 0.445$ GeV may be calculated using 3.1.

The square of the four-momentum is given by

$$Q^2 = q^2 - \omega^2 = 0.802 \text{ (GeV/c)}^2. \tag{3.4}$$

Drawing this together, the Björken variable x for this measurement is

$$x = \frac{Q^2}{2m_p\omega} = 0.960. \tag{3.5}$$

A summary of the pertinent probe parameters is presented in Table 3.1.

Variable	Value
$\vec{q}$	1.0 GeV/c
ω	0.445 GeV
Q^2	0.802 (GeV/c)^2
x	0.960

Table 3.1: E89-003 probe parameters.

3.1.2 Energies

There are some considerations to be made when choosing the electron beam energy that an experiment will be performed at. While in principle, almost any energy up to a nominal value of 4.0 GeV is available to the experimenter at Jefferson Lab, certain energies are much easier to attain and run at.

The Jefferson Lab accelerator consists of a 0.045 GeV injector followed by a pair of 0.4 GeV recirculating superconducting CW LINACs configured in racetrack fashion. Extraction may be performed after each pass through both LINACs, and the apparatus is currently rated for 5-pass beam. Table 3.2 presents the beam energies which are thus "readily" available to the experimenter.

Pass	E_{beam} (GeV)
1	0.845
2	1.645
3	2.445
4	3.245
5	4.045

Table 3.2: "Easily" obtainable beam energies.

In selecting the electron beam energies for this experiment, ϵ (the polarization of the virtual photon) was considered, as it defines a "separation lever arm" for the parallel kinematics measurements. Basically, the larger the variation in ϵ between the various measurements which constitute the separation, the smaller the systematic errors on the extracted response functions.

The variation in ϵ as a function of beam energy is shown in Fig. 3.3, along with the "readily" attainable beam energies presented in Table 3.2.

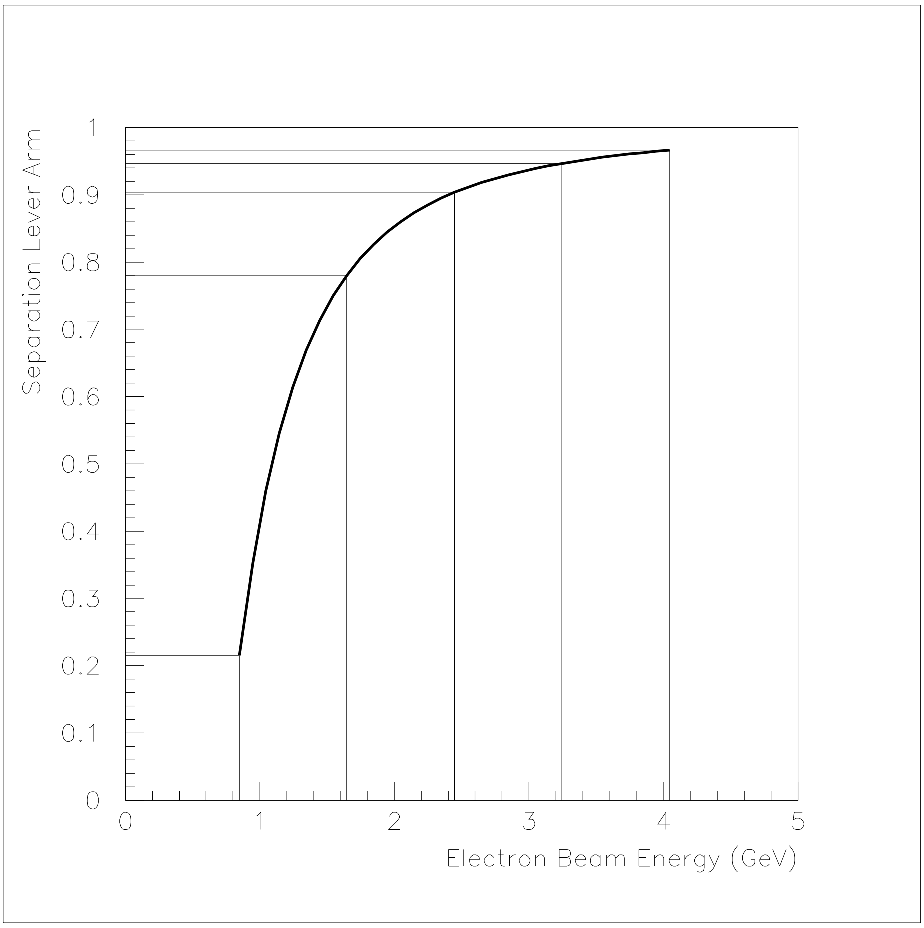

Figure 3.3: ϵ for $\vec{q} = 1.0$ GeV/c and $\omega = 0.445$ GeV.

Clearly, the virtual photon polarization "saturates" as the electron beam energy approaches 4.045 GeV. In fact, there is little separation lever arm to be gained above 2.445 GeV. This, coupled to the fact that the lowest "readily" available beam energy is 0.845 GeV has resulted in our choosing these electron beam energies as the extremes for our measurement. We will also perform an intermediary measurement at 1.645 GeV which will be used to monitor the structure function extraction systematics for the experiment. Table 3.3 summarizes the beam energies and ϵ's we have chosen to employ.

Pass	E_{beam} (GeV)	ϵ
1	0.845	0.215
2	1.645	0.780
3	2.445	0.904

Table 3.3: E89-003 beam energies and virtual photon polarizations.

The Mott cross section σ_M for the chosen beam energies is shown in Fig. 3.4. Since the electron scattering cross section is proportional to σ_M, the magnitude of σ_M gives a good first approximation to the runtime necessary for a given kinematics.

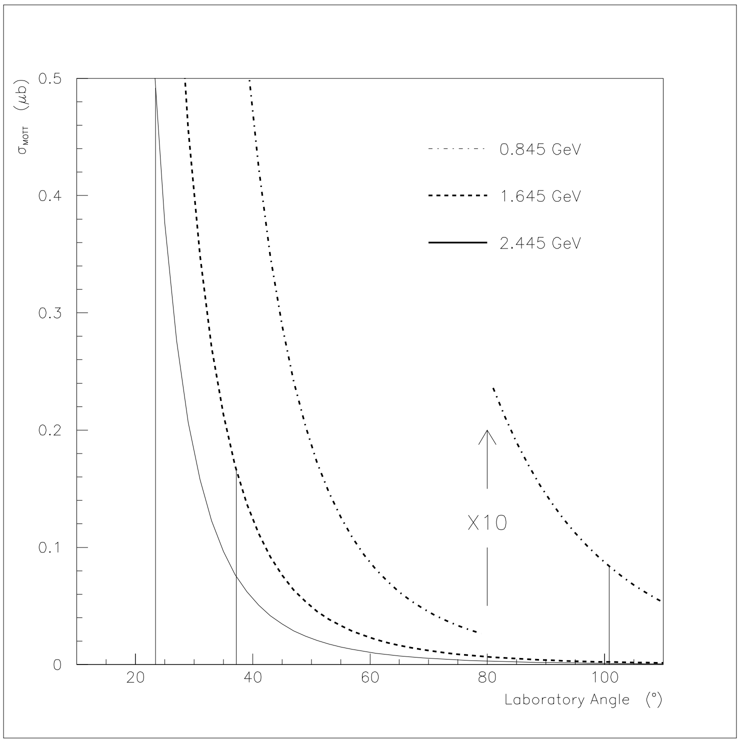

Figure 3.4: The Mott cross section as a function of θ_e.

Table 3.4 summarizes the anticipated beam requirements.

Parameter	Requirement
current	50 - 100 μA
charge determination	$< 1\%$
horizontal spotsize	± 100 μm (4σ)
vertical spotsize	± 100 μm (4σ)
energy stability	1×10^{-4}
energy resolution	1×10^{-4} FWHM
absolute energy	1×10^{-3}
current monitoring	as available
positional stability	± 25 μm
directional stability	± 100 μr
rastering	not required

Table 3.4: Anticipated beam requirements.

3.2 Target

3.2.1 Preamble

The target that has been chosen for our investigation is ^{16}O. The naïve shell model of this nucleus is presented in Fig. 3.5 as a reminder.

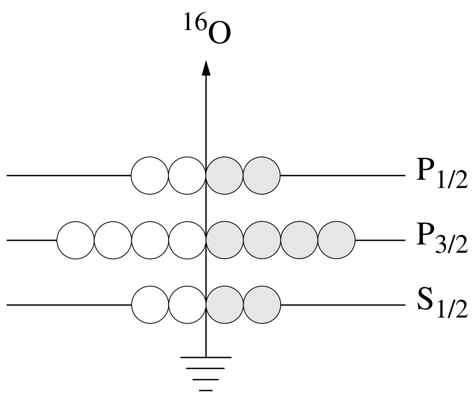

Figure 3.5: Shell model of ^{16}O.

The ^{16}O itself will be made available in the form of a waterfall (H_2O) target. The waterfall target was constructed by a group from INFN, and the basic design configuration for the apparatus is presented in detail in [3]. Waterfall targets have been used for ^{16}O(e,e$'$p) experiments successfully in the past at Mainz, NIKHEF-K, and Saclay [4, 5, 6, 7].

A waterfall target is particularly useful for our purposes because of the H content of the water molecule. By performing several discrete luminosity measurements on the kinematically-overdetermined p(e,e$'$p) reaction, both the absolute normalization of the experiment and the precise direction of $\vec{q}$ (very important for the separation) can be determined. Further, the singles rates in the HRS$_e$ spectrometer for the p(e,e$'$) reaction can be used to extract a relative normalization of the experiment at any point in time. Combined, these two normalization measurements serve as a continuous luminosity monitor, and thus the experiment is both self-calibrating and self-normalizing. It is projected that in this manner, we will be able to monitor the thickness stability of the target foils to $< \pm 0.5\%$.

The waterfall target is currently onsite at Jefferson Lab and is installed and running in Hall A. It has been used for the HRS^2 coincidence commissioning studies. A remote interface to and operations manual for the target are both located in the Hall A Counting House.

3.2.2 Windows

Crucial to our use of the waterfall target is its windows. Because we intend to employ beam currents in excess of 50 μA, care must be taken in choosing the window material such that it does not melt!

Consider the general case of a circular beam spot and a circular target window, as illustrated in Figure 3.6.

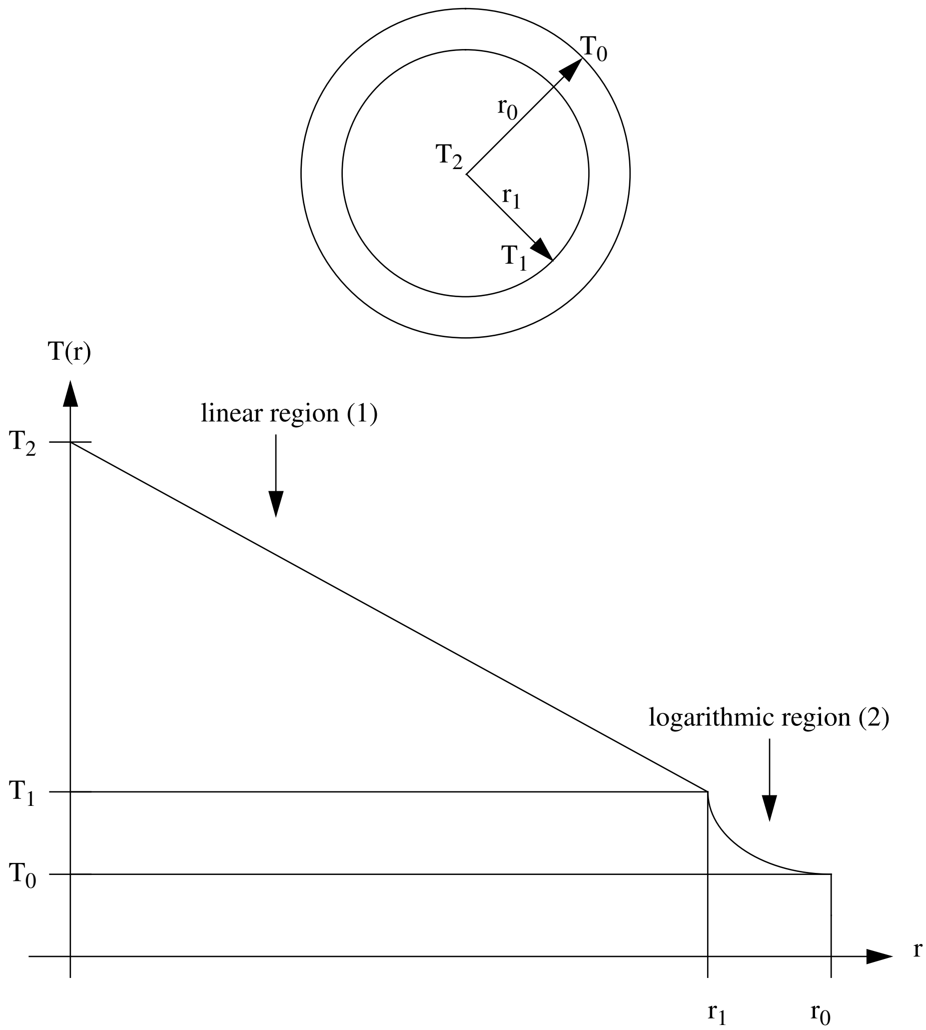

Figure 3.6: Window heating.

Further, suppose there is a continuous heat sink surrounding the window which is maintained at temperature T_0 and located a distance r_0 from the center of the beam spot. The beam spot radius is r_1.

The heating pattern which develops is characterized by two distinct regions. In the logarithmic region, this heating is given by

$$\Delta T_1 = T_1 - T_0 = \frac{i\rho}{2\pi\kappa}\frac{dE}{dx}\ln(\frac{r_0}{r_1}), \tag{3.6}$$

while in the linear region, the heating is given by

$$\Delta T_2 = T_2 - T_1 = \frac{i\rho}{4\pi\kappa}\frac{dE}{dx}. \tag{3.7}$$

In both cases, i is the beam current (in μA), ρ is the target density, κ is the thermal conductivity and dE/dx is the differential energy loss.

The total temperature rise above the maintained heatsink temperature T_0 is thus

$$\Delta T = \Delta T_1 + \Delta T_2 = \frac{i\rho}{4\pi\kappa}\frac{dE}{dx}\left[1 + 2\ln(\frac{r_0}{r_1})\right]. \tag{3.8}$$

If a 100 μA beam of radius 25 μm and a window of radius 3 cm are considered (*very* extreme situations), Table 3.5 results.

Material	ρ (g/cm^2)	$\frac{dE}{dx}$ $(\frac{\text{MeV}}{\text{g/cm}^2})$	κ $(\frac{\text{MeV}^\circ\text{C}}{\mu\text{A}})$	T_{melt} (°C)	ΔT (°C)
Al	2.7	1.62	2.37	660	223
Fe	7.9	1.48	0.8	1530	1765
Ti	4.5	1.51	0.22	1660	3731
Cu	8.96	1.44	4.0	1083	390
Be	1.85	1.61	2.1	1278	171
W	19.3	1.16	1.75	3410	1545
Ta	16.65	1.2(?)	0.58	2996	4161

Table 3.5: Target window heating.

Thus, Be windows were chosen for the beam entrance and exit windows for the INFN waterfall target can. These windows are 3 mil thick and 30 mm in diameter. Because Be is poisonous, they have been plated with .5 mil of Ni and a whisper of Au (which also serves to improve heat conductivity). The lateral windows, which the scattered electrons and knocked out protons must traverse, are made of Kapton and are 75 μm thick. A temporary Kevlar explosion shield may be put in place around the windows during access for safety purposes.

3.2.3 Foils

A three-waterfall offset configuration has been chosen, with each each waterfall to be nominally 125 mg/cm^2 thick and oriented at 30° to the incident beam direction. Note that the thickness of the waterfalls may be fine-tuned by varying the target pump speed. This configuration is superior to, for example, a single waterfall 3 times thicker because energy loss in the target is reduced. Further, a consistent reaction vertex reduces the number of accidentals, and allows the energy loss to be *partly* corrected for. The particular waterfall target configuration that will be used is shown in Figures 3.7 and 3.8. The target design was performed by Gao, and care was taken to optimize the foil configuration with respect to the spectrometer acceptance and ejectile trajectory.

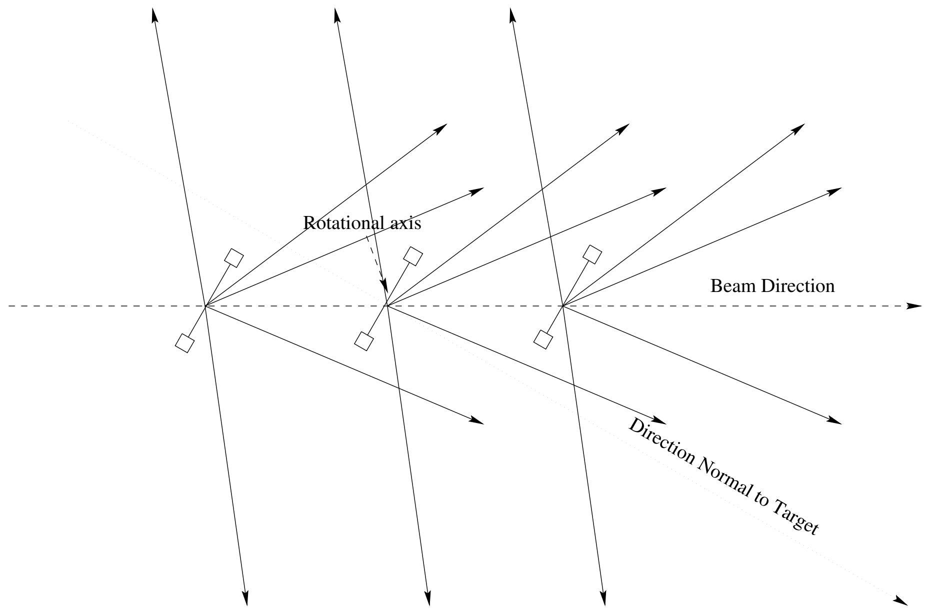

Figure 3.7: The waterfall target: kinematical overview.

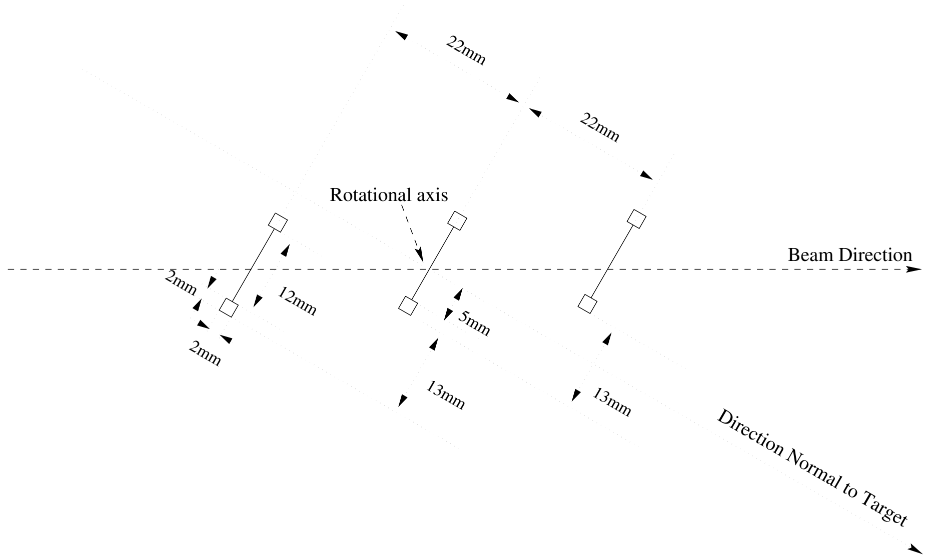

Figure 3.8: The waterfall target: configuration.

In Fig. 3.8, the three water foils are identical, 12 mm wide, and guided by poles which are 2 mm $\times$ 2 mm. In the direction normal to the target, the foils are separated by 22 mm. Along the target, the first foil is shifted down the page by 13 mm and second up the page by 13 mm. The rotational axis occurs at the intersection of the incident electron beam and the central foil. The distance from the rotational axis to the nearest pole is 5 mm. The foils are parallel, and the angle between the beam direction and the direction normal to the target is 30°. The tolerance of the machining was less than 0.15 mm.

3.3 Spectrometers

Parameter	Requirement
absolute momentum	5×10^{-4}
momentum resolution	2×10^{-4}
positioning requirement	0.2 mr (0.01°)
collimators	5 msr/sieve slit/0.6 msr
TOF resolution	1 ns FWHM
detector stack	standard configuration

Table 3.6: Anticipated spectrometer requirements.

Table 3.6 summarizes the anticipated spectrometer requirements.

Chapter 4

Experimental considerations

4.1 Preamble

Experiment E89-003 at Jefferson Lab will investigate the ^{16}O(e,e$'$p) reaction using the Hall A High Resolution Spectrometers. A proven waterfall target will be employed which will allow for precise monitoring of the luminosity and thus provide excellent knowledge of the absolute normalization. The ^{1}P$_{1/2}$, ^{1}P$_{3/2}$, and ^{1}S$_{1/2}$ states as well as part of the continuum at Q^2 = 0.802 (GeV/c)^2, ω = 0.445 GeV, and $\vec{q}$ = 1.0 GeV/c will be studied. Measurements in both parallel kinematics (to extract the structure functions $\mathbf{R_l}$ and $\mathbf{R_t}$), and quasi-perpendicular kinematics (to extract the structure functions and combinations $\mathbf{R_{lt}}$, $\mathbf{R_t}$, and $\mathbf{R_l} + \frac{v_{tt}}{v_l}\mathbf{R_{tt}}$) will be performed. The parallel kinematics measurements will be configured to investigate a missing momentum range $0 \leq |\vec{p}_{miss}| \leq$ 0.10 GeV/c. The quasi-perpendicular kinematics measurements will be configured to investigate a missing momentum range 0.05 GeV/c $\leq |\vec{p}_{miss}| \leq$ 0.40 GeV/c.

4.2 Angular settings

The angular settings for the spectrometers for the various kinematics to be investigated are summarized in Tables 4.1 (^{1}H) and 4.2 (^{16}O). These kinematics have been calculated using the program `eepkin`, and have been cross-checked against several other codes. The settings have been extracted within a constant center-of-mass energy framework.

4.2.1 ^{1}H

$\lvert\vec{q}\rvert$ (GeV/c)	E_{beam} (GeV)	E_{scat} (GeV)	ε	θ_e (°)	θ_q (°)	θ_{pq} (°)	θ_h (°)	kin	$\lvert\vec{p}_{miss}\rvert$ (GeV/c)
1.004	0.845	0.408	0.217	100.76	23.53	0	23.53	$\parallel$	0.00
0.999	1.645	1.213	0.782	37.17	47.19	0	47.19	$\parallel$	0.00
0.997	2.445	2.014	0.905	23.36	53.28	0	53.28	$\parallel$	0.00

Table 4.1: Angular settings for ^{1}H.

The corresponding kinematics for electron scattering from ^{1}H are presented in Fig. 4.1.

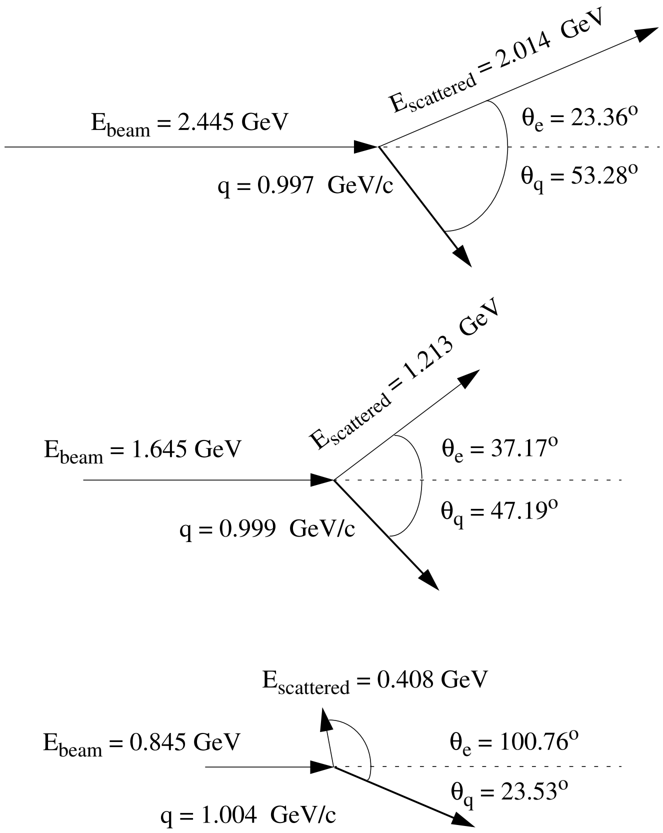

Figure 4.1: A sketch of the ^{1}H kinematics.

4.2.2 ^{16}O

E_{beam} (GeV)	Kin	E_{scat} (GeV)	ε	θ_e (°)	θ_q (°)	θ_{pq} (°)	θ_h (°)	$\lvert\vec{p}_{miss}\rvert$ (GeV/c)
0.845	$\parallel$	0.400	0.215	100.76	23.12	0	23.12	0.00
	$\Sigma 3$					6	29.12	0.11
						8	31.12	0.14
						9	32.12	0.16
						12	35.12	0.21
						16	39.12	0.28
						18	41.12	0.31
						19	42.12	0.33
						20	43.12	0.35
1.645	$\Sigma 4$	1.200	0.780	37.17	46.45	-12	34.45	0.21
						-9	37.45	0.16
						-8	38.45	0.14
	$\parallel$					0	46.45	0.00
	$\Sigma 5$					8	54.45	0.14
						9	55.45	0.16
						12	58.45	0.21
2.445	$\Sigma 2$	2.000	0.904	23.36	52.47	-20	32.47	0.35
						-19	33.47	0.33
						-18	34.47	0.31
						-16	36.47	0.28
						-12	40.47	0.21
						-9	43.47	0.16
						-8	44.47	0.14
						-6	46.47	0.10
	$\parallel$					0	52.47	0.00
	$\Sigma 1$					6	58.47	0.10
						8	60.47	0.14
						9	61.47	0.16
						12	64.47	0.21
						16	68.47	0.28
						18	70.47	0.31
						19	71.47	0.33
						20	72.47	0.35
						30	82.47	0.51

Table 4.2: Angular settings for ^{16}O.

Figure 4.2 presents a sketch of these kinematics for ^{16}O.

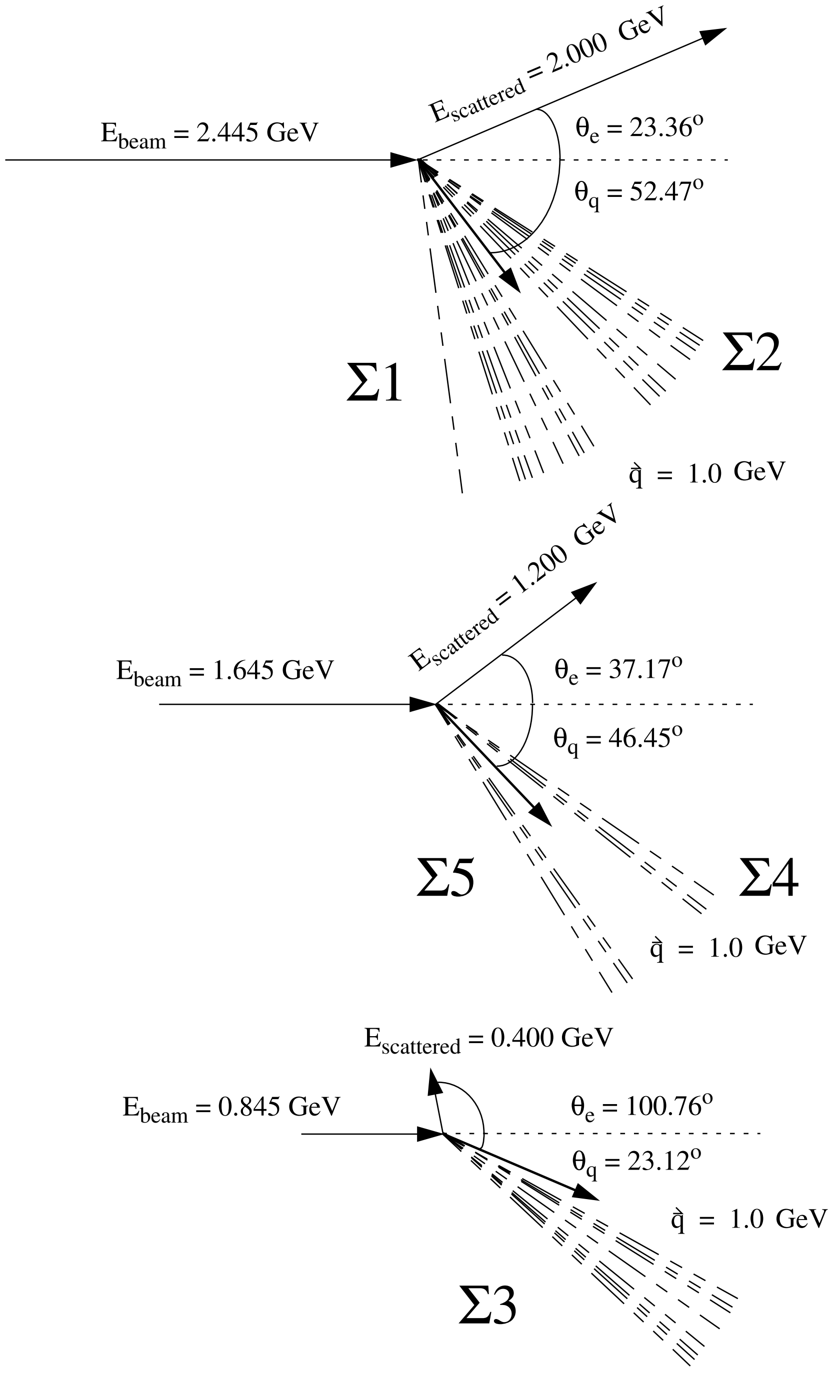

Figure 4.2: A sketch of the ^{16}O kinematics.

4.3 Rate estimates and run time projections

4.3.1 MCEEP setup parameters

The following tables summarize the count rate estimates performed by Fissum for this experiment using Ulmer's Monte Carlo code `MCEEP`. The input parameters are presented below:

- target: three 125 mg/cm^2 foils of H_2O oriented such that the perpendicular to the surface of the foil makes an angle of 30° with respect to the beam.

Target	Thickness (mg/cm^2)
H_2O	145 mg/cm^2
^{16}O	130 mg/cm^2
^1H	15 mg/cm^2

Table 4.3: Nominal effective per-foil target thicknesses.

- acceptance weighting: 2.45. This constant is intended to represent, *on average*, the affect of the spectrometer acceptance on the luminosity. Note that for the `MCEEP` calculations, the total effective target thickness is taken to have the form of a *single* central target.

Target	Thickness (mg/cm^2)
H_2O	355 mg/cm^2
^{16}O	320 mg/cm^2
^1H	35 mg/cm^2

Table 4.4: Total target thicknesses.

- HRS_h fields: adjusted by 20 MeV so that the center of the HRS^2 acceptance is at about E_{miss} = 32 MeV (20 MeV above the $^1P_{1/2}$ state.
- beam current: 65 μA.
- luminosity: 20 $\mu A/cm^2 = 5 \times 10^{36}$ cm^{-2}s^{-1} for ^{16}O and 2.5 $\mu A/cm^2 = 1 \times 10^{36}$ cm^{-2}s^{-1} for ^1H.
- ^{16}O model: Van Orden[2] (the employed central E_m values and spectroscopic factors are presented in Table 4.5.)

State	E_{miss} (MeV)	Spectroscopic Factor
$^1P_{1/2}$	12.1	0.63 [6]
$^1P_{3/2}$	18.4	0.51 [6]
$^1S_{1/2}$	37.0	0.55 [4]

Table 4.5: Spectroscopic Factors.

The P-shell momentum distributions of Van Orden employed by MCEEP are shown below.

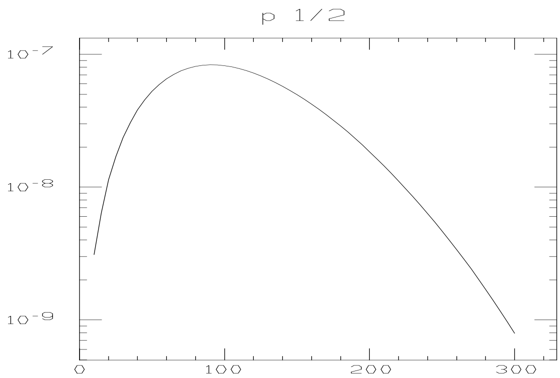

Figure 4.3: The $^1P_{\frac{1}{2}}$ momentum distribution used in MCEEP.

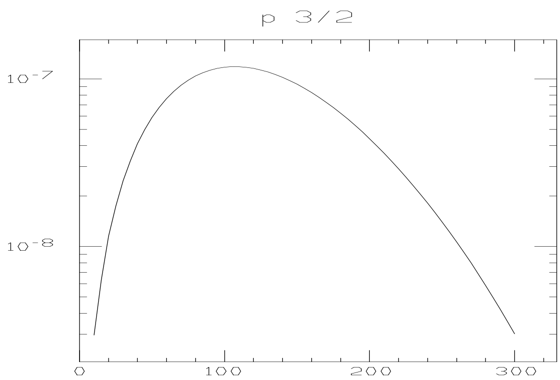

Figure 4.4: The $^1P_{\frac{3}{2}}$ momentum distribution used in MCEEP.

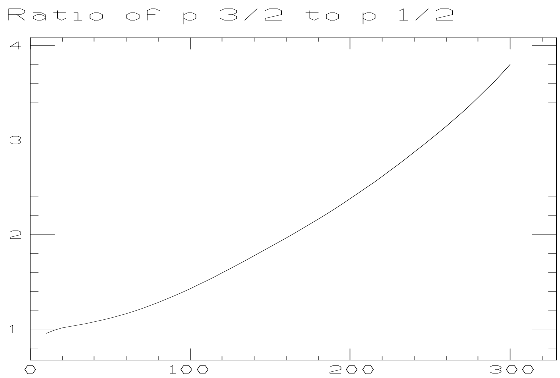

Figure 4.5: The ratio of the momentum distributions.

Refer to Appendix A for a complete listing of the MCEEP output variable summaries.

4.3.2 Cross section and rate summaries

^{1}H

Tables 4.6 and 4.7 summarize the projected cross sections and rates for p(e,e′).

E_{beam}	Kinematics	σ (μb/sr)
0.845	all	0.0014286
1.645	all	0.015688
2.445	all	0.047602

Table 4.6: Projected p(e,e′) σ (μb/sr).

E_{beam}	Kinematics	Rate (/hr)
0.845	all	226800
1.645	all	2502000
2.445	all	7588800

Table 4.7: Projected hourly p(e,e′) rate.

Tables 4.8 and 4.9 summarize the projected cross sections and rates for p(e,e′p).

E_{beam}	Kinematics	Full $\Delta\Omega$ (μb/sr)
0.845	$\|\|$	0.0014286
1.645	$\|\|$	0.015383
2.445	$\|\|$	0.046348

Table 4.8: Projected p(e,e′p) σ (μb/sr).

E_{beam}	Full $\Delta\Omega$ Rate	$\vec{q}$-llimator Rate (/hr)
0.845	226800	38
1.645	1170000	416
2.445	1278000	1258

Table 4.9: Projected hourly p(e,e′p) rate.

The $\vec{q}$-llimator rate is that left after a cut has been placed on the central pinhole of the sieve slit collimator. It is the projected rate to be used to calculate the beamtime necessary to determine $\vec{q}$.

^{16}O

Table 4.10 presents raw projected cross sections and rates for ^{16}O(e,e′p). The column labeled "pinhole" was extracted using pinhole (0.1 mr $\times$ 0.1 mr) aperatures for the HRS^2, a $\pm$ 0.1% Δp/p acceptance for the HRS_e, and a p-shell harmonic oscillator potential with an oscillator parameter of 1.67.

E_{beam} (GeV)	Kin	θ_{pq} (°)	σ ($\times 10^{-3} \frac{\mu b}{sr^2 \cdot GeV}$)			
			$^1P_{1/2}$	$^1P_{3/2}$	$^1S_{1/2}$	pinhole
0.845	$\parallel$	0	60.248	53.090	77.252	0.0048133
	Σ3	6	150.98	121.51	126.71	51.834
		9	90.488	71.009	73.007	46.350
		12	33.518	26.000	27.110	22.229
		16	4.8428	3.7201	4.0284	3.8073
		18	1.3741	1.0643	1.1839	1.1654
		19	0.67680	0.52111	0.58916	0.60060
		20	0.30771	0.23866	0.27477	0.29562
1.645	Σ4	-12	79.870	75.972	130.71	86.610
		-9	272.58	248.03	370.79	209.60
	$\parallel$	0	661.59	536.79	627.61	0.10826
	Σ5	9	768.05	579.18	482.52	360.24
		12	349.27	250.99	180.57	177.57
2.445	Σ2	-20	1.1459	1.2729	3.0365	2.0332
		-19	2.6355	2.8357	6.3306	4.3284
		-18	5.7392	6.0796	12.934	8.8075
		-16	22.344	22.683	43.779	31.712
		-12	201.12	192.01	318.03	226.52
		-9	676.35	616.73	900.66	551.97
		-6	1537.0	1319.2	1629.6	723.44
	$\parallel$	0	1973.9	1596.6	1830.7	0.62824
	Σ1	6	2713.8	2147.9	2090.7	1059.6
		9	1884.8	1399.0	1157.4	979.56
		12	853.08	599.31	429.49	484.00
		16	169.60	111.98	66.492	85.814
		18	58.299	36.937	19.682	26.673
		19	32.585	20.325	10.086	13.846
		20	16.999	10.264	4.7758	6.8630
		30	0.0049618	0.0031718	0.0027774	0.00058025

Table 4.10: Projected cross sections to the various states (no $\omega\vec{q}$ matching).

E_{beam}	Kin	θ_{pq} ($^\circ$)	$^1P_{1/2}$	$^1P_{3/2}$	$^1S_{1/2}$
0.845	$\parallel$	0	695	797	3707
	$\Sigma3$	6	1763	2492	1931
		9	1022	1866	825
		12	378	862	251
		16	54	167	28
		18	16	56	7
		19	8	30	3
		20	4	15	1
1.645	$\Sigma4$	-12	1875	4522	2191
		-9	6422	11862	7749
	$\parallel$	0	15799	15730	42804
	$\Sigma5$	9	18387	25951	9499
		12	8380	13987	2955
2.445	$\Sigma2$	-20	27	137	25
		-19	62	283	59
		-18	136	562	138
		-16	534	1818	560
		-12	4829	11613	5306
		-9	16312	30114	18621
		-6	37152	51858	46760
	$\parallel$	0	48168	50216	99644
	$\Sigma1$	6	66910	81400	51073
		9	46429	65156	22137
		12	21099	34415	6879
		16	4211	8517	818
		18	1453	3234	196
		19	811	1914	88
		20	424	1040	35
		30	1	4	1

Table 4.11: Projected hourly raw rates (no $\omega\vec{q}$ matching).

Since each of the structure functions and combinations of structure functions to be separated are functions of $\vec{q}$, ω, E_m and $\vec{p}_{\text{miss}}$, and since they must necessarily be extracted for the same *ranges* of the aforementioned variables, it is important to apply *matching* cuts to the yields. The matching cut takes the form of a parallelogram in $\omega\vec{q}$ space (see Figure 4.6).

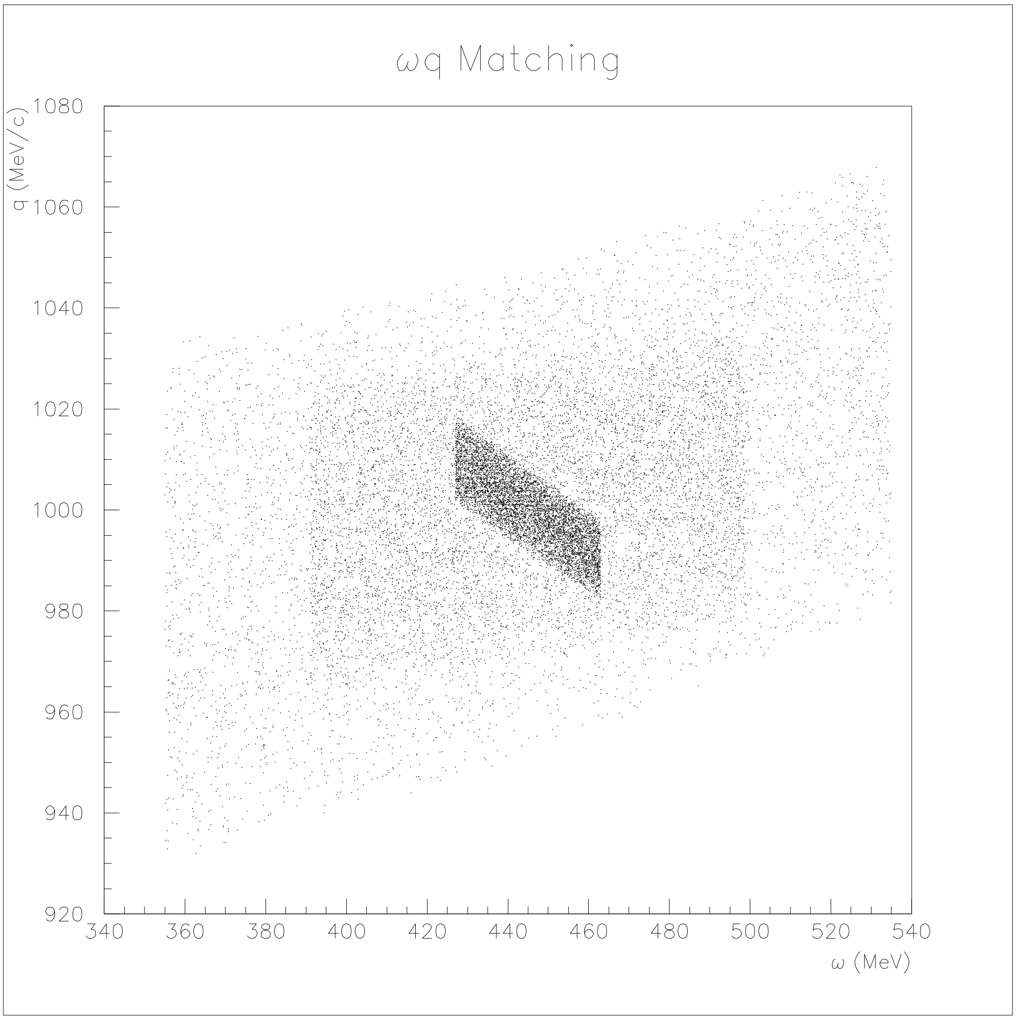

Figure 4.6: $\omega\vec{q}$ phase space.

The dark, central region represents the $\omega\vec{q}$ distribution at $\mathrm{E_{beam}} = 0.845$ GeV, the medium-shaded region represents the $\omega\vec{q}$ distribution at $\mathrm{E_{beam}} = 1.645$ GeV, and the lightest region represents the $\omega\vec{q}$ distribution at $\mathrm{E_{beam}} = 2.445$ GeV. Thus, it is the $\omega\vec{q}$ distribution at $\mathrm{E_{beam}} = 0.845$ GeV to which the spectra obtained at the other beam energies must be matched. A cut was applied which selected this darkest central region, and the rates were re-evaluated subject to this cut. The figures shown in Appendix B clearly illustrate the affect of applying this cut on both the $\vec{p}_{\mathrm{miss}}E_m$ phase space and implicitly, the count rate.

Figure 4.7 illustrates the overall $\omega\vec{q}$-matched $\vec{p}_{\mathrm{miss}}E_m$ phase space to be investigated in this experiment. Our exact *sampling* of this space will be decided as we go along, and get a feeling for the true rates.

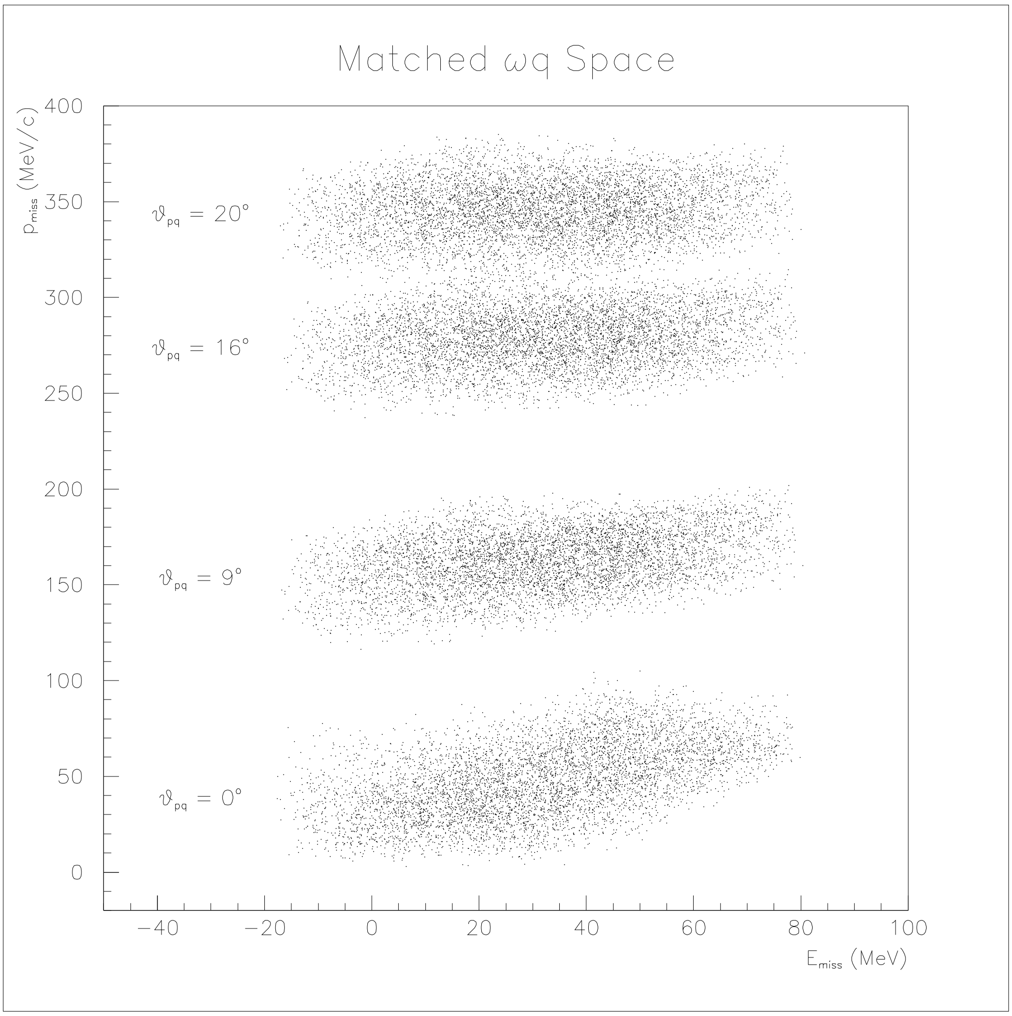

Figure 4.7: $\omega\vec{q}$ matched $\vec{p}_{\mathrm{miss}}$ vs. E_m space.

The following table presents the matched count rate estimates for this experiment. It is anticipated that these rates are good to the 10% level. It will be interesting to see how well they actually do!

E_{beam}	Kin	θ_{pq} (°)	$^1P_{1/2}$	$^1P_{3/2}$	$^1S_{1/2}$
0.845	$\parallel$	0	695	797	3707
	$\Sigma 3$	6	1763	2492	1931
		9	1022	1866	825
		12	378	862	251
		16	54	167	28
		18	16	56	7
		19	8	30	3
		20	4	15	1
1.645	$\Sigma 4$	-12	402	1097	344
		-9	1302	2728	1263
	$\parallel$	0	2176	2684	7848
	$\Sigma 5$	9	2373	4521	1894
		12	896	2113	589
2.445	$\Sigma 2$	-20	3	21	2
		-19	8	43	5
		-18	17	87	11
		-16	66	273	51
		-12	609	1705	515
		-9	1993	4296	1875
		-6	4485	6953	4856
	$\parallel$	0	4821	6147	11390
	$\Sigma 1$	6	6580	9999	6293
		9	3779	7051	2777
		12	1427	3257	869
		16	211	639	100
		18	62	216	24
		19	30	115	10
		20	14	57	4

Table 4.12: Projected hourly $\omega\vec{q}$-matched rates.

4.3.3 Singles and accidentals

Overview

The singles and accidentals calculations for E89-003 were performed by Sarty assuming the same experiment parameters that went into the `MCEEP` work of section 4.3.

The code `QFS` was used to generate (e,e′) singles, while the code `EPS` was used to generate (e,ep), (e,π^+), and (e,π^-) singles. The (e,e′) and (e,ep) results were scanned across 50 bins of the momentum in the HRS^2, and 50 bins of the scattering angle. The accidental (e,e′p) rate for each of those bins was then calculated, along with the apparent missing energy (for ^{16}O) of the bin.

Singles

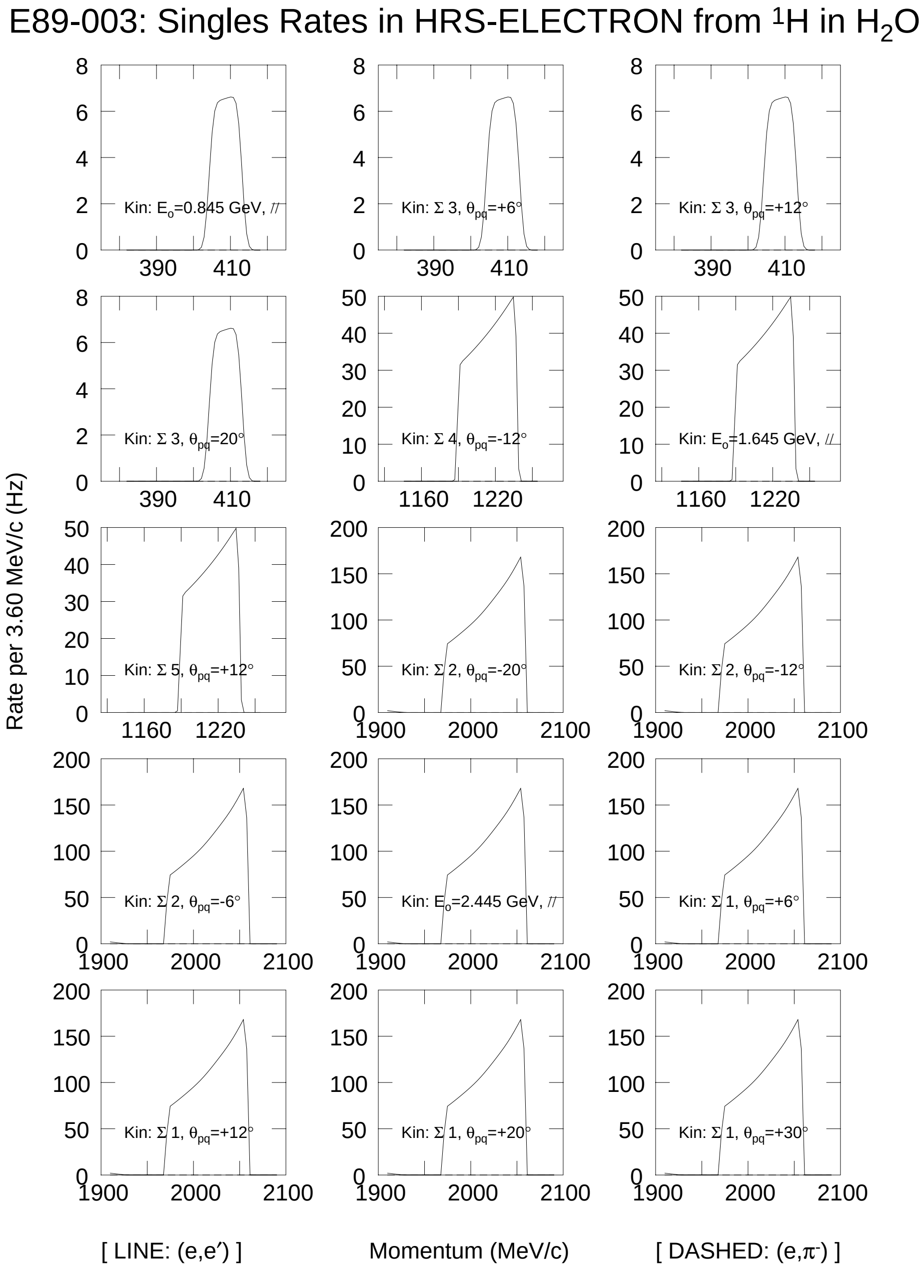

Figure 4.8: HRS_e singles from ^1H.

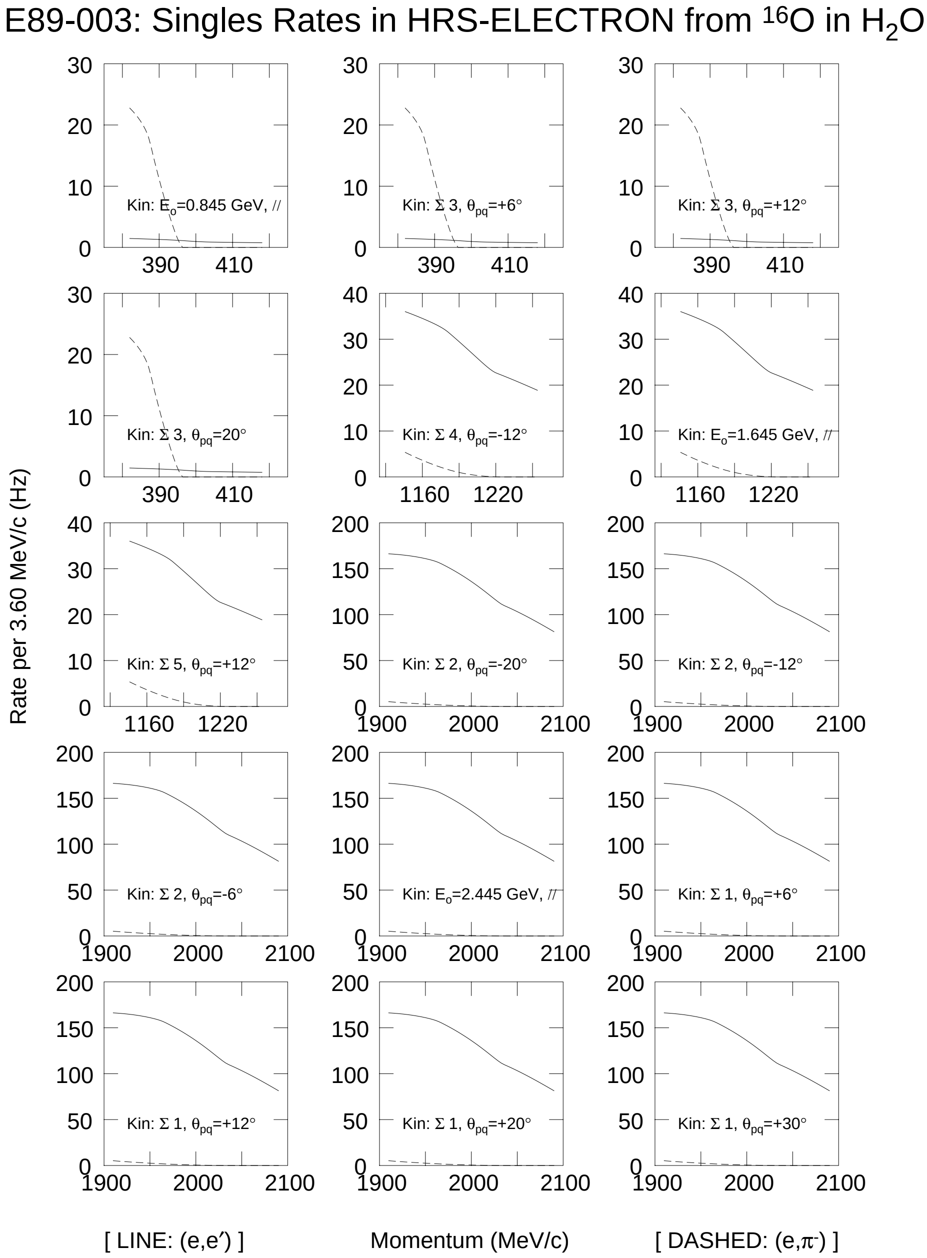

Figure 4.9: HRS_e singles from ^{16}O.

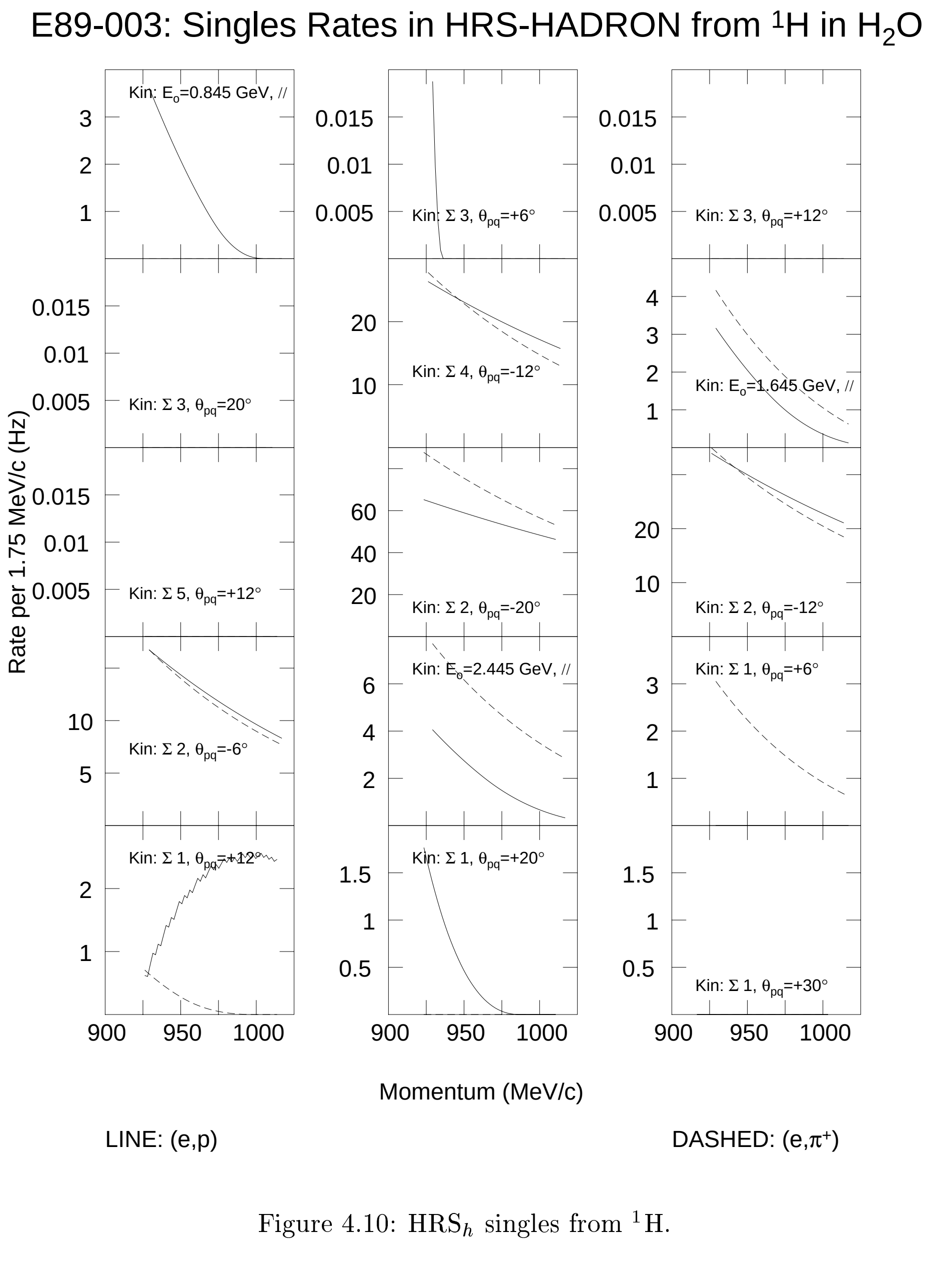

Figure 4.10: HRS_h singles from ^{1}H.

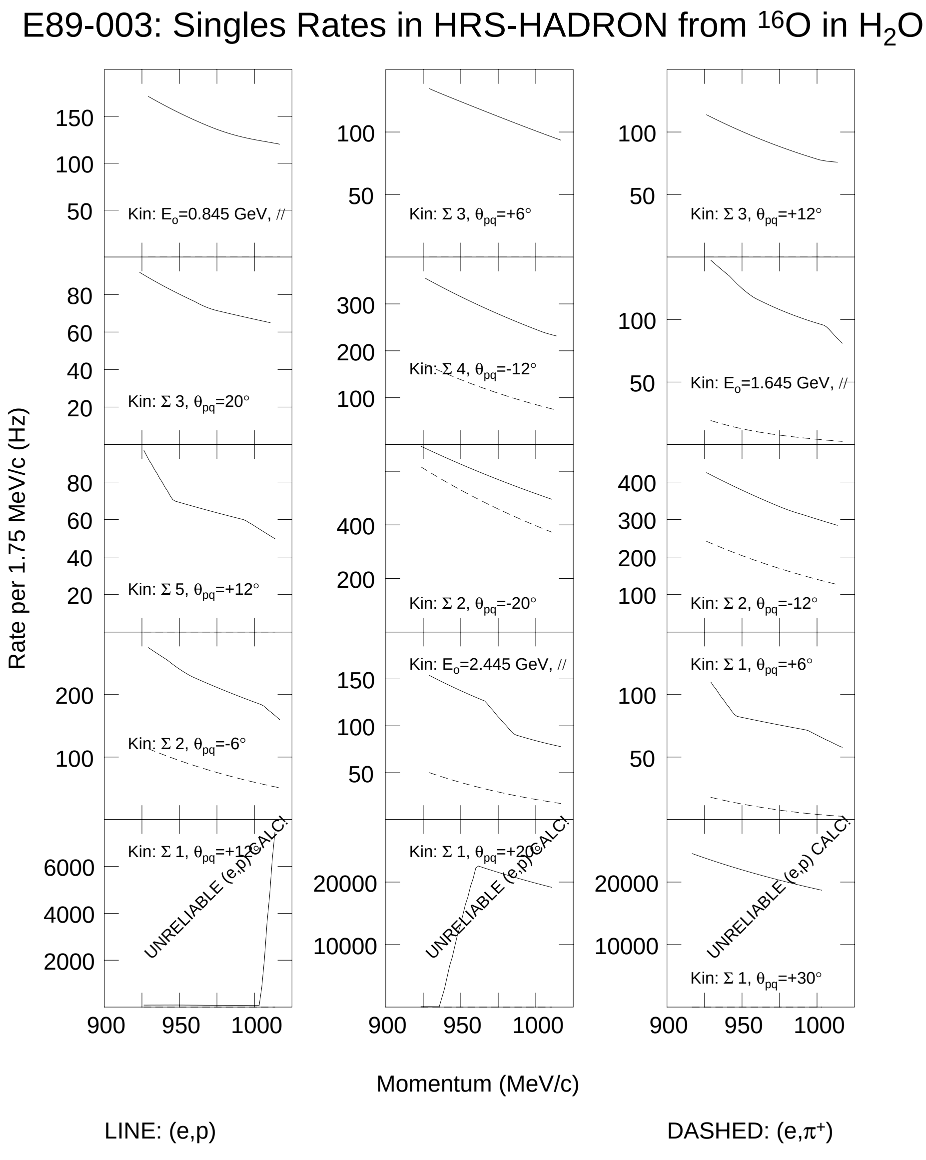

Figure 4.11: HRS_h singles from ^{16}O.

Accidentals

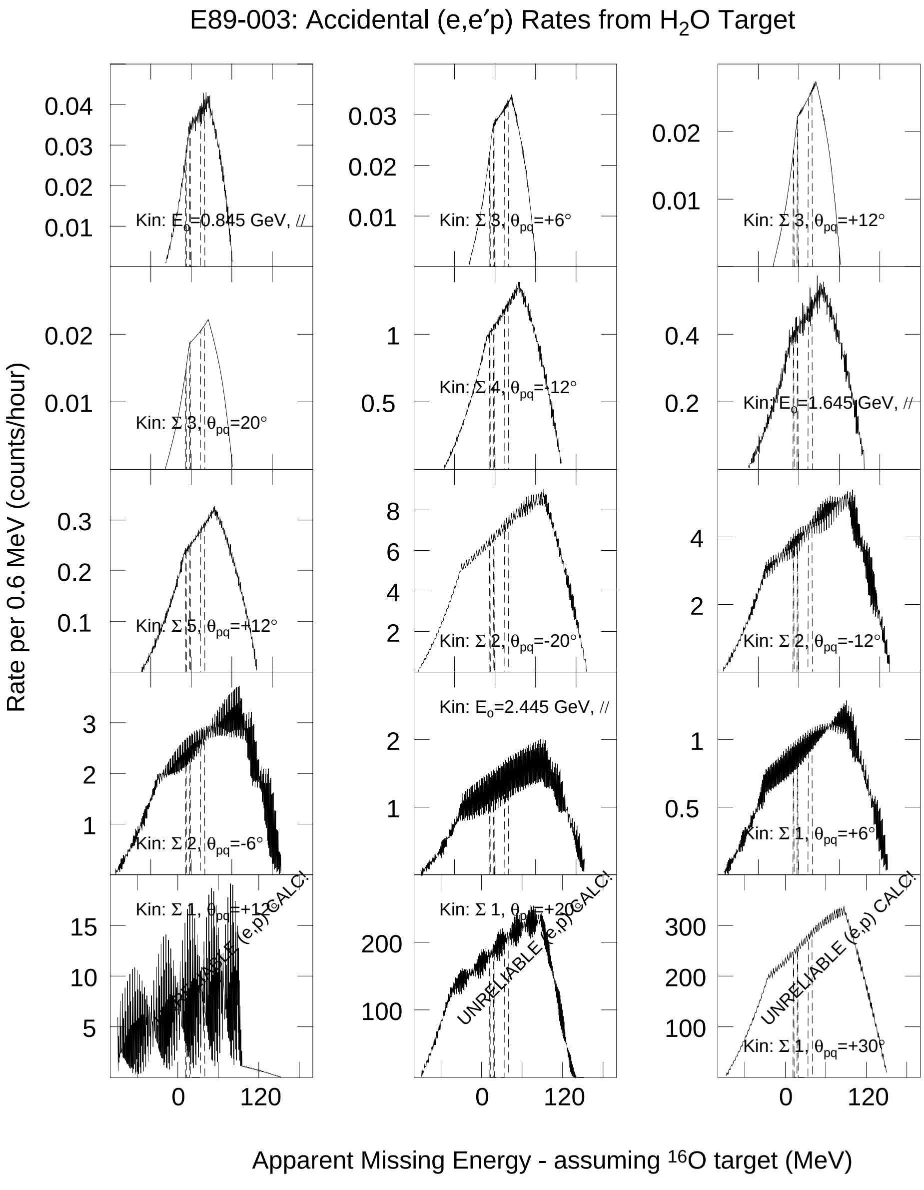

Figure 4.12: Accidental coincidences.

			accidental rates (hr^{-1})			
				$^1P_{\frac{1}{2}}$ region	$^3P_{\frac{1}{2}}$ region	$^1S_{\frac{1}{2}}$ region
		θ_{pq}	Full $\Delta\Omega$	[11.6 - 12.8]	[17.6 - 18.8]	[33.8 - 39.8]
E_{beam}	Kin	(°)	(5 msr)	(MeV)	(MeV)	(MeV)
0.845	$\parallel$	0	4.1	0.06	0.07	0.39
	$\Sigma3$	6	3.3	0.05	0.06	0.32
		12	2.7	0.03	0.04	0.25
		20	2.2	0.03	0.04	0.21
1.645	$\Sigma4$	-12	221.0	2.0	2.1	12.0
	$\parallel$	0	85.9	0.81	0.83	4.8
		12	51.2	0.48	0.50	2.9
2.445	$\Sigma2$	-20	2179.3	12.7	13.6	72.4
		-12	1283.6	7.7	7.9	42.8
		-6	799.1	4.6	5.0	27.0
	$\parallel$	0	416.8	2.5	2.6	14.1
	$\Sigma1$	6	286.1	1.7	1.8	9.8

Table 4.13: A summary of the projected accidental rates.

			HRS_e rate (kHz)				HRS_h rate (kHz)			
			(e,e′)		(e,π^-)		(e,p)		(e,π^+)	
E_{beam}	Kin	θ_{pq} (°)	^{1}H	^{16}O	^{1}H	^{16}O	^{1}H	^{16}O	^{1}H	^{16}O
0.845	$\parallel$	0	0.08	0.05	0.00	0.26	0.06	7.17	0.00	0.00
	$\Sigma3$	6	0.08	0.05	0.00	0.26	0.00	5.79	0.00	0.00
		12	0.08	0.05	0.00	0.26	0.00	4.68	0.00	0.00
		20	0.08	0.05	0.00	0.26	0.00	3.86	0.00	0.00
1.645	$\Sigma4$	-12	1.39	0.90	0.00	0.07	1.06	14.68	1.00	5.99
	$\parallel$	0	1.39	0.90	0.00	0.07	0.07	5.71	0.11	0.45
		12	1.39	0.90	0.00	0.07	0.00	3.40	0.00	0.00
2.445	$\Sigma2$	-20	2.81	6.71	0.00	0.07	2.82	30.08	3.53	24.78
		-12	2.81	6.71	0.00	0.07	1.38	17.71	1.32	9.12
		-6	2.81	6.71	0.00	0.07	0.62	11.03	0.60	4.01
	$\parallel$	0	2.81	6.71	0.00	0.07	0.09	5.75	0.25	1.60
	$\Sigma1$	6	2.81	6.71	0.00	0.07	0.00	3.95	0.08	0.44
		12	2.81	6.71	0.00	0.07	-	-	0.01	0.04
		20	2.81	6.71	0.00	0.07	-	-	0.00	0.00
		30	2.81	6.71	0.00	0.07	-	-	0.00	0.00

Table 4.14: A summary of the projected singles rates in the HRS^2.

E_{beam}	Kin	θ_{pq} (°)	Full $\Delta\Omega$ (5 msr)	signal-to-noise ratio $^1P_{\frac{1}{2}}$ region [11.6 - 12.8] (MeV)	$^3P_{\frac{1}{2}}$ region [17.6 - 18.8] (MeV)	$^1S_{\frac{1}{2}}$ region [33.8 - 39.8] (MeV)
0.845	$\parallel$	0	-	11583	11386	9505
	$\Sigma 3$	6	-	35260	41533	6034
		12	-	12600	21550	1004
		20	-	133	375	4.8
1.645	$\Sigma 4$	-12	-	9375	2153	183
	$\parallel$	0	-	19505	18952	2667
		12	-	17458	27974	1019
2.445	$\Sigma 2$	-20	-	2.1	10.1	0.34
		-12	-	627	1470	124
		-6	-	8077	10372	1732
	$\parallel$	0	-	19267	19314	7067
	$\Sigma 1$	6	-	39359	45222	5212
		12	-	-	-	-
		20	-	-	-	-
		30	-	-	-	-

Table 4.15: A summary of the projected signal-to-noise ratios.

4.4 Runplan

The experiment runplan was developed by a team of people, including Weinstein, Ulmer, Templon, Saha, Liang and Fissum. The work was overseen and coordinated by Weinstein, who also wrote this section.

4.4.1 Measurements

Our intention in E89-003 is to separate $\mathbf{R_l}$, $\mathbf{R_t}$, $\mathbf{R_{lt}}$, and $\mathbf{R_{l+tt}}$ at $|\vec{q}| = 1.0$ GeV/c for four angles, $\theta_{pq} = 0°, 8°, 12°$ and $16°$ using beam energies of 0.845, 1.645 and 2.445 GeV. At 2.445 MeV, we will also separate $\mathbf{R_{lt}}$ at $\theta_{pq} = 20°$ and, time permitting, make an exploratory measurement of the cross section at $\theta_{pq} = 30°$. The measurement of the 0° and 8° points at 1.645 GeV is crucial: it provides a check of our systematic uncertainties which is absolutely necessary for a high precision experiment performed on brand new equipment.

This run plan is based on our count rate estimates (see section 4.3). If the actual count rate is significantly higher than estimated (by a factor of four or more) at the largest angles θ_{pq}, then we will also measure $\mathbf{R_{lt}}$ and $\mathbf{R_{l+tt}}$ at $\theta_{pq} = 20°$. If the count rate is significantly smaller than estimated, then we will skip the $\theta_{pq} = 12°$ measurement. The $\theta_{pq} = 8°$ measurement matches the largest angle to be measured by E89-033. This both saves beam time (in that they will measure the $\theta_{pq} = +8°$ point at $E_{beam} = 2.445$ GeV for us), and provides a useful physics overlap so that, between the two experiments, we measure a large set of response functions at common kinematics.

The plan uses 365 hours of beam time, of which 163 hours is used for ^{16}O(e,e′p) data taking, 48 hours for changing angles 12 times, and 154 hours for normalizations and calibrations. This is approximately 50% of the 29 days of calendar time allocated to the experiment and is consistent with the 1996 Hall C experience with accelerator and experimental equipment reliability.

The 163 hours of ^{16}O(e,e′p) data taking is far less than the 280 hours EXPINT allocated. At the time the proposal was written, no normalizations or calibrations were included in the beam time because the spectrometers were unknown quantities. At least 48 hours is needed at each beam energy for calibrations. *It is likely that some extra commissioning time will be needed later for some further studies.*

The 48 hours allocated for 12 spectrometer angle changes is likely optimistic. Achieving this speed will require practice. Practice while the beam is off will be valuable.

The run plan lists the kinematic conditions and expected times for run periods from May 15 to June 23. The period from June 26 to June 29 will be used as a makeup period in case of accelerator or equipment failure. And finally, in the case of excessive down time, the period from August 8 to August 11 might also be needed.

The beamtimes shown in Table 4.16 have been awarded to us.

Period	Start	Stop	E_{beam} (GeV)
1	May 15	May 23	0.845
2	June 6	June 9	1.645
3	June 12	June 23	2.445
4	June 26	June 29	2.445
5	July 17	August 8	2.445
6	August 8	August 11	2.445

Table 4.16: E89-003/E-89033 beamtime.

Kinematics			Run Type	"Real" Counts (cut)	PWIA Counts (cut)	$^1P_{\frac{1}{2}}$ PW Rate (cut)	Time (hrs)
E_{beam} (GeV)	θ_{pq} (°)	θ_h (°)					
0.845	0	23.12	calibration	NA	NA	NA	48
0.845	0	23.12	sieve slit	NA	NA	NA	12
0.845	0	23.12	production	2500	7500	695	11
0.845	8	31.12	angle change	NA	NA	NA	4
0.845	8	31.12	production	1700	5000	1000	5
0.845	16	39.12	angle change	NA	NA	NA	4
0.845	16	39.12	production	234	700	54	13
0.845	12	35.12	angle change	NA	NA	NA	4
0.845	12	35.12	production	1300	4000	378	11
Total ^{16}O(e,e′p)							40
Total							112

Table 4.17: 0.845 GeV: May 15-23, 1997.

Kinematics			Run Type	"Real" Counts (cut)	PWIA Counts (cut)	$^1P_{\frac{1}{2}}$ PW Rate (cut)	Time (hrs)
E_{beam} (GeV)	θ_{pq} (°)	θ_h (°)					
1.645	0	46.45	calibration	NA	NA	NA	38
1.645	0	46.45	sieve slit	NA	NA	NA	4
1.645	0	46.45	production	2500	7500	2198	4
1.645	-8	38.45	angle change	NA	NA	NA	4
1.645	-8	38.45	production	2500	7500	1300	6
1.645	+8	54.45	angle change	NA	NA	NA	4
1.645	+8	54.45	production	2500	7500	2400	4
Total ^{16}O(e,e′p)							14
Total							64

Table 4.18: 1.645 GeV: June 6-9, 1997.

Kinematics			Run	"Real"	PWIA	$^{1}P_{\frac{1}{2}}$	Time
E_{beam} (GeV)	θ_{pq} (°)	θ_h (°)	Type	Counts (cut)	Counts (cut)	PW Rate (cut)	(hrs)
2.445	0	52.47	calibration	NA	NA	NA	48
2.445	0	52.47	sieve slit	NA	NA	NA	4
2.445	0	52.47	production	2500	7500	4680	2
2.445	-16	36.47	angle change	NA	NA	NA	4
2.445	-16	36.47	production	290	860	66	13
2.445	-12	40.47	angle change	NA	NA	NA	4
2.445	-12	40.47	production	2500	7500	609	13
2.445	-8	44.47	angle change	NA	NA	NA	4
2.445	-8	44.47	production	2500	7500	2800	2
2.445	16	68.47	angle change	NA	NA	NA	4
2.445	16	68.47	production	1700	5000	211	24
2.445	12	64.47	angle change	NA	NA	NA	4
2.445	12	64.47	production	2500	7500	1400	5
2.445	-20	32.47	angle change	NA	NA	NA	4
2.445	-20	32.47	production	20	60	3	20
2.445	+20	72.47	angle change	NA	NA	NA	4
2.445	+20	72.47	production	140	420	14	30
measured only if time remains							
2.445	+30	82.47	angle change	NA	NA	NA	4
2.445	+30	82.47	production	<1	<1	<1	?
Total ^{16}O(e,e′p)							109
Total							189

Table 4.19: 2.445 GeV: June 12-23, 1997.

4.4.2 Normalizations

The following is the plan for the calibration measurements for the ^{16}O(e,e′p) experiment, E89-003. We intend to perform these checks at each of the three beam energies. We want to measure both relative and absolute efficiencies, which will be a combination of detector efficiency and the (four-dimensional) spectrometer acceptance. We will then, time permitting, check spectrometer field reproducibility.

We plan to measure the relative efficiency as a function of δ for each of the HRS[2] by measuring a flat spectrum at five closely-spaced momentum settings in a procedure commonly-refered to as *white spectra measurement*. We plan to take about 250,000 counts at each momentum setting. The count rates are adequate to do this in one hour of data taking at each point. We need to do this at each energy and angle for HRS_e and at a variety of angles for HRS_h (since the efficiency will vary with target position).

The motivation for measuring "white spectra" efficiencies is as follows:

- the spectrometer acceptance depends on four variables δ, θ_t, ϕ_t, and y_t (where the subscript "t" refers to that variable at the target)
- the term "efficiency" includes both spectrometer acceptance and detector efficiencies (which may or may not be flat over the focal plane)
- elastic scattering does not measure an unbiased efficiency for two reasons:
  1. δ and the scattering angle ϕ_t are highly correlated (at least for hydrogen)
  2. the cross-section is strongly forward peaked (that is, it disproportionately samples the forward angle part of the collimator)

The event distribution (as a function of δ) measured at the focal plane is a convolution of the physical cross section and the spectrometer efficiency. We want to take enough measurements to deconvolute the two so we can use the measured spectrometer efficiency to understand the "real" measurement. The procedure for doing this is as follows:

- tune the spectrometer to a magnetic field where the cross-section is relatively featureless (flat or smoothly sloped) and the count rate is high enough. For our purposes, we defined "flat" to be reasonably-approximated by the QE peak. Use the normal Quad/Dipole tune.
- acquire about 250,000 events
- repeat the above six more times, lowering the magnetic field by 1.5% each time. This scans the spectrum across the focal plane.

The conceptual procedure for analyzing the "white spectra" efficiencies is as follows:

- the same cross section ($\sigma(P)$) has now been measured at several points along the focal plane. The **relative** efficiency of each of those points is just their relative number of counts (divided by the indiviual run normalizations [which includes integrated luminosity and dead time] and bin size).
- further, several different cross sections have been measured at the same point in the focal plane. The relative cross-section for each of those momenta is just their relative number of counts (divided by the indiviual run normalizations [the bin size is now the same]).

At each of several spectrometer central momentum settings $P_\circ^m$, data have been acquired consisting of events distributed across the focal plane. Each run, m, will have a normalization factor f_m which includes the integrated luminosity of the run, the solid angle of the spectrometer, and the dead time of the run.

The following guidelines/observations for the analysis are to be kept in mind:

- split the focal plane up into momentum bins. For each run m, bin i will have a certain number of counts N_i^m.
- the momentum of bin i in run m is $P(m,i) = P_\circ(m)\delta(i)$.
- each momentum bin has efficiency ϵ_i (unknown).
- the cross-section is $\sigma(P)$. The cross-section for bin i in run m is $\sigma(P(m,i))$.

The cross section may be parametrized using Legendre polynomials (or other orthogonal functions) as

$$\sigma(P) = \sum_{j=1}^{j_{max}} a_j F_j(P)$$

where j_{max} is the number of functions used, a_j is the coefficient of the j^{th} function, and F_j is the j^{th} order function. The a_j are also unknown. The reason for measuring the cross section where it is flat is to *minimize the order of the required cross section polynomial.*

The next step is to fit the ϵ_i and the a_j to the data. The χ^2 of our fit will be:

$$\chi^2 = \sum_m \sum_i \left[\frac{N_i^m - f_m \epsilon_i \sigma(P(m,i))}{N_i^m} \right]^2$$

where the N_i^m in the denominator is the statistical variance in the number of counts for Poisson statistics. Standard iterative fitting techniques may then be applied to minimize χ^2.

One final detail: The overall normalization of the cross section and the efficiency are not fixed. There are two reasonable criteria for normalizing the efficiencies:

- set the maximum efficiency to 1.00. If you do this you have to be careful in propagating statistical errors during analysis of coincidence data because the number of "efficiency corrected" counts will be different from the number of counts so Poisson statistics will no longer be valid.
- set the average efficiency to be 1.00. This way the number of "efficiency corrected" counts will be the same as the number of counts so Poisson statistics will be approximately valid.

The result will be twofold: both a fit to the cross section, and the relative efficiency of each momentum bin of the focal plane.

E_{beam} (GeV)	particle	p_f (GeV/c)	angle (°)	σ $(\frac{\text{nb}}{\text{sr}\cdot\text{MeV/c}})$	Rate (Hz)	Rate (hr^{-1})
0.845	p	1.0	23.1	2.5	4300	3.6×10^6
2.445	p	1.0	52.5	1.6	2700	3.6×10^6
0.845	e	0.345	100.7	0.10	60	2.2×10^6
0.845	e	0.295	100.7	0.16	80	2.9×10^6
2.445	e	1.9	23.4	1.6	500	1.8×10^6
2.445	e	1.8	23.4	1.5	500	1.8×10^6

Table 4.20: Rates for the white spectra measurements.

HRS_e			HRS_h			time
δ (%)	collimator	activity	δ (%)	collimator	activity	(hrs)
relative efficiencies - FLAT spectra in both spectrometers						14
+4.5	5.0	production		5.0	change B	1
	5.0	change B	+4.5	5.0	production	1
+3.0	5.0	production		5.0	change B	1
	5.0	change B	+3.0	5.0	production	1
+1.5	5.0	production		5.0	change B	1
	5.0	change B	+1.5	5.0	production	1
+0.0	5.0	production		5.0	change B	1
	5.0	change B	+0.0	5.0	production	1
-1.5	5.0	production		5.0	change B	1
	5.0	change B	-1.5	5.0	production	1
-3.0	5.0	production		5.0	change B	1
	5.0	change B	-3.0	5.0	production	1
-4.5	5.0	production		5.0	change B	1
	5.0	change B	-4.5	5.0	production	1

Table 4.21: Relative efficiency white spectra measurements.

We then plan to measure H(e,e′p), H(e,e′), and H(e,p) as a function of peak position in the electron spectrometer for both electron spectrometer collimators. We will then repeat this measurement as a function of peak position in the hadron arm for both hadron spectrometer collimators. Measurement of the H(e,e′) and H(e,p) single-arm cross sections with the small collimators will tell us the non-solid-angle contributions to the spectrometer efficiency (such as detector inefficiencies), and will allow us to absolutely normalize the spectrometers for that aperture. Measurement of the H(e,e′) and H(e,p) single-arm cross sections with the full size (5 msr) collimators will tell us the solid angle contributions to the efficiency and will allow us to absolutely normalize the spectrometers for the experimental aperture. We will then use the H(e,e′p) data to tell us the combined two-spectrometer efficiency. Using the different collimator combinations will allow us to understand the spectrometer acceptances and efficiencies. Note that the H(e,e′p) calibration data will have to be used with caution due to the high degree of kinematic correlation in the data. Also note that the magnetic fields will be different for the relative efficiency measurements (which require flat spectra) and the H(e,e′p) measurements (which require peaks).

HRS_e			HRS_h			time
δ (%)	collimator	activity	δ (%)	collimator	activity	(hrs)
$^1H(e,e'p)$: vary δ_e - ^1H peak centered in HRS_h						21
+4.5		change B	+0.0	5.0		1
+4.5	5.0	production	+0.0	5.0	production	1
+4.5	0.6	production	+0.0	5.0	production	1
+3.0		change B	+0.0	5.0		1
+3.0	5.0	production	+0.0	5.0	production	1
+3.0	0.6	production	+0.0	5.0	production	1
+1.5		change B	+0.0	5.0		1
+1.5	5.0	production	+0.0	5.0	production	1
+1.5	0.6	production	+0.0	5.0	production	1
+0.0		change B	+0.0	5.0		1
+0.0	5.0	production	+0.0	5.0	production	1
+0.0	0.6	production	+0.0	5.0	production	1
-1.5		change B	+0.0	5.0		1
-1.5	5.0	production	+0.0	5.0	production	1
-1.5	0.6	production	+0.0	5.0	production	1
-3.0		change B	+0.0	5.0		1
-3.0	5.0	production	+0.0	5.0	production	1
-3.0	0.6	production	+0.0	5.0	production	1
-4.5		change B	+0.0	5.0		1
-4.5	5.0	production	+0.0	5.0	production	1
-4.5	0.6	production	+0.0	5.0	production	1

Table 4.22: HRS_e $^1H(e,e'p)$ studies.

HRS$_e$			HRS$_h$			time
δ (%)	collimator	activity	δ (%)	collimator	activity	(hrs)
$^1H(e,e'p)$: vary δ_h - ^1H peak centered in HRS_e						21
+0.0	5.0		+4.5	5.0	change B	1
+0.0	5.0	production	+4.5	5.0	production	1
+0.0	5.0	production	+4.5	0.6	production	1
+0.0	5.0		+3.0	5.0	change B	1
+0.0	5.0	production	+3.0	5.0	production	1
+0.0	5.0	production	+3.0	0.6	production	1
+0.0	5.0		+1.5	5.0	change B	1
+0.0	5.0	production	+1.5	5.0	production	1
+0.0	5.0	production	+1.5	0.6	production	1
+0.0	5.0		+0.0	5.0	change B	1
+0.0	5.0	production	+0.0	5.0	production	1
+0.0	5.0	production	+0.0	0.6	production	1
+0.0	5.0		-1.5	5.0	change B	1
+0.0	5.0	production	-1.5	5.0	production	1
+0.0	5.0	production	-1.5	0.6	production	1
+0.0	5.0		-3.0	5.0	change B	1
+0.0	5.0	production	-3.0	5.0	production	1
+0.0	5.0	production	-3.0	0.6	production	1
+0.0	5.0		-4.5	5.0	change B	1
+0.0	5.0	production	-4.5	5.0	production	1
+0.0	5.0	production	-4.5	0.6	production	1

Table 4.23: HRS$_h$ ^{1}H(e,e$'$p) studies.

HRS$_e$			HRS$_h$			time
δ (%)	collimator	activity	δ (%)	collimator	activity	(hrs)
$^1H(e,e'p)$: vary δ_h - ^1H peak centered in HRS_e						10
+0.0	5.0			5.0	change B	1
+0.0	5.0		B = 0	5.0	production	1
+0.0	5.0			5.0	change B	2
+0.0	5.0		0.0	5.0	production	1
	5.0	change B	0.0	5.0		1
B = 0	5.0	production	0.0	5.0		1
	5.0	change B	0.0	5.0		2
0.0	5.0	production	0.0	5.0		1

Table 4.24: Magnet reproducibility studies: ^{1}H(e,e$'$p).

4.5 Errors, resolutions and uncertainties

4.5.1 On errors

This section was written by Ulmer and describes the effect of kinematical uncertainties on the determination of the coincidence cross section. How the resulting cross section uncertainties propagate to uncertainties in the various response functions is described elsewhere.

This experiment, being the first Hall A experiment and a separation measurement requiring strict control over systematics, relies heavily on a calibration technique involving ^{1}H(e,e$'$p) elastic scattering in conjunction with a pinhole collimator on the electron arm (actually a sieve slit will be used, so throughout this section the term "pinhole" refers to any of the holes in the sieve). Scattering from hydrogen in the waterfall target serves two purposes. For those kinematics which include elastic scattering from hydrogen, this process serves as an absolute cross section normalization for the ^{16}O(e,e$'$p) measurement. In addition, hydrogen elastic scattering through a pinhole in the electron arm gives a well defined ray bundle in the proton arm for coincidence events. This ray bundle determines $\vec{q}$ for a fiducial point for the electron arm (that point which corresponds to hydrogen elastic scattering at the precise angle defined by the pinhole). It is this aspect of the calibration which is discussed below in connection with the kinematical uncertainties.

The canonical tolerances on kinematical quantities for Hall A separation experiments are 0.1 mr for angles and 10^{-4} for momenta. As will be shown below, these are still the required tolerances (except for the beam energy). However, use of the pinhole technique implies these tolerances are relative to fiducial rays in each spectrometer. Thus, only differences in angles and momenta relative to these fiducuial rays need to be known with this accuracy. This is what makes this experiment feasible so early in the Hall A program.

The error estimates made here assume that the dominant kinematical errors arise from the rapid variation of the momentum distribution, $|\phi(p_r)|^2$. With this assumption, only the determination of the recoil momentum is important. For $|\phi(p_r)|^2$, a $1p$ harmonic oscillator is assumed:

$$F = |\phi(p_r)|^2 = \frac{2b^3}{3\pi^{3/2}} p_r b \exp(-(p_r b)^2) \tag{4.1}$$

where p_r is the recoil momentum and the oscillator constant b is taken to be 1.67 fm. The relative error in F due to an error in p_r of δp_r is:

$$\frac{\delta F}{F} = \frac{1}{F}\frac{dF}{dp_r}\delta p_r = \left(\frac{\delta p_r}{p_r}\right)\left[1 - 2(bp_r)^2\right]. \tag{4.2}$$

In the factorized PWIA model, the coincidence cross section is proportional to F, so that this is the dominant error. The relative error in the cross section is the same as the relative error in F. The next step is to determine the uncertainty in p_r.

The error in p_r has two sources: uncertainty in q $(= |\vec{q}\,|)$ and uncertainty in θ_{pq}. This can be seen since $\vec{p_r} = \vec{q} - \vec{p}$ (where $\vec{p}$ is the proton momentum), so that

$$p_r^2 = q^2 + p^2 - 2pq\cos\theta_{pq}. \tag{4.3}$$

To find the uncertainty in p_r, we need to take derivatives of the above expression with respect to q and θ_{pq}. Since the proton momentum is measured directly, the derivatives are taken at **fixed** p. For discrete states, the errors may be reduced somewhat by requiring a fixed missing mass. We get:

$$\frac{\delta p_r}{p_r} = \frac{\delta q}{q}\Big(1 + \frac{\vec{p_r}\cdot\vec{p}}{p_r^2}\Big) \qquad \text{(from } \delta\text{q)} \tag{4.4}$$

$$\frac{\delta p_r}{p_r} = \delta\theta_{pq}\Big(\frac{pq}{p_r^2}\sin\theta_{pq}\Big) \qquad \text{(from } \delta\theta_{\mathrm{pq}}\text{)}. \tag{4.5}$$

For "perpendicular" kinematics (defined by $\vec{p_r}\cdot\vec{p} = 0$) these reduce to:

$$\delta p_r = \delta q\big(\frac{p_r}{q}\big) \tag{4.6}$$

$$\delta p_r = q\,\delta\theta_{pq}\cos\theta_{pq} = p\,\delta\theta_{pq}. \tag{4.7}$$

Note that for perpendicular kinematics, an uncertainty in q results in a reduced uncertainty in p_r by the factor p_r/q. The worst case is for parallel kinematics where $\delta p_r = \delta q$.

Now that we have the error in p_r from errors in q and θ_{pq}, we need to determine the uncertainties in q and θ_{pq}. To simplify things, we assume in-plane kinematics and only examine dependences on the momenta and in-plane angles. Then we need to find the uncertainty in q and θ_{pq} with respect to four kinematic variables: e (beam energy), e' (scattered electron energy), θ_e (scattering angle) and θ_p (emission angle of the proton relative to the beam direction). The uncertainty with respect to the proton momentum is ignored here. In any case, for discrete states in (e,e′p) (for fixed missing mass), the proton momentum is determined from the above four quantitites (and the missing mass).

First consider the beam energy. The error in the angle of $\vec{q}$ due to an error in e is assumed to be zero, since the direction of $\vec{q}$ is determined directly via the pinhole and ^{1}H(e,e′p) elastic scattering (the direction of the coincident protons gives the direction of $\vec{q}$). The same is true for the magnitude of $\vec{q}$ since this is determined directly by the proton momentum measurement. So, assuming that only the determination of the recoil momentum matters, we needn't worry about the beam energy provided we determine $\vec{q}$ in this way. Note that even though our absolute determination of $\vec{q}$ may be imprecise (without a good absolute spectrometer momentum calibration for example), we can still relate $\vec{q}$ for the various separation measurements by requiring that we image the proton ray bundle for pinhole scattering to the same place on the focal plane for each kinematics. Any deviations will have to be corrected for though. The problem then reduces to relating various rays within the full acceptances of the spectrometer to fiducial rays for ^{1}H(e,e′p) elastic scattering through the pinhole.

For the other three variables (e', θ_e and θ_p) we need to relate these quantities to those for our fiducial rays. First, it is necessary to determine Δq and $\Delta\theta_{pq}$ from the deviations ($\Delta\theta_e$, $\Delta e'$ and $\Delta\theta_p$) from the fiducial rays. Note that we use a capital delta to denote a deviation from the fiducial ray and a small delta to denote an uncertainty in a kinematical quantity. Then we can compute the errors in q and θ_{pq} due to errors in the measurement of these deviations (again, this implies that only measurement of particular rays **relative** to fiducial rays matters). To determine uncertainties in q and θ_{pq}, various partial derivatives are needed:

$$\frac{\partial\theta_q}{\partial e'} = \frac{1}{q}\sin(\theta_e + \theta_q) \tag{4.8}$$

$$\frac{\partial\theta_q}{\partial\theta_e} = \frac{e'}{q}\cos(\theta_e + \theta_q) \tag{4.9}$$

$$\frac{\partial q}{\partial e'} = -\cos(\theta_e + \theta_q) \tag{4.10}$$

$$\frac{\partial q}{\partial\theta_e} = e'\sin(\theta_e + \theta_q) \tag{4.11}$$

For the ^{1}H(e,e'p) kinematics these derivatives are:

Kinematics	$\partial\theta_q/\partial e'$ (rad/GeV)	$\partial\theta_q/\partial\theta_e$	$\partial q/\partial e'$	$\partial q/\partial\theta_e$ (GeV/rad)
Forward	0.98	0.47	−0.23	1.96
Intermediate	1.00	0.12	−0.098	1.21
Backward	0.82	−0.23	0.56	0.34

Table 4.25: General derivatives for ^{1}H(e,e'p).

If we take uncertainties of:

$$\delta(\Delta\theta_e) = 1 \text{ mr} \tag{4.12}$$

$$\frac{\delta(\Delta e')}{e'} = 10^{-3}, \tag{4.13}$$

we get:

Kinematics	$\|\delta(\Delta\theta_q)\|$ from e' (mr)	$\|\delta(\Delta\theta_q)\|$ from θ_e (mr)	$\|\delta(\Delta q)\|$ from e' (MeV)	$\|\delta(\Delta q)\|$ from θ_e (MeV)
Forward	1.97	0.47	0.46	1.96
Intermediate	1.21	0.12	0.12	1.21
Backward	0.34	0.23	0.23	0.34

Table 4.26: Specific derivatives for ^{1}H(e,e'p).

Note that the near equality of various columns results from the value of q for our case: 1 GeV/c. Within the assumptions of this analysis, an error in θ_p is equivalent to an error in θ_q. Therefore, for $\delta(\Delta\theta_p) = 1$ mr, we have $\delta(\Delta\theta_q) = 1$ mr. Adding all the errors in quadrature for the forward kinematics (worst case) gives:

$$\delta(\Delta\theta_q) = 2.3 \text{ mr} \tag{4.14}$$

$$\delta(\Delta q) = 2.1 \text{ MeV}. \tag{4.15}$$

We had: $\delta p_r \approx \delta q$ (pessimistically) due to an error in q, and $\delta p_r \approx q\,\delta\theta_{pq}$ due to an error in θ_{pq}. For $q = 1$ GeV and for $\delta(\Delta\theta_{pq}) = 2.3$ mr and $\delta(\Delta q) = 2.1$ MeV, we have $\delta p_r \sim 3$ MeV/c, where the two errors have been added in quadrature.

Now, using the $1p$ harmonic oscillator momentum distribution we get:

p_r (MeV/c)	$\delta F/F$
100	1.3
200	7.1
300	12.0

Table 4.27: Estimated errors.

Clearly, errors this large cannot be tolerated. Thus, we need to do better than 1 mr on the angles and 10^{-3} on momenta. Provided we can measure angles at the 0.1 mr level and momenta at the 10^{-4} level, we can keep the errors at or below the 1% level for p_r up to 300 MeV/c. But again, note that these errors reflect uncertainties in quantities relative to *fiducial* rays within the acceptance of each spectrometer.

4.5.2 Missing energy resolution

The anticipated missing energy resolution is presented in Table 4.28.

Quantity	Parameters	Spread
scattered electron	2.0 GeV $\times$ 2 $\times$ 10^{-4}	0.4 MeV
electron dE/dx in target	-	0.2 MeV
scattered proton	2.0 GeV $\times$ 2 $\times$ 10^{-4}	0.2 MeV
proton dE/dx in target	-	0.4 MeV

Table 4.28: Anticipated missing energy resolution.

The quadratic sum of these values is 0.63 MeV.

4.5.3 Estimated Uncertainties

Overview

Table 4.29 presents a summary of the anticipated systematic uncertainties in the cross section measurements.

Contributor	Value	Magnitude	$\delta\sigma$
spectrometer	magnitude of $\lvert\vec{q}\rvert$	$\pm 5 \times 10^{-4}$	$\pm 0.3\%$
	knowledge of θ_{pq}	± 0.2 mr	$\pm 0.9\%$
	acceptance: relative variation (normalized to H)	-	$\pm 0.9\%$
measurement of σ(p(e,ep))	variation in θ_e	± 0.2 mr	$\pm 0.4\%$
	p_e momentum resolution	$\pm 5 \times 10^{-4}$	$\pm 0.4\%$
knowledge of σ(p(e,ep))	-	-	$\pm 0.4\%$

Table 4.29: A summary of anticipated uncertainties.

θ_{pq} and $\lvert\vec{q}\rvert$

For the purpose of determining the effect of our knowledge of θ_{pq} on the extracted cross section, we assume knowledge of this angle to the standard survey level ± 0.2 mr ($\pm 0.011°$). The cross section is most sensitive to this variable at $E_{beam} = 0.845$ GeV, $\theta_{pq} = 20°$. The rate for $^1P_{1/2}$ protons for this "pristine" angular setting was then calculated and compared to the rate obtained if the HRS_h spectrometer is changed by ± 0.2 mr ($\pm 0.011°$). Because θ_q is fixed and the cross section depends most strongly on the missing momentum (which is a function of θ_{pq}), this approach yields the desired estimate.

For the purpose of determining the effect of our knowledge of $\vec{q}$ on the extracted cross section, we assume knowledge of the relative error in this quantity to a level of $\pm 5 \times 10^{-4}$. As the cross section is again most sensitive to this variable at $E_{beam} = 0.845$ GeV and $\theta_{pq} = 20°$, we select this setting for our investigation. We then fix E_{beam}, θ_e, the proton momentum, and θ_{pq}, and calculate the rate for $^1P_{1/2}$ protons. We then increment $\lvert\vec{q}\rvert$ by 0.0005 GeV (by shifting the electron momentum and θ_h), and recalculate the rate.

Both calculations were performed according to the previously-mentioned prescriptions of Van Orden using MCEEP. The results are presented in Table 4.30. Note that the effect of variations in these parameters is on the 1% level.

Kin	θ_h (°)	$\|\vec{q}\|$ (MeV/c)	Central $\vec{p}_{miss}$ (MeV/c)	Rate (/hr)	Δ Rate (%)
pristine	37.75	1004.11	350.868	5.67366	-
θ_{pq} + dθ_{pq}	37.761	-	351.059	5.62165	-0.92
θ_{pq} - dθ_{pq}	37.739	-	350.677	5.71261	+0.69
$\|\vec{q}\|$+d$\|\vec{q}\|$	-	1004.61	350.883	5.69126	+0.31
$\|\vec{q}\|-$d$\|\vec{q}\|$	-	1003.61	350.749	5.66305	-0.19

Table 4.30: Rate effects due to uncertainties in θ_{pq} and $|\vec{q}|$.

The uncertainties assumed to contribute to the Hydrogen elastic cross section are $\theta_e = \pm 0.2$ mr and $\Delta p_e/p_e = \pm 5 \times 10^{-4}$. Table 4.31 summarizes the results.

E_{beam} (GeV)	Kin	p_e (MeV/c)	θ_e (°)	σ (nb/sr)	$\Delta\sigma$ (%)
2.4	pristine	1968.298	23.900	33.129	-
	θ_e^+	1968.298	23.957	32.527	-0.4%
	θ_e^-	1968.298	23.843	33.743	+0.4%
	p_e^+	1969.282	23.900	33.0067	-0.4%
	p_e^-	1967.314	23.900	33.2521	+0.4%
1.6	pristine	1165.546	38.610	10.550	-
	θ_e^+	1165.546	38.667	10.439	-1.1%
	θ_e^-	1165.546	38.553	10.661	+1.1%
	p_e^+	1166.129	38.610	10.507	-0.4%
	p_e^-	1164.963	38.610	10.592	+0.4%
0.8	pristine	357.073	117.055	0.814	-
	θ_e^+	357.073	117.112	0.812	-0.2%
	θ_e^-	357.073	116.998	0.815	+0.2%
	p_e^+	357.248	117.055	0.809	-0.6%
	p_e^-	356.894	117.055	0.818	+0.6%

Table 4.31: Anticipated uncertainty in the hydrogen elastic cross section.

Separations

These calculations were performed by Zhao. They following assumptions were made:

At $\theta_{pq} = 0^o, \pm 6^o$,

$(\delta\sigma/\sigma)_{stat.} = 1.0\%$, $(\delta\sigma/\sigma)_{syst.} = 3.0\%$, $(\delta\sigma/\sigma)_{tot.} = 3.2\%$

At $\theta_{pq} = \pm 12^o$,

$(\delta\sigma/\sigma)_{stat.} = 1.5\%$, $(\delta\sigma/\sigma)_{syst.} = 3.0\%$, $(\delta\sigma/\sigma)_{tot.} = 3.4\%$

At $\theta_{pq} = \pm 20^o$,

Forward:

$(\delta\sigma/\sigma)_{stat.} = 2.5\%$, $(\delta\sigma/\sigma)_{syst.} = 3.0\%$, $(\delta\sigma/\sigma)_{tot.} = 3.9\%$

Backward:

$(\delta\sigma/\sigma)_{stat.} = 3.5\%$, $(\delta\sigma/\sigma)_{syst.} = 3.0\%$, $(\delta\sigma/\sigma)_{tot.} = 4.6\%$

The uncertainty estimates are presented in Tables 4.33 and 4.32.

θ_{pq}	$(\delta\sigma/\sigma)$	$\frac{(R_L+cR_{TT})}{R_T}$	R_{LT}/R_T	$\frac{\delta(R_L+c\cdot R_{TT})}{(R_L+c\cdot R_{TT})}$	$\delta R_T/R_T$	$\delta R_{LT}/R_{LT}$
$\pm 6^o$	3.2%	1.0	1.0	5.2 %	3.5 %	4.6 %
		0.5	0.5	7.0 %	3.7 %	7.5 %
		0.3	0.3	9.5 %	3.7 %	12 %
		0.1	0.1	22 %	3.8 %	33 %
$\pm 12^o$	3.4%	1.0	1.0	5.6 %	3.8 %	4.8 %
		0.5	0.5	7.5 %	3.9 %	8.0 %
		0.3	0.3	10 %	4.0 %	12 %
		0.1	0.1	24 %	4.0 %	35 %
$\pm 20^o$	3.9%	1.0	1.0	6.4 %	5.0 %	5.8 %
	4.6%	0.5	0.5	8.6 %	5.2 %	9.9 %
		0.3	0.3	12 %	5.3 %	16 %
		0.1	0.1	27 %	5.4 %	45 %

Table 4.32: Uncertainty estimates for perpendicular kinematics.

θ_{pq}	$(\delta\sigma/\sigma)$	R_L/R_T	$\delta R_T/R_T$	$\delta R_L/R_L$
0^o	3.2%	1.0	4.7%	7.1%
		0.5	4.2%	11%
		0.3	4.0%	16%
		0.1	3.9%	40%

Table 4.33: Uncertainty estimates for parallel kinematics.

Appendix A

MCEEP variable summaries

A.1 p(e,e′p)

Variable	Central	Average	Centroid	Minimum	Maximum
θ_e (°)	100.760	100.760	100.738	99.331	102.182
ω (MeV)	445.000	436.520	436.455	432.120	440.816
$\lvert\vec{q}\rvert$ (MeV/c)	1000.116	1004.839	1004.750	998.812	1010.710
Q^2 ((GeV/c)^2)	.802	.819	.819	.811	.827
θ_q (°)	-23.136	-23.528	-23.536	-24.073	-23.010
ϕ_q (°)	.000	.010	.010	-1.395	1.396
X	.961	1.000	1.000	1.000	1.000
ϵ	.216	.218	.218	.209	.227
$\lvert\vec{p}\,'\rvert$ (MeV/c)	973.000	1004.839	1004.750	998.812	1010.7 10
$\lvert\vec{p}_R\rvert$ (MeV/c)	27.117	0.000	0.000	.000	0.000
θ_{pq} (°)	.016	0.000	0.000	-.000	0.000
ϕ_x (°)	.000	173.772	173.696	.000	360.000
E_{miss} (MeV)	16.181	0.000	0.000	0.000	0.000
W (GeV)	.956	.938	.938	.938	.938
θ_{CM} (°)	177.426	48.781	48.754	-.000	180.000

Table A.1: $E_e = 0.845$ GeV: p(e,e′p), full $\Delta\Omega$.

Variable	Central	Average	Centroid	Minimum	Maximum
θ_e ($^\circ$)	37.170	37.288	37.256	36.366	37.972
ω (MeV)	445.000	433.969	433.440	418.710	445.261
$\lvert\vec{q}\rvert$ (MeV/c)	1000.038	1001.326	1000.601	980.332	1016.768
Q^2 ((GeV/c)^2)	.802	.814	.813	.786	.836
θ_q ($^\circ$)	-46.468	-47.087	-47.114	-47.877	-46.462
ϕ_q ($^\circ$)	.000	-.017	-.012	-3.419	3.432
X	.960	1.000	1.000	1.000	1.000
ϵ	.780	.781	.781	.773	.791
$\lvert\vec{p}\,'\rvert$ (MeV/c)	973.000	1001.326	1000.601	980.332	1016.7 68
$\lvert\vec{p}_R\rvert$ (MeV/c)	27.040	0.000	0.000	.000	0.000
θ_{pq} ($^\circ$)	.018	0.000	0.000	-.000	0.000
ϕ_x ($^\circ$)	.000	164.986	164.839	.000	359.999
E_{miss} (MeV)	16.310	0.000	0.000	0.000	0.000
W (GeV)	.956	.938	.938	.938	.938
θ_{CM} ($^\circ$)	177.112	64.653	64.719	-.000	180.000

Table A.2: E_e = 1.645 GeV: p(e,e$'$p), full $\Delta\Omega$.

Variable	Central	Average	Centroid	Minimum	Maximum
θ_e ($^\circ$)	23.360	23.442	23.422	22.879	23.858
ω (MeV)	445.000	432.793	432.198	415.956	445.273
$\lvert\vec{q}\rvert$ (MeV/c)	999.838	999.709	998.893	976.516	1016.784
Q^2 ((GeV/c)^2)	.802	.812	.811	.781	.836
θ_q ($^\circ$)	-52.480	-53.181	-53.205	-53.883	-52.642
ϕ_q ($^\circ$)	.000	-.030	-.022	-3.342	3.404
X	.960	1.000	1.000	1.000	1.000
ϵ	.904	.904	.904	.901	.909
$\lvert\vec{p}\,'\rvert$ (MeV/c)	973.000	999.709	998.893	976.516	1016.784
$\lvert\vec{p}_R\rvert$ (MeV/c)	26.838	0.000	0.000	.000	0.000
θ_{pq} ($^\circ$)	.010	0.000	0.000	-.000	0.000
ϕ_x ($^\circ$)	.000	162.180	162.302	.000	359.966
E_{miss} (MeV)	16.639	0.000	0.000	0.000	0.000
W (GeV)	.956	.938	.938	.938	.938
θ_{CM} ($^\circ$)	178.291	65.911	65.915	.000	180.000

Table A.3: E_e = 2.445 GeV: p(e,e$'$p), full $\Delta\Omega$.

Variable	Central	Average	Centroid	Minimum	Maximum
θ_e ($^\circ$)	100.760	100.760	100.760	100.731	100.788
ω (MeV)	445.000	436.535	436.535	436.448	436.621
$\|\vec{q}\|$ (MeV/c)	1000.116	1004.862	1004.861	1004.742	1004.980
Q^2 ((GeV/c)^2)	.802	.819	.819	.819	.819
θ_q ($^\circ$)	-23.136	-23.537	-23.537	-23.548	-23.526
ϕ_q ($^\circ$)	.000	0.000	0.000	-.012	.012
X	.961	1.000	1.000	1.000	1.000
ϵ	.216	.218	.218	.217	.218
$\|\vec{p}\,'\|$ (MeV/c)	973.000	1004.862	1004.861	1004.742	1004. 980
$\|\vec{p}_R\|$ (MeV/c)	27.117	0.000	0.000	.000	0.000
θ_{pq} ($^\circ$)	.016	0.000	0.000	-.000	0.000
ϕ_x ($^\circ$)	.000	174.252	174.253	.000	360.000
E_{miss} (MeV)	16.181	0.000	0.000	0.000	0.000
W (GeV)	.956	.938	.938	.938	.938
θ_{CM} ($^\circ$)	177.426	47.567	47.567	-.000	180.000

Table A.4: E_e = 0.845 GeV: p(e,e$'$p), $\vec{q}$-llimator.

Variable	Central	Average	Centroid	Minimum	Maximum
θ_e ($^\circ$)	37.170	37.170	37.170	37.141	37.198
ω (MeV)	445.000	432.027	432.027	431.553	432.496
$\|\vec{q}\|$ (MeV/c)	1000.038	998.685	998.685	998.035	999.329
Q^2 ((GeV/c)^2)	.802	.811	.811	.810	.812
θ_q ($^\circ$)	-46.468	-47.208	-47.208	-47.231	-47.184
ϕ_q ($^\circ$)	.000	0.000	0.000	-.035	.035
X	.960	1.000	1.000	1.000	1.000
ϵ	.780	.782	.782	.782	.783
$\|\vec{p}\,'\|$ (MeV/c)	973.000	998.685	998.685	998.035	999.329
$\|\vec{p}_R\|$ (MeV/c)	27.040	0.000	0.000	.000	0.000
θ_{pq} ($^\circ$)	.018	0.000	0.000	-.000	0.000
ϕ_x ($^\circ$)	.000	165.566	165.570	.000	360.000
E_{miss} (MeV)	16.310	0.000	0.000	0.000	0.000
W (GeV)	.956	.938	.938	.938	.938
θ_{CM} ($^\circ$)	177.112	63.202	63.202	-.000	180.000

Table A.5: E_e = 1.645 GeV: p(e,e$'$p), $\vec{q}$-llimator.

Variable	Central	Average	Centroid	Minimum	Maximum
θ_e (°)	23.360	23.360	23.360	23.331	23.388
ω (MeV)	445.000	430.329	430.327	429.470	431.178
$\|\vec{q}\|$ (MeV/c)	999.838	996.354	996.351	995.174	997.519
Q^2 ((GeV/c)^2)	.802	.808	.808	.806	.809
θ_q (°)	-52.480	-53.298	-53.298	-53.333	-53.264
ϕ_q (°)	.000	0.000	0.000	-.058	.058
X	.960	1.000	1.000	1.000	1.000
ϵ	.904	.905	.905	.905	.905
$\|\vec{p}\,'\|$ (MeV/c)	973.000	996.354	996.351	995.174	997.519
$\|\vec{p}_R\|$ (MeV/c)	26.838	0.000	0.000	.000	0.000
θ_{pq} (°)	.010	0.000	0.000	-.000	0.000
ϕ_x (°)	.000	163.905	163.908	.000	360.000
E_{miss} (MeV)	16.639	0.000	0.000	0.000	0.000
W (GeV)	.956	.938	.938	.938	.938
θ_{CM} (°)	178.291	67.902	67.907	-.000	180.000

Table A.6: E_e = 2.445 GeV: p(e,e$'$p), $\vec{q}$-llimator.

A.2 The $^1P_{1/2}$ state of ^{16}O

Variable	Central	Average	Centroid	Minimum	Maximum
θ_e (°)	100.760	100.754	100.732	99.331	102.192
ω (MeV)	445.000	442.316	441.799	427.010	457.465
$\|\vec{q}\|$ (MeV/c)	1000.116	1001.592	1001.762	985.640	1018.341
Q^2 ((GeV/c)^2)	.802	.808	.808	.763	.854
θ_q (°)	-23.136	-23.252	-23.281	-24.282	-22.273
ϕ_q (°)	.000	-.003	.012	-1.396	1.393
X	.961	.974	.976	.889	1.065
ϵ	.216	.216	.216	.206	.227
$\|\vec{p}\,'\|$ (MeV/c)	973.000	996.086	995.339	974.870	1016.783
$\|\vec{p}_R\|$ (MeV/c)	27.117	36.918	45.330	2.910	83.276
θ_{pq} (°)	.016	1.813	2.302	.029	4.649
ϕ_x (°)	.000	179.947	180.202	.168	359.889
E_{miss} (MeV)	31.552	12.100	12.100	12.100	12.100
W (GeV)	15.316	15.314	15.313	15.297	15.330
θ_{CM} (°)	.018	1.988	2.523	.031	5.092

Table A.7: E_e = 0.845 GeV: $^1P_{1/2}$ state, $\|$ Kinematics.

Variable	Central	Average	Centroid	Minimum	Maximum
θ_e $(^\circ)$	100.760	100.754	100.724	99.331	102.192
ω (MeV)	445.000	442.507	442.576	427.010	458.034
$\lvert\vec{q}\rvert$ (MeV/c)	1000.116	1001.487	1001.276	985.263	1018.341
Q^2 ((GeV/c)^2)	.802	.807	.807	.761	.854
θ_q $(^\circ)$	-23.136	-23.243	-23.247	-24.282	-22.232
ϕ_q $(^\circ)$	.000	-.004	-.005	-1.396	1.393
X	.961	.973	.972	.887	1.065
ϵ	.216	.216	.216	.205	.227
$\lvert\vec{p}\,'\rvert$ (MeV/c)	973.000	995.833	995.937	974.373	1016.768
$\lvert\vec{p}_R\rvert$ (MeV/c)	106.483	108.820	108.015	68.714	146.254
θ_{pq} $(^\circ)$	5.984	6.150	6.105	3.656	8.256
ϕ_x $(^\circ)$	180.000	180.060	180.051	136.617	222.818
E_{miss} (MeV)	31.173	12.100	12.100	12.100	12.100
W (GeV)	15.316	15.314	15.314	15.297	15.330
θ_{CM} $(^\circ)$	6.564	6.739	6.690	4.012	9.032

Table A.8: $E_e = 0.845$ GeV: $^1P_{1/2}$ state, $\Sigma3$ Kinematics, $\theta_{pq} = 6^\circ$.

Variable	Central	Average	Centroid	Minimum	Maximum
θ_e $(^\circ)$	100.760	100.755	100.700	99.331	102.192
ω (MeV)	445.000	442.013	441.423	427.010	457.075
$\lvert\vec{q}\rvert$ (MeV/c)	1000.116	1001.768	1001.774	985.825	1018.341
Q^2 ((GeV/c)^2)	.802	.808	.809	.763	.8542
θ_q $(^\circ)$	-23.136	-23.267	-23.307	-24.282	-22.299
ϕ_q $(^\circ)$	.000	-.004	-.005	-1.396	1.393
X	.961	.975	.977	.891	1.065
ϵ	.216	.216	.217	.206	.227
$\lvert\vec{p}\,'\rvert$ (MeV/c)	971.000	994.506	993.744	973.684	1014.685
$\lvert\vec{p}_R\rvert$ (MeV/c)	157.076	158.416	155.182	118.070	197.267
θ_{pq} $(^\circ)$	8.984	9.037	8.852	6.654	11.218
ϕ_x $(^\circ)$	180.000	180.058	180.012	148.878	210.913
E_{miss} (MeV)	32.136	12.100	12.100	12.100	12.100
W (GeV)	15.316	15.313	15.313	15.297	15.329
θ_{CM} $(^\circ)$	9.853	9.902	9.700	7.301	12.275

Table A.9: $E_e = 0.845$ GeV: $^1P_{1/2}$ state, $\Sigma3$ Kinematics, $\theta_{pq} = 9^\circ$.

Variable	Central	Average	Centroid	Minimum	Maximum
θ_e (°)	100.760	100.756	100.680	99.331	102.192
ω (MeV)	445.000	441.979	440.845	427.010	457.075
$\lvert\vec{q}\rvert$ (MeV/c)	1000.116	1001.794	1001.984	985.877	1018.341
Q^2 ((GeV/c)^2)	.802	.808	.810	.764	.854
θ_q (°)	-23.136	-23.268	-23.339	-24.282	-22.299
ϕ_q (°)	.000	-.005	-.004	-1.396	1.393
X	.961	.975	.979	.892	1.065
ϵ	.216	.216	.217	.206	.227
$\lvert\vec{p}\,'\rvert$ (MeV/c)	970.000	993.538	992.082	972.732	1013.628
$\lvert\vec{p}_R\rvert$ (MeV/c)	207.822	209.294	204.262	168.764	249.072
θ_{pq} (°)	11.984	11.990	11.703	9.653	14.201
ϕ_x (°)	180.000	180.050	179.997	155.695	204.393
E_{miss} (MeV)	32.193	12.100	12.100	12.100	12.100
W (GeV)	15.316	15.313	15.312	15.297	15.329
θ_{CM} (°)	13.140	13.134	12.821	10.589	15.535

Table A.10: $E_e = 0.845$ GeV: $^1P_{1/2}$ state, $\Sigma3$ Kinematics, $\theta_{pq} = 12°$.

Variable	Central	Average	Centroid	Minimum	Maximum
θ_e (°)	100.760	100.757	100.654	99.331	102.192
ω (MeV)	445.000	441.826	440.021	427.010	457.075
$\lvert\vec{q}\rvert$ (MeV/c)	1000.116	1001.884	1002.287	986.415	1018.341
Q^2 ((GeV/c)^2)	.802	.809	.811	.765	.854
θ_q (°)	-23.136	-23.275	-23.384	-24.282	-22.299
ϕ_q (°)	.000	-.005	-.003	-1.396	1.393
X	.961	.976	.983	.892	1.065
ϵ	.216	.216	.217	.206	.227
$\lvert\vec{p}\,'\rvert$ (MeV/c)	968.000	991.701	989.410	971.057	1011.551
$\lvert\vec{p}_R\rvert$ (MeV/c)	275.472	277.312	270.084	236.719	317.942
θ_{pq} (°)	15.984	15.950	15.539	13.653	18.188
ϕ_x (°)	180.000	180.042	179.983	160.989	199.260
E_{miss} (MeV)	32.462	12.100	12.100	12.100	12.100
W (GeV)	15.316	15.313	15.311	15.297	15.329
θ_{CM} (°)	17.517	17.463	17.017	14.970	19.883

Table A.11: $E_e = 0.845$ GeV: $^1P_{1/2}$ state, $\Sigma3$ Kinematics, $\theta_{pq} = 16°$.

Variable	Central	Average	Centroid	Minimum	Maximum
θ_e ($^\circ$)	100.760	100.757	100.635	99.331	102.192
ω (MeV)	445.000	442.251	439.873	427.010	457.668
$\lvert\vec{q}\rvert$ (MeV/c)	1000.116	1001.644	1002.261	985.640	1018.341
Q^2 ((GeV/c)^2)	.802	.808	.811	.763	.854
θ_q ($^\circ$)	-23.136	-23.255	-23.396	-24.282	-22.252
ϕ_q ($^\circ$)	.000	-.004	-.002	-1.396	1.393
X	.961	.974	.983	.889	1.065
ϵ	.216	.216	.217	.205	.227
$\lvert\vec{p}\,'\rvert$ (MeV/c)	968.000	991.286	988.278	970.046	1011.540
$\lvert\vec{p}_R\rvert$ (MeV/c)	309.234	311.699	302.930	270.659	352.548
θ_{pq} ($^\circ$)	17.984	17.958	17.461	15.653	20.201
ϕ_x ($^\circ$)	180.000	180.030	179.973	162.708	197.507
E_{miss} (MeV)	31.757	12.100	12.100	12.100	12.100
W (GeV)	15.316	15.314	15.311	15.297	15.330
θ_{CM} ($^\circ$)	19.701	19.654	19.116	17.158	22.072

Table A.12: $E_e = 0.845$ GeV: $^1P_{1/2}$ state, $\Sigma3$ Kinematics, $\theta_{pq} = 18^\circ$.

Variable	Central	Average	Centroid	Minimum	Maximum
θ_e ($^\circ$)	100.760	100.757	100.625	99.331	102.192
ω (MeV)	445.000	442.058	439.471	427.010	457.480
$\lvert\vec{q}\rvert$ (MeV/c)	1000.116	1001.754	1002.425	985.640	1018.341
Q^2 ((GeV/c)^2)	.802	.808	.812	.763	.854
θ_q ($^\circ$)	-23.136	-23.264	-23.417	-24.282	-22.299
ϕ_q ($^\circ$)	.000	-.004	-.001	-1.396	1.393
X	.961	.975	.985	.889	1.065
ϵ	.216	.216	.218	.206	.227
$\lvert\vec{p}\,'\rvert$ (MeV/c)	967.000	990.491	987.233	969.491	1010.506
$\lvert\vec{p}_R\rvert$ (MeV/c)	326.030	328.509	318.966	287.599	369.624
θ_{pq} ($^\circ$)	18.984	18.944	18.404	16.653	21.200
ϕ_x ($^\circ$)	180.000	180.029	179.970	163.426	196.765
E_{miss} (MeV)	32.094	12.100	12.100	12.100	12.100
W (GeV)	15.316	15.313	15.311	15.297	15.329
θ_{CM} ($^\circ$)	20.794	20.731	20.146	18.251	23.158

Table A.13: $E_e = 0.845$ GeV: $^1P_{1/2}$ state, $\Sigma3$ Kinematics, $\theta_{pq} = 19^\circ$.

Variable	Central	Average	Centroid	Minimum	Maximum
θ_e (°)	100.760	100.757	100.612	99.331	102.192
ω (MeV)	445.000	442.280	439.318	427.010	458.023
$\lvert\vec{q}\rvert$ (MeV/c)	1000.116	1001.628	1002.437	985.640	1018.341
Q^2 ((GeV/c)^2)	.802	.808	.812	.763	.854
θ_q (°)	-23.136	-23.254	-23.427	-24.282	-22.252
ϕ_q (°)	.000	-.004	-.001	-1.396	1.393
X	.961	.974	.985	.889	1.065
ϵ	.216	.216	.218	.205	.227
$\lvert\vec{p}\,'\rvert$ (MeV/c)	967.000	990.226	986.500	968.909	1010.492
$\lvert\vec{p}_R\rvert$ (MeV/c)	342.863	345.656	335.152	304.515	386.662
θ_{pq} (°)	19.984	19.950	19.356	17.652	22.198
ϕ_x (°)	180.000	180.023	179.964	164.076	196.094
E_{miss} (MeV)	31.692	12.100	12.100	12.100	12.100
W (GeV)	15.316	15.314	15.311	15.297	15.330
θ_{CM} (°)	21.884	21.827	21.185	19.344	24.244

Table A.14: E_e = 0.845 GeV: $^1P_{1/2}$ state, Σ3 Kinematics, θ_{pq} = 20°.

Variable	Central	Average	Centroid	Minimum	Maximum
θ_e (°)	37.170	37.205	37.042	35.742	38.602
ω (MeV)	445.000	425.729	433.897	394.503	456.704
$\lvert\vec{q}\rvert$ (MeV/c)	1000.038	998.996	996.305	965.966	1030.503
Q^2 ((GeV/c)^2)	.802	.817	.804	.738	.896
θ_q (°)	-46.468	-47.531	-47.047	-49.370	-45.591
ϕ_q (°)	.000	-.003	-.013	-4.232	4.212
X	.960	1.025	.990	.862	1.202
ϵ	.780	.783	.783	.767	.800
$\lvert\vec{p}\,'\rvert$ (MeV/c)	970.000	970.435	982.096	926.360	1013.605
$\lvert\vec{p}_R\rvert$ (MeV/c)	208.387	231.925	218.408	175.779	290.159
θ_{pq} (°)	12.018	13.354	12.582	9.978	16.640
ϕ_x (°)	.000	176.869	175.703	.002	359.998
E_{miss} (MeV)	32.185	12.100	12.100	12.100	12.100
W (GeV)	15.316	15.297	15.306	15.265	15.330
θ_{CM} (°)	13.177	14.641	13.784	10.902	18.281

Table A.15: E_e = 1.645 GeV: $^1P_{1/2}$ state, Σ4 Kinematics, θ_{pq} = -12°.

Variable	Central	Average	Centroid	Minimum	Maximum
θ_e (°)	37.170	37.205	37.063	35.742	38.602
ω (MeV)	445.000	425.738	432.457	394.503	457.089
$\lvert\vec{q}\rvert$ (MeV/c)	1000.038	998.987	996.603	965.966	1030.503
Q^2 ((GeV/c)^2)	.802	.817	.806	.738	.898
θ_q (°)	-46.468	-47.531	-47.132	-49.426	-45.591
ϕ_q (°)	.000	0.000	-.009	-4.232	4.212
X	.960	1.025	.995	.862	1.212
ϵ	.780	.783	.783	.767	.800
$\lvert\vec{p}\,'\rvert$ (MeV/c)	971.000	971.458	981.004	927.316	1014.685
$\lvert\vec{p}_R\rvert$ (MeV/c)	157.637	182.763	171.304	124.521	245.235
θ_{pq} (°)	9.018	10.432	9.807	6.979	13.800
ϕ_x (°)	.000	176.867	175.278	.003	359.968
E_{miss} (MeV)	32.129	12.100	12.100	12.100	12.100
W (GeV)	15.316	15.297	15.304	15.264	15.330
θ_{CM} (°)	9.891	11.442	10.749	7.627	15.169

Table A.16: E_e = 1.645 GeV: $^1P_{1/2}$ state, Σ4 Kinematics, θ_{pq} = -9°.

Variable	Central	Average	Centroid	Minimum	Maximum
θ_e (°)	37.170	37.204	37.179	35.742	38.602
ω (MeV)	445.000	426.144	423.299	394.540	457.689
$\lvert\vec{q}\rvert$ (MeV/c)	1000.038	999.013	998.230	965.966	1030.503
Q^2 ((GeV/c)^2)	.802	.816	.817	.738	.898
θ_q (°)	-46.468	-47.507	-47.663	-49.426	-45.552
ϕ_q (°)	.000	-.009	.001	-4.232	4.212
X	.960	1.023	1.031	.862	1.212
ϵ	.780	.783	.784	.767	.800
$\lvert\vec{p}\,'\rvert$ (MeV/c)	973.000	973.490	969.482	929.226	1016.743
$\lvert\vec{p}_R\rvert$ (MeV/c)	27.040	60.566	69.578	2.820	147.095
θ_{pq} (°)	.018	2.829	3.309	.041	7.617
ϕ_x (°)	.000	178.682	178.541	.160	359.956
E_{miss} (MeV)	31.552	12.100	12.100	12.100	12.100
W (GeV)	15.316	15.298	15.295	15.264	15.330
θ_{CM} (°)	.020	3.104	3.631	.045	8.378

Table A.17: E_e = 1.645 GeV: $^1P_{1/2}$ state, $\|$ Kinematics.

Variable	Central	Average	Centroid	Minimum	Maximum
θ_e (°)	37.170	37.205	37.091	35.742	38.602
ω (MeV)	445.000	425.477	422.910	393.620	457.139
$\lvert\vec{q}\rvert$ (MeV/c)	1000.038	998.979	996.298	965.966	1030.503
Q^2 ((GeV/c)^2)	.802	.817	.814	.738	.898
θ_q (°)	-46.468	-47.545	-47.682	-49.480	-45.561
ϕ_q (°)	.000	-.003	-.002	-4.232	4.212
X	.960	1.026	1.028	.862	1.212
ϵ	.780	.783	.784	.767	.800
$\lvert\vec{p}\,'\rvert$ (MeV/c)	971.000	971.655	968.173	927.362	1014.646
$\lvert\vec{p}_R\rvert$ (MeV/c)	157.027	149.207	143.786	94.796	212.866
θ_{pq} (°)	8.982	8.342	8.044	4.784	12.101
ϕ_x (°)	180.000	179.789	179.745	127.471	229.176
E_{miss} (MeV)	32.136	12.100	12.100	12.100	12.100
W (GeV)	15.316	15.297	15.295	15.263	15.330
θ_{CM} (°)	9.851	9.149	8.821	5.275	13.248

Table A.18: E_e = 1.645 GeV: $^1P_{1/2}$ state, Σ5 Kinematics, θ_{pq} = 9°.

Variable	Central	Average	Centroid	Minimum	Maximum
θ_e (°)	37.170	37.206	37.071	35.742	38.602
ω (MeV)	445.000	425.389	420.042	393.245	457.139
$\lvert\vec{q}\rvert$ (MeV/c)	1000.038	998.982	995.620	965.966	1030.503
Q^2 ((GeV/c)^2)	.802	.817	.815	.738	.898
θ_q (°)	-46.468	-47.551	-47.845	-49.487	-45.561
ϕ_q (°)	.000	.002	.009	-4.232	4.212
X	.960	1.026	1.036	.862	1.213
ϵ	.780	.783	.785	.767	.800
$\lvert\vec{p}\,'\rvert$ (MeV/c)	970.000	970.708	963.451	926.374	1013.649
$\lvert\vec{p}_R\rvert$ (MeV/c)	207.774	197.056	187.726	141.032	256.888
θ_{pq} (°)	11.982	11.220	10.698	7.763	14.636
ϕ_x (°)	180.000	179.864	179.865	138.832	218.436
E_{miss} (MeV)	32.194	12.100	12.100	12.100	12.100
W (GeV)	15.316	15.297	15.292	15.263	15.330
θ_{CM} (°)	13.138	12.302	11.731	8.558	16.010

Table A.19: E_e = 1.645 GeV: $^1P_{1/2}$ state, Σ5 Kinematics, θ_{pq} = 12°.

Variable	Central	Average	Centroid	Minimum	Maximum
θ_e (°)	23.360	23.429	22.899	21.932	24.792
ω (MeV)	445.000	426.417	436.384	394.912	457.715
$\|\vec{q}\|$ (MeV/c)	999.838	998.028	982.235	942.374	1049.801
Q^2 ((GeV/c)^2)	.802	.815	.775	.708	.917
θ_q (°)	-52.480	-53.458	-52.664	-55.605	-51.220
ϕ_q (°)	.000	-.048	-.140	-6.940	6.866
X	.960	1.020	.947	.838	1.220
ϵ	.904	.905	.907	.894	.916
$\|\vec{p}\,'\|$ (MeV/c)	967.000	967.398	982.129	923.498	1010.511
$\|\vec{p}_R\|$ (MeV/c)	343.237	365.993	341.899	309.736	423.410
θ_{pq} (°)	20.010	21.328	19.995	17.913	24.916
ϕ_x (°)	.000	176.221	170.280	.003	359.994
E_{miss} (MeV)	31.683	12.100	12.100	12.100	12.100
W (GeV)	15.316	15.298	15.309	15.266	15.330
θ_{CM} (°)	21.913	23.349	21.847	19.539	27.330

Table A.20: E_e = 2.445 GeV: $^1P_{1/2}$ state, Σ2 Kinematics, θ_{pq} = -20°.

Variable	Central	Average	Centroid	Minimum	Maximum
θ_e (°)	23.360	23.426	22.926	21.932	24.792
ω (MeV)	445.000	425.890	435.694	394.627	457.042
$\|\vec{q}\|$ (MeV/c)	999.838	997.784	982.979	942.374	1048.101
Q^2 ((GeV/c)^2)	.802	.814	.777	.708	.917
θ_q (°)	-52.480	-53.485	-52.715	-55.640	-51.220
ϕ_q (°)	.000	-.041	-.137	-6.940	6.866
X	.960	1.021	.951	.838	1.220
ϵ	.904	.905	.907	.894	.916
$\|\vec{p}\,'\|$ (MeV/c)	967.000	967.235	981.669	923.504	1010.479
$\|\vec{p}_R\|$ (MeV/c)	326.405	349.894	326.747	292.981	407.999
θ_{pq} (°)	19.010	20.370	19.090	16.917	23.961
ϕ_x (°)	.000	176.499	171.375	.012	359.994
E_{miss} (MeV)	32.085	12.100	12.100	12.100	12.100
W (GeV)	15.316	15.297	15.308	15.265	15.329
θ_{CM} (°)	20.822	22.305	20.864	18.454	26.288

Table A.21: E_e = 2.445 GeV: $^1P_{1/2}$ state, Σ2 Kinematics, θ_{pq} = -19°.

Variable	Central	Average	Centroid	Minimum	Maximum
θ_e ($^\circ$)	23.360	23.428	22.960	21.932	24.792
ω (MeV)	445.000	426.146	435.415	394.912	457.545
$\lvert\vec{q}\rvert$ (MeV/c)	999.838	997.923	984.059	942.374	1049.801
Q^2 ((GeV/c)^2)	.802	.815	.779	.708	.917
θ_q ($^\circ$)	-52.480	-53.472	-52.746	-55.640	-51.220
ϕ_q ($^\circ$)	.000	-.043	-.122	-6.940	6.866
X	.960	1.021	.955	.838	1.220
ϵ	.904	.905	.907	.894	.916
$\lvert\vec{p}\,'\rvert$ (MeV/c)	968.000	968.155	981.763	924.486	1011.498
$\lvert\vec{p}_R\rvert$ (MeV/c)	309.612	333.370	311.468	276.218	392.622
θ_{pq} ($^\circ$)	18.010	19.377	18.170	15.920	23.009
ϕ_x ($^\circ$)	.000	176.174	172.555	.021	359.987
E_{miss} (MeV)	31.749	12.100	12.100	12.100	12.100
W (GeV)	15.316	15.298	15.308	15.265	15.330
θ_{CM} ($^\circ$)	19.730	21.222	19.865	17.370	25.249

Table A.22: E_e = 2.445 GeV: $^1P_{1/2}$ state, $\Sigma 2$ Kinematics, θ_{pq} = -18°.

Variable	Central	Average	Centroid	Minimum	Maximum
θ_e ($^\circ$)	23.360	23.424	23.005	21.932	24.792
ω (MeV)	445.000	425.324	434.005	394.286	456.981
$\lvert\vec{q}\rvert$ (MeV/c)	999.838	997.588	985.265	942.374	1048.101
Q^2 ((GeV/c)^2)	.802	.815	.783	.708	.917
θ_q ($^\circ$)	-52.480	-53.517	-52.848	-55.660	-51.220
ϕ_q ($^\circ$)	.000	-.027	-.100	-6.940	6.866
X	.960	1.023	.963	.838	1.220
ϵ	.904	.905	.907	.894	.916
$\lvert\vec{p}\,'\rvert$ (MeV/c)	968.000	968.024	980.697	924.447	1011.538
$\lvert\vec{p}_R\rvert$ (MeV/c)	275.851	301.175	280.963	242.702	362.019
θ_{pq} ($^\circ$)	16.010	17.464	16.357	13.929	21.117
ϕ_x ($^\circ$)	.000	176.411	173.162	.009	359.998
E_{miss} (MeV)	32.455	12.100	12.100	12.100	12.100
W (GeV)	15.316	15.297	15.306	15.265	15.329
θ_{CM} ($^\circ$)	17.545	19.134	17.892	15.201	23.183

Table A.23: E_e = 2.445 GeV: $^1P_{1/2}$ state, $\Sigma 2$ Kinematics, θ_{pq} = -16°.

Variable	Central	Average	Centroid	Minimum	Maximum
θ_e (°)	23.360	23.424	23.083	21.932	24.792
ω (MeV)	445.000	425.509	432.739	394.286	457.042
$\|\vec{q}\|$ (MeV/c)	999.838	997.650	987.627	942.374	1048.101
Q^2 ((GeV/c)^2)	.802	.815	.788	.708	.917
θ_q (°)	-52.480	-53.506	-52.955	-55.660	-51.220
ϕ_q (°)	.000	-.028	-.089	-6.940	6.866
X	.960	1.022	.973	.838	1.220
ϵ	.904	.905	.906	.894	.916
$\|\vec{p}\ '\|$ (MeV/c)	970.000	970.020	980.472	926.359	1013.606
$\|\vec{p}_R\|$ (MeV/c)	208.204	236.084	218.801	176.031	301.869
θ_{pq} (°)	12.010	13.584	12.656	9.954	17.405
ϕ_x (°)	.000	175.582	173.062	.005	359.992
E_{miss} (MeV)	32.187	12.100	12.100	12.100	12.100
W (GeV)	15.316	15.297	15.305	15.265	15.329
θ_{CM} (°)	13.169	14.891	13.855	10.868	19.121

Table A.24: E_e = 2.445 GeV: $^1P_{1/2}$ state, Σ2 Kinematics, θ_{pq} = -12°.

Variable	Central	Average	Centroid	Minimum	Maximum
θ_e (°)	23.360	23.425	23.135	21.932	24.792
ω (MeV)	445.000	425.483	431.426	394.286	457.042
$\|\vec{q}\|$ (MeV/c)	999.838	997.665	989.079	942.374	1049.801
Q^2 ((GeV/c)^2)	.802	.815	.792	.708	.917
θ_q (°)	-52.480	-53.508	-53.053	-55.660	-51.220
ϕ_q (°)	.000	-.026	-.068	-6.940	6.866
X	.960	1.022	.981	.838	1.220
ϵ	.904	.905	.906	.894	.916
$\|\vec{p}\ '\|$ (MeV/c)	971.000	970.986	979.529	927.364	1014.678
$\|\vec{p}_R\|$ (MeV/c)	157.452	188.399	173.271	127.112	259.231
θ_{pq} (°)	9.010	10.741	9.948	6.993	14.886
ϕ_x (°)	.000	176.180	173.779	.013	359.966
E_{miss} (MeV)	32.131	12.100	12.100	12.100	12.100
W (GeV)	15.316	15.297	15.304	15.265	15.330
θ_{CM} (°)	9.882	11.779	10.897	7.637	16.339

Table A.25: E_e = 2.445 GeV: $^1P_{1/2}$ state, Σ2 Kinematics, θ_{pq} = -9°.

Variable	Central	Average	Centroid	Minimum	Maximum
θ_e (°)	23.360	23.431	23.195	21.932	24.792
ω (MeV)	445.000	426.659	430.646	395.074	458.040
$\lvert\vec{q}\rvert$ (MeV/c)	999.838	998.147	990.950	942.374	1049.801
Q^2 ((GeV/c)^2)	.802	.815	.797	.708	.917
θ_q (°)	-52.480	-53.445	-53.124	-55.640	-51.050
ϕ_q (°)	.000	-.040	-.058	-6.940	6.866
X	.960	1.020	.988	.833	1.220
ϵ	.904	.905	.906	.894	.916
$\lvert\vec{p}\,'\rvert$ (MeV/c)	973.000	973.381	979.089	929.215	1016.751
$\lvert\vec{p}_R\rvert$ (MeV/c)	106.842	141.745	129.961	75.406	222.625
θ_{pq} (°)	6.010	7.937	7.342	4.087	12.696
ϕ_x (°)	.000	176.427	175.094	.047	359.978
E_{miss} (MeV)	31.170	12.100	12.100	12.100	12.100
W (GeV)	15.316	15.298	15.303	15.265	15.331
θ_{CM} (°)	6.593	8.706	8.046	4.464	13.939

Table A.26: E$_e$ = 2.445 GeV: ^{1}P$_{1/2}$ state, Σ2 Kinematics, θ_{pq} = -6°.

Variable	Central	Average	Centroid	Minimum	Maximum
θ_e (°)	23.360	23.425	23.343	21.932	24.792
ω (MeV)	445.000	425.909	425.515	394.590	457.662
$\lvert\vec{q}\rvert$ (MeV/c)	999.838	997.764	994.887	942.374	1049.801
Q^2 ((GeV/c)^2)	.802	.814	.809	.708	.917
θ_q (°)	-52.480	-53.484	-53.461	-55.701	-51.050
ϕ_q (°)	.000	-.028	-.053	-6.940	6.866
X	.960	1.021	1.016	.833	1.220
ϵ	.904	.905	.905	.894	.916
$\lvert\vec{p}\,'\rvert$ (MeV/c)	973.000	973.032	972.454	929.226	1016.782
$\lvert\vec{p}_R\rvert$ (MeV/c)	26.838	76.038	81.183	2.041	175.728
θ_{pq} (°)	.010	3.733	4.075	.047	10.100
ϕ_x (°)	.000	177.588	177.634	.030	359.809
E_{miss} (MeV)	31.552	12.100	12.100	12.100	12.100
W (GeV)	15.316	15.297	15.297	15.264	15.331
θ_{CM} (°)	.011	4.095	4.469	.052	11.080

Table A.27: E$_e$ = 2.445 GeV: ^{1}P$_{1/2}$ state, $\|$ Kinematics.

Variable	Central	Average	Centroid	Minimum	Maximum
θ_e ($^\circ$)	23.360	23.424	23.271	21.932	24.792
ω (MeV)	445.000	426.292	425.977	394.590	458.425
$\lvert\vec{q}\rvert$ (MeV/c)	999.838	997.841	992.497	942.374	1049.801
Q^2 ((GeV/c)^2)	.802	.814	.804	.707	.917
θ_q ($^\circ$)	-52.480	-53.463	-53.420	-55.701	-50.980
ϕ_q ($^\circ$)	.000	-.033	-.037	-6.940	6.866
X	.960	1.020	1.008	.822	1.220
ϵ	.904	.905	.906	.894	.916
$\lvert\vec{p}\,'\rvert$ (MeV/c)	973.000	973.205	972.829	929.226	1016.762
$\lvert\vec{p}_R\rvert$ (MeV/c)	106.502	115.918	111.392	49.604	201.116
θ_{pq} ($^\circ$)	5.990	6.247	6.064	2.125	11.447
ϕ_x ($^\circ$)	180.000	179.276	179.210	104.992	258.007
E_{miss} (MeV)	31.173	12.100	12.100	12.100	12.100
W (GeV)	15.316	15.298	15.298	15.264	15.332
θ_{CM} ($^\circ$)	6.570	6.850	6.646	2.333	12.509

Table A.28: E_e = 2.445 GeV: $^1P_{1/2}$ state, $\Sigma 1$ Kinematics, θ_{pq} = 6°.

Variable	Central	Average	Centroid	Minimum	Maximum
θ_e ($^\circ$)	23.360	23.422	23.250	21.932	24.792
ω (MeV)	445.000	425.107	421.750	393.472	457.412
$\lvert\vec{q}\rvert$ (MeV/c)	999.838	997.494	990.805	942.374	1049.801
Q^2 ((GeV/c)^2)	.802	.815	.804	.708	.917
θ_q ($^\circ$)	-52.480	-53.528	-53.654	-55.788	-51.132
ϕ_q ($^\circ$)	.000	-.024	-.015	-6.940	7.031
X	.960	1.023	1.018	.838	1.238
ϵ	.904	.905	.906	.894	.916
$\lvert\vec{p}\,'\rvert$ (MeV/c)	971.000	970.998	966.466	927.368	1014.687
$\lvert\vec{p}_R\rvert$ (MeV/c)	157.108	157.501	148.917	96.590	237.031
θ_{pq} ($^\circ$)	8.990	8.810	8.380	5.054	13.503
ϕ_x ($^\circ$)	180.000	179.497	179.418	117.112	238.642
E_{miss} (MeV)	32.135	12.100	12.100	12.100	12.100
W (GeV)	15.316	15.297	15.294	15.263	15.331
θ_{CM} ($^\circ$)	9.860	9.661	9.186	5.564	14.752

Table A.29: E_e = 2.445 GeV: $^1P_{1/2}$ state, $\Sigma 1$ Kinematics, θ_{pq} = 9°.

Variable	Central	Average	Centroid	Minimum	Maximum
θ_e (°)	23.360	23.423	23.242	21.932	24.792
ω (MeV)	445.000	424.953	418.711	393.361	457.412
$\vert\vec{q}\vert$ (MeV/c)	999.838	997.483	989.823	942.374	1049.801
Q^2 ((GeV/c)^2)	.802	.815	.805	.708	.917
θ_q (°)	-52.480	-53.537	-53.823	-55.788	-51.168
ϕ_q (°)	.000	-.022	-.007	-6.940	7.031
X	.960	1.024	1.026	.838	1.238
ϵ	.904	.905	.907	.894	.916
$\vert\vec{p}\,'\vert$ (MeV/c)	970.000	969.958	961.513	926.360	1013.634
$\vert\vec{p}_R\vert$ (MeV/c)	207.859	203.529	191.381	143.359	279.674
θ_{pq} (°)	11.990	11.588	10.963	7.932	15.890
ϕ_x (°)	180.000	179.618	179.526	129.319	228.283
E_{miss} (MeV)	32.193	12.100	12.100	12.100	12.100
W (GeV)	15.316	15.296	15.291	15.263	15.330
θ_{CM} (°)	13.146	12.703	12.016	8.731	17.407

Table A.30: E_e = 2.445 GeV: $^1P_{1/2}$ state, Σ1 Kinematics, $\theta_{pq} = 12°$.

Variable	Central	Average	Centroid	Minimum	Maximum
θ_e (°)	23.360	23.423	23.223	21.932	24.792
ω (MeV)	445.000	424.659	414.758	392.763	457.412
$\vert\vec{q}\vert$ (MeV/c)	999.838	997.435	988.289	942.374	1049.801
Q^2 ((GeV/c)^2)	.802	.815	.805	.708	.923
θ_q (°)	-52.480	-53.554	-54.039	-55.889	-51.168
ϕ_q (°)	.000	-.029	-.006	-6.940	7.031
X	.960	1.025	1.036	.838	1.250
ϵ	.904	.905	.907	.894	.916
$\vert\vec{p}\,'\vert$ (MeV/c)	968.000	968.051	954.700	924.450	1011.529
$\vert\vec{p}_R\vert$ (MeV/c)	275.507	267.337	250.020	206.966	340.418
θ_{pq} (°)	15.990	15.406	14.531	11.863	19.389
ϕ_x (°)	180.000	179.692	179.615	140.397	219.150
E_{miss} (MeV)	32.462	12.100	12.100	12.100	12.100
W (GeV)	15.316	15.296	15.287	15.262	15.330
θ_{CM} (°)	17.523	16.881	15.923	13.057	21.228

Table A.31: E_e = 2.445 GeV: $^1P_{1/2}$ state, Σ1 Kinematics, $\theta_{pq} = 16°$.

Variable	Central	Average	Centroid	Minimum	Maximum
θ_e ($^\circ$)	23.360	23.422	23.213	21.932	24.792
ω (MeV)	445.000	425.364	413.294	393.361	458.076
$\lvert\vec{q}\rvert$ (MeV/c)	999.838	997.565	987.602	942.374	1049.801
Q^2 ((GeV/c)^2)	.802	.814	.805	.707	.917
θ_q ($^\circ$)	-52.480	-53.514	-54.118	-55.788	-50.980
ϕ_q ($^\circ$)	.000	-.035	-.010	-6.940	6.866
X	.960	1.023	1.039	.822	1.238
ϵ	.904	.905	.907	.894	.916
$\lvert\vec{p}\,'\rvert$ (MeV/c)	968.000	968.093	951.864	924.479	1011.524
$\lvert\vec{p}_R\rvert$ (MeV/c)	309.267	300.560	279.927	239.197	371.741
θ_{pq} ($^\circ$)	17.990	17.387	16.358	13.819	21.204
ϕ_x ($^\circ$)	180.000	179.713	179.615	144.326	215.714
E_{miss} (MeV)	31.756	12.100	12.100	12.100	12.100
W (GeV)	15.316	15.297	15.285	15.263	15.332
θ_{CM} ($^\circ$)	19.707	19.046	17.922	15.206	23.208

Table A.32: $E_e = 2.445$ GeV: $^1P_{1/2}$ state, $\Sigma1$ Kinematics, $\theta_{pq} = 18^\circ$.

Variable	Central	Average	Centroid	Minimum	Maximum
θ_e ($^\circ$)	23.360	23.423	23.202	21.932	24.792
ω (MeV)	445.000	425.026	411.994	392.981	457.662
$\lvert\vec{q}\rvert$ (MeV/c)	999.838	997.516	986.945	942.374	1049.801
Q^2 ((GeV/c)^2)	.802	.815	.805	.708	.917
θ_q ($^\circ$)	-52.480	-53.533	-54.188	-55.788	-51.050
ϕ_q ($^\circ$)	.000	-.032	.011	-6.940	7.031
X	.960	1.024	1.042	.833	1.238
ϵ	.904	.905	.907	.894	.916
$\lvert\vec{p}\,'\rvert$ (MeV/c)	967.000	967.131	949.631	923.497	1010.507
$\lvert\vec{p}_R\rvert$ (MeV/c)	326.062	316.535	294.292	255.350	387.551
θ_{pq} ($^\circ$)	18.990	18.346	17.247	14.802	22.124
ϕ_x ($^\circ$)	180.000	179.724	179.686	145.937	214.209
E_{miss} (MeV)	32.093	12.100	12.100	12.100	12.100
W (GeV)	15.316	15.297	15.284	15.263	15.331
θ_{CM} ($^\circ$)	20.800	20.093	18.893	16.285	24.209

Table A.33: $E_e = 2.445$ GeV: $^1P_{1/2}$ state, $\Sigma1$ Kinematics, $\theta_{pq} = 19^\circ$.

Variable	Central	Average	Centroid	Minimum	Maximum
θ_e ($^\circ$)	23.360	23.421	23.192	21.932	24.792
ω (MeV)	445.000	425.393	411.047	393.086	458.361
$\|\vec{q}\|$ (MeV/c)	999.838	997.542	986.367	942.374	1049.801
Q^2 ((GeV/c)^2)	.802	.814	.804	.707	.917
θ_q ($^\circ$)	-52.480	-53.512	-54.237	-55.788	-50.980
ϕ_q ($^\circ$)	.000	-.033	.005	-6.940	6.866
X	.960	1.023	1.044	.822	1.238
ϵ	.904	.905	.907	.894	.916
$\|\vec{p}\ '\|$ (MeV/c)	967.000	967.100	947.867	923.520	1010.500
$\|\vec{p}_R\|$ (MeV/c)	342.894	333.253	308.849	271.513	403.435
θ_{pq} ($^\circ$)	19.990	19.343	18.147	15.786	23.050
ϕ_x ($^\circ$)	180.000	179.742	179.684	147.409	212.825
E_{miss} (MeV)	31.691	12.100	12.100	12.100	12.100
W (GeV)	15.316	15.297	15.283	15.263	15.332
θ_{CM} ($^\circ$)	21.890	21.182	19.876	17.366	25.217

Table A.34: E_e = 2.445 GeV: $^1P_{1/2}$ state, $\Sigma 1$ Kinematics, $\theta_{pq} = 20^\circ$.

Variable	Central	Average	Centroid	Minimum	Maximum
θ_e ($^\circ$)	23.360	23.421	23.153	21.932	24.792
ω (MeV)	445.000	425.184	410.294	392.558	458.425
$\|\vec{q}\|$ (MeV/c)	999.838	997.492	984.891	942.374	1049.801
Q^2 ((GeV/c)^2)	.802	.814	.802	.707	.917
θ_q ($^\circ$)	-52.480	-53.524	-54.258	-55.788	-50.980
ϕ_q ($^\circ$)	.000	-.031	.007	-6.940	7.031
X	.960	1.023	1.043	.822	1.238
ϵ	.904	.905	.908	.894	.916
$\|\vec{p}\ '\|$ (MeV/c)	960.000	960.076	940.401	916.801	1003.197
$\|\vec{p}_R\|$ (MeV/c)	508.533	495.852	470.570	431.241	564.113
θ_{pq} ($^\circ$)	29.990	29.192	28.105	25.698	32.751
ϕ_x ($^\circ$)	180.000	179.831	179.820	157.168	203.447
E_{miss} (MeV)	31.671	12.100	12.100	12.100	12.100
W (GeV)	15.316	15.297	15.283	15.263	15.332
θ_{CM} ($^\circ$)	32.764	31.896	30.715	28.212	35.609

Table A.35: E_e = 2.445 GeV: $^1P_{1/2}$ state, $\Sigma 1$ Kinematics, $\theta_{pq} = 30^\circ$.

A.3 The $^1P_{3/2}$ state of ^{16}O

Variable	Central	Average	Centroid	Minimum	Maximum
θ_e (°)	100.760	100.753	100.748	99.331	102.192
ω (MeV)	445.000	444.959	443.801	427.010	462.997
$\|\vec{q}\|$ (MeV/c)	1000.116	1000.124	1000.750	982.693	1018.341
Q^2 ((GeV/c)^2)	.802	.802	.804	.751	.854
θ_q (°)	-23.136	-23.126	-23.181	-24.282	-21.986
ϕ_q (°)	.000	-.003	.011	-1.396	1.393
X	.961	.962	.967	.865	1.065
ϵ	.216	.216	.216	.204	.227
$\|\vec{p}\,'\|$ (MeV/c)	973.000	991.034	989.395	966.076	1015.792
$\|\vec{p}_R\|$ (MeV/c)	27.117	38.996	47.740	1.154	86.739
θ_{pq} (°)	.016	1.824	2.303	.029	4.649
ϕ_x (°)	.000	180.808	180.764	.168	359.889
E_{miss} (MeV)	31.552	18.400	18.400	18.400	18.400
W (GeV)	15.316	15.316	15.315	15.297	15.336
θ_{CM} (°)	.018	1.999	2.525	.031	5.094

Table A.36: E_e = 0.845 GeV: $^1P_{3/2}$ state, $\|$ Kinematics.

Variable	Central	Average	Centroid	Minimum	Maximum
θ_e (°)	100.760	100.753	100.732	99.331	102.192
ω (MeV)	445.000	444.959	445.399	427.010	462.997
$\|\vec{q}\|$ (MeV/c)	1000.116	1000.124	999.758	982.693	1018.341
Q^2 ((GeV/c)^2)	.802	.802	.801	.751	.854
θ_q (°)	-23.136	-23.126	-23.110	-24.282	-21.986
ϕ_q (°)	.000	-.003	-.004	-1.396	1.393
X	.961	.962	.960	.865	1.065
ϵ	.216	.216	.216	.204	.227
$\|\vec{p}\,'\|$ (MeV/c)	973.000	990.502	991.105	965.579	1015.260
$\|\vec{p}_R\|$ (MeV/c)	106.483	111.174	111.402	71.311	149.797
θ_{pq} (°)	5.984	6.260	6.279	3.656	8.535
ϕ_x (°)	180.000	180.183	180.206	136.617	222.818
E_{miss} (MeV)	31.173	18.400	18.400	18.400	18.400
W (GeV)	15.316	15.316	15.317	15.297	15.336
θ_{CM} (°)	6.564	6.861	6.881	4.013	9.340

Table A.37: E_e = 0.845 GeV: $^1P_{3/2}$ state, $\Sigma 3$ Kinematics, θ_{pq} = 6°.

Variable	Central	Average	Centroid	Minimum	Maximum
θ_e ($^\circ$)	100.760	100.753	100.696	99.331	102.192
ω (MeV)	445.000	444.959	444.172	427.010	462.997
$\lvert\vec{q}\rvert$ (MeV/c)	1000.116	1000.124	1000.228	982.693	1018.341
Q^2 ((GeV/c)^2)	.802	.802	.803	.751	.854
θ_q ($^\circ$)	-23.136	-23.126	-23.177	-24.282	-21.986
ϕ_q ($^\circ$)	.000	-.003	-.004	-1.396	1.393
X	.961	.962	.965	.865	1.065
ϵ	.216	.216	.216	.204	.227
$\lvert\vec{p}\,'\rvert$ (MeV/c)	971.000	989.836	988.807	964.893	1014.623
$\lvert\vec{p}_R\rvert$ (MeV/c)	157.076	160.826	157.413	119.937	201.044
θ_{pq} ($^\circ$)	8.984	9.172	8.974	6.654	11.440
ϕ_x ($^\circ$)	180.000	180.130	180.095	148.878	210.913
E_{miss} (MeV)	32.136	18.400	18.400	18.400	18.400
W (GeV)	15.316	15.316	15.316	15.297	15.336
θ_{CM} ($^\circ$)	9.853	10.050	9.835	7.304	12.514

Table A.38: E_e = 0.845 GeV: $^1P_{3/2}$ state, $\Sigma3$ Kinematics, $\theta_{pq} = 9^\circ$.

Variable	Central	Average	Centroid	Minimum	Maximum
θ_e ($^\circ$)	100.760	100.754	100.687	99.331	102.192
ω (MeV)	445.000	444.944	443.791	427.010	462.997
$\lvert\vec{q}\rvert$ (MeV/c)	1000.116	1000.134	1000.387	982.693	1018.341
Q^2 ((GeV/c)^2)	.802	.802	.804	.751	.854
θ_q ($^\circ$)	-23.136	-23.127	-23.197	-24.282	-21.986
ϕ_q ($^\circ$)	.000	-.003	-.003	-1.396	1.393
X	.961	.962	.966	.865	1.065
ϵ	.216	.216	.216	.204	.227
$\lvert\vec{p}\,'\rvert$ (MeV/c)	970.000	988.888	987.387	963.944	1013.582
$\lvert\vec{p}_R\rvert$ (MeV/c)	207.822	211.434	207.170	169.727	252.577
θ_{pq} ($^\circ$)	11.984	12.127	11.881	9.653	14.417
ϕ_x ($^\circ$)	180.000	180.101	180.068	155.695	204.393
E_{miss} (MeV)	32.193	18.400	18.400	18.400	18.400
W (GeV)	15.316	15.316	15.315	15.297	15.336
θ_{CM} ($^\circ$)	13.140	13.284	13.017	10.594	15.764

Table A.39: E_e = 0.845 GeV: $^1P_{3/2}$ state, $\Sigma3$ Kinematics, $\theta_{pq} = 12^\circ$.

Variable	Central	Average	Centroid	Minimum	Maximum
θ_e (°)	100.760	100.755	100.649	99.331	102.192
ω (MeV)	445.000	444.895	442.395	427.010	462.997
$\lvert\vec{q}\rvert$ (MeV/c)	1000.116	1000.167	1000.946	982.693	1018.341
Q^2 ((GeV/c)^2)	.802	.802	.806	.751	.854
θ_q (°)	-23.136	-23.129	-23.272	-24.282	-21.986
ϕ_q (°)	.000	-.003	-.002	-1.396	1.393
X	.961	.962	.972	.865	1.065
ϵ	.216	.216	.217	.204	.227
$\lvert\vec{p}\,'\rvert$ (MeV/c)	968.000	987.180	983.943	962.277	1011.550
$\lvert\vec{p}_R\rvert$ (MeV/c)	275.472	279.231	271.467	236.934	321.161
θ_{pq} (°)	15.984	16.092	15.648	13.653	18.397
ϕ_x (°)	180.000	180.072	180.021	160.989	199.260
E_{miss} (MeV)	32.462	18.400	18.400	18.400	18.400
W (GeV)	15.316	15.316	15.314	15.297	15.336
θ_{CM} (°)	17.517	17.618	17.137	14.976	20.105

Table A.40: $E_e = 0.845$ GeV: $^1P_{3/2}$ state, $\Sigma3$ Kinematics, $\theta_{pq} = 16°$.

Variable	Central	Average	Centroid	Minimum	Maximum
θ_e (°)	100.760	100.753	100.630	99.331	102.192
ω (MeV)	445.000	444.959	441.853	427.010	462.997
$\lvert\vec{q}\rvert$ (MeV/c)	1000.116	1000.124	1001.138	982.693	1018.341
Q^2 ((GeV/c)^2)	.802	.802	.807	.751	.854
θ_q (°)	-23.136	-23.126	-23.302	-24.282	-21.986
ϕ_q (°)	.000	-.003	-.001	-1.396	1.393
X	.961	.962	.974	.865	1.065
ϵ	.216	.216	.217	.204	.227
$\lvert\vec{p}\,'\rvert$ (MeV/c)	968.000	986.279	982.275	961.267	1011.196
$\lvert\vec{p}_R\rvert$ (MeV/c)	309.234	313.089	303.808	270.587	355.307
θ_{pq} (°)	17.984	18.079	17.550	15.653	20.391
ϕ_x (°)	180.000	180.068	180.012	162.708	197.507
E_{miss} (MeV)	31.757	18.400	18.400	18.400	18.400
W (GeV)	15.316	15.316	15.313	15.297	15.336
θ_{CM} (°)	19.701	19.788	19.216	17.165	22.276

Table A.41: $E_e = 0.845$ GeV: $^1P_{3/2}$ state, $\Sigma3$ Kinematics, $\theta_{pq} = 18°$.

Variable	Central	Average	Centroid	Minimum	Maximum
θ_e ($^\circ$)	100.760	100.754	100.620	99.331	102.192
ω (MeV)	445.000	444.947	441.474	427.010	462.997
$\|\vec{q}\|$ (MeV/c)	1000.116	1000.133	1001.289	982.693	1018.341
Q^2 ((GeV/c)^2)	.802	.802	.808	.751	.854
θ_q ($^\circ$)	-23.136	-23.127	-23.322	-24.282	-21.986
ϕ_q ($^\circ$)	.000	-.003	-.001	-1.396	1.393
X	.961	.962	.976	.865	1.065
ϵ	.216	.216	.217	.204	.227
$\|\vec{p}\,'\|$ (MeV/c)	967.000	985.727	981.258	960.715	1010.497
$\|\vec{p}_R\|$ (MeV/c)	326.030	329.994	319.816	287.398	372.332
θ_{pq} ($^\circ$)	18.984	19.075	18.495	16.653	21.388
ϕ_x ($^\circ$)	180.000	180.065	180.006	163.426	196.765
E_{miss} (MeV)	32.094	18.400	18.400	18.400	18.400
W (GeV)	15.316	15.316	15.313	15.297	15.336
θ_{CM} ($^\circ$)	20.794	20.874	20.249	18.259	23.360

Table A.42: $E_e = 0.845$ GeV: $^1P_{3/2}$ state, $\Sigma3$ Kinematics, $\theta_{pq} = 19^\circ$.

Variable	Central	Average	Centroid	Minimum	Maximum
θ_e ($^\circ$)	100.760	100.753	100.620	99.331	102.192
ω (MeV)	445.000	444.959	441.498	427.010	462.997
$\|\vec{q}\|$ (MeV/c)	1000.116	1000.124	1001.276	982.693	1018.341
Q^2 ((GeV/c)^2)	.802	.802	.808	.751	.854
θ_q ($^\circ$)	-23.136	-23.126	-23.321	-24.282	-21.986
ϕ_q ($^\circ$)	.000	-.003	-.001	-1.396	1.393
X	.961	.962	.976	.865	1.065
ϵ	.216	.216	.217	.204	.227
$\|\vec{p}\,'\|$ (MeV/c)	967.000	985.179	980.741	960.135	1010.140
$\|\vec{p}_R\|$ (MeV/c)	342.863	346.865	336.768	304.191	389.320
θ_{pq} ($^\circ$)	19.984	20.070	19.496	17.652	22.385
ϕ_x ($^\circ$)	180.000	180.061	180.006	164.076	196.094
E_{miss} (MeV)	31.692	18.400	18.400	18.400	18.400
W (GeV)	15.316	15.316	15.313	15.297	15.336
θ_{CM} ($^\circ$)	21.884	21.959	21.340	19.352	24.445

Table A.43: $E_e = 0.845$ GeV: $^1P_{3/2}$ state, $\Sigma3$ Kinematics, $\theta_{pq} = 20^\circ$.

Variable	Central	Average	Centroid	Minimum	Maximum
θ_e (°)	37.170	37.210	37.051	35.742	38.602
ω (MeV)	445.000	431.612	438.588	400.612	462.986
$\lvert\vec{q}\rvert$ (MeV/c)	1000.038	999.643	996.997	966.221	1030.754
Q^2 ((GeV/c)^2)	.802	.813	.802	.735	.891
θ_q (°)	-46.468	-47.196	-46.780	-49.031	-45.229
ϕ_q (°)	.000	-.020	-.032	-4.232	4.212
X	.960	1.006	.976	.851	1.178
ϵ	.780	.782	.782	.766	.799
$\lvert\vec{p}\,'\rvert$ (MeV/c)	970.000	969.980	979.938	926.356	1013.641
$\lvert\vec{p}_R\rvert$ (MeV/c)	208.387	226.465	214.916	170.043	285.711
θ_{pq} (°)	12.018	13.019	12.372	9.662	16.269
ϕ_x (°)	.000	176.645	177.500	.002	359.998
E_{miss} (MeV)	32.185	18.400	18.400	18.400	18.400
W (GeV)	15.316	15.303	15.310	15.272	15.336
θ_{CM} (°)	13.177	14.275	13.556	10.567	17.862

Table A.44: E_e = 1.645 GeV: $^1P_{3/2}$ state, $\Sigma 4$ Kinematics, θ_{pq} = -12°.

Variable	Central	Average	Centroid	Minimum	Maximum
θ_e (°)	37.170	37.210	37.063	35.742	38.602
ω (MeV)	445.000	431.665	438.269	400.612	462.986
$\lvert\vec{q}\rvert$ (MeV/c)	1000.038	999.664	997.207	966.221	1030.754
Q^2 ((GeV/c)^2)	.802	.813	.802	.735	.891
θ_q (°)	-46.468	-47.193	-46.800	-49.031	-45.229
ϕ_q (°)	.000	-.018	-.030	-4.232	4.212
X	.960	1.006	.977	.851	1.178
ϵ	.780	.782	.782	.766	.799
$\lvert\vec{p}\,'\rvert$ (MeV/c)	971.000	971.037	980.414	927.350	1014.689
$\lvert\vec{p}_R\rvert$ (MeV/c)	157.637	177.355	166.065	118.771	241.157
θ_{pq} (°)	9.018	10.097	9.491	6.683	13.433
ϕ_x (°)	.000	176.116	175.916	.003	359.968
E_{miss} (MeV)	32.129	18.400	18.400	18.400	18.400
W (GeV)	15.316	15.303	15.310	15.272	15.336
θ_{CM} (°)	9.891	11.076	10.403	7.310	14.755

Table A.45: E_e = 1.645 GeV: $^1P_{3/2}$ state, $\Sigma 4$ Kinematics, θ_{pq} = -9°.

Variable	Central	Average	Centroid	Minimum	Maximum
θ_e (°)	37.170	37.211	37.213	35.742	38.602
ω (MeV)	445.000	432.060	428.730	400.870	463.999
$\|\vec{q}\|$ (MeV/c)	1000.038	999.716	999.473	966.221	1030.754
Q^2 ((GeV/c)^2)	.802	.813	.815	.735	.892
θ_q (°)	-46.468	-47.170	-47.354	-49.052	-45.193
ϕ_q (°)	.000	-.013	.006	-4.232	4.212
X	.960	1.005	1.016	.851	1.184
ϵ	.780	.782	.782	.766	.799
$\|\vec{p}\,'\|$ (MeV/c)	973.000	972.963	968.258	929.228	1016.747
$\|\vec{p}_R\|$ (MeV/c)	27.040	59.710	71.125	3.180	139.908
θ_{pq} (°)	.018	2.711	3.306	.041	7.352
ϕ_x (°)	.000	177.765	177.468	.160	359.956
E_{miss} (MeV)	31.552	18.400	18.400	18.400	18.400
W (GeV)	15.316	15.303	15.300	15.271	15.336
θ_{CM} (°)	.020	2.975	3.628	.045	8.083

Table A.46: E_e = 1.645 GeV: $^1P_{3/2}$ state, $\|$ Kinematics.

Variable	Central	Average	Centroid	Minimum	Maximum
θ_e (°)	37.170	37.209	37.094	35.742	38.602
ω (MeV)	445.000	431.437	428.581	399.779	463.545
$\|\vec{q}\|$ (MeV/c)	1000.038	999.630	996.895	966.221	1030.754
Q^2 ((GeV/c)^2)	.802	.813	.810	.735	.892
θ_q (°)	-46.468	-47.206	-47.358	-49.086	-45.229
ϕ_q (°)	.000	-.011	-.013	-4.232	4.212
X	.960	1.007	1.009	.851	1.184
ϵ	.780	.782	.783	.766	.799
$\|\vec{p}\,'\|$ (MeV/c)	971.000	971.098	967.220	927.318	1014.685
$\|\vec{p}_R\|$ (MeV/c)	157.027	154.787	149.019	99.713	221.281
θ_{pq} (°)	8.982	8.663	8.343	5.284	12.592
ϕ_x (°)	180.000	179.700	179.586	132.530	229.176
E_{miss} (MeV)	32.136	18.400	18.400	18.400	18.400
W (GeV)	15.316	15.303	15.300	15.271	15.336
θ_{CM} (°)	9.851	9.501	9.150	5.800	13.777

Table A.47: E_e = 1.645 GeV: $^1P_{3/2}$ state, $\Sigma 5$ Kinematics, θ_{pq} = 9°.

Variable	Central	Average	Centroid	Minimum	Maximum
θ_e (°)	37.170	37.209	37.088	35.742	38.602
ω (MeV)	445.000	431.359	427.003	399.704	463.545
$\|\vec{q}\|$ (MeV/c)	1000.038	999.616	996.631	966.221	1030.754
Q^2 ((GeV/c)^2)	.802	.813	.811	.735	.892
θ_q (°)	-46.468	-47.210	-47.448	-49.112	-45.229
ϕ_q (°)	.000	-.009	-.011	-4.232	4.212
X	.960	1.007	1.014	.851	1.184
ϵ	.780	.782	.784	.766	.799
$\|\vec{p}\,'\|$ (MeV/c)	970.000	970.134	964.228	926.387	1013.630
$\|\vec{p}_R\|$ (MeV/c)	207.774	202.824	195.186	146.456	268.495
θ_{pq} (°)	11.982	11.552	11.130	8.283	15.312
ϕ_x (°)	180.000	179.788	179.690	142.356	218.436
E_{miss} (MeV)	32.194	18.400	18.400	18.400	18.400
W (GeV)	15.316	15.303	15.299	15.270	15.336
θ_{CM} (°)	13.138	12.666	12.205	9.089	16.748

Table A.48: E_e = 1.645 GeV: $^1P_{3/2}$ state, Σ5 Kinematics, θ_{pq} = 12°.

Variable	Central	Average	Centroid	Minimum	Maximum
θ_e (°)	23.360	23.433	22.914	21.932	24.792
ω (MeV)	445.000	432.554	442.335	401.349	463.778
$\|\vec{q}\|$ (MeV/c)	999.838	999.568	984.235	942.459	1051.421
Q^2 ((GeV/c)^2)	.802	.812	.773	.704	.917
θ_q (°)	-52.480	-53.116	-52.334	-55.353	-50.741
ϕ_q (°)	.000	-.015	.009	-6.848	6.860
X	.960	1.003	.933	.813	1.212
ϵ	.904	.904	.907	.893	.915
$\|\vec{p}\,'\|$ (MeV/c)	967.000	967.367	981.800	923.537	1010.504
$\|\vec{p}_R\|$ (MeV/c)	343.237	360.661	337.243	299.141	421.130
θ_{pq} (°)	20.010	20.984	19.697	17.265	24.424
ϕ_x (°)	.000	175.858	171.272	.003	359.994
E_{miss} (MeV)	31.683	18.400	18.400	18.400	18.400
W (GeV)	15.316	15.304	15.315	15.272	15.336
θ_{CM} (°)	21.913	22.977	21.526	18.829	26.772

Table A.49: E_e = 2.445 GeV: $^1P_{3/2}$ state, Σ2 Kinematics, θ_{pq} = -20°.

Variable	Central	Average	Centroid	Minimum	Maximum
θ_e ($^\circ$)	23.360	23.435	22.915	21.932	24.792
ω (MeV)	445.000	432.212	442.193	400.691	463.778
$\vert\vec{q}\vert$ (MeV/c)	999.838	999.529	984.230	942.459	1051.421
Q^2 ((GeV/c)^2)	.802	.813	.773	.704	.917
θ_q ($^\circ$)	-52.480	-53.135	-52.343	-55.353	-50.741
ϕ_q ($^\circ$)	.000	-.026	-.003	-6.848	6.860
X	.960	1.004	.933	.813	1.212
ϵ	.904	.904	.907	.893	.915
$\vert\vec{p}\,'\vert$ (MeV/c)	967.000	967.455	982.140	923.613	1010.455
$\vert\vec{p}_R\vert$ (MeV/c)	326.405	344.575	320.738	282.359	404.932
θ_{pq} ($^\circ$)	19.010	20.024	18.713	16.266	23.505
ϕ_x ($^\circ$)	.000	176.225	172.541	.012	359.994
E_{miss} (MeV)	32.085	18.400	18.400	18.400	18.400
W (GeV)	15.316	15.304	15.315	15.271	15.336
θ_{CM} ($^\circ$)	20.822	21.930	20.455	17.742	25.771

Table A.50: E_e = 2.445 GeV: $^1P_{3/2}$ state, $\Sigma 2$ Kinematics, θ_{pq} = -19°.

Variable	Central	Average	Centroid	Minimum	Maximum
θ_e ($^\circ$)	23.360	23.434	22.949	21.932	24.792
ω (MeV)	445.000	432.512	442.048	401.349	463.778
$\vert\vec{q}\vert$ (MeV/c)	999.838	999.575	985.338	942.459	1051.421
Q^2 ((GeV/c)^2)	.802	.812	.776	.704	.917
θ_q ($^\circ$)	-52.480	-53.118	-52.367	-55.353	-50.741
ϕ_q ($^\circ$)	.000	-.022	.003	-6.848	6.860
X	.960	1.003	.937	.813	1.212
ϵ	.904	.904	.906	.893	.915
$\vert\vec{p}\,'\vert$ (MeV/c)	968.000	968.430	982.414	924.491	1011.545
$\vert\vec{p}_R\vert$ (MeV/c)	309.612	327.931	305.321	265.569	388.734
θ_{pq} ($^\circ$)	18.010	19.026	17.785	15.268	22.593
ϕ_x ($^\circ$)	.000	175.810	173.386	.021	359.987
E_{miss} (MeV)	31.749	18.400	18.400	18.400	18.400
W (GeV)	15.316	15.304	15.314	15.271	15.336
θ_{CM} ($^\circ$)	19.730	20.841	19.446	16.656	24.775

Table A.51: E_e = 2.445 GeV: $^1P_{3/2}$ state, $\Sigma 2$ Kinematics, θ_{pq} = -18°.

Variable	Central	Average	Centroid	Minimum	Maximum
θ_e (°)	23.360	23.433	22.999	21.932	24.792
ω (MeV)	445.000	431.709	440.494	400.257	462.690
$\lvert\vec{q}\rvert$ (MeV/c)	999.838	999.349	986.646	942.459	1051.421
Q^2 ((GeV/c)^2)	.802	.813	.780	.704	.917
θ_q (°)	-52.480	-53.163	-52.478	-55.353	-50.741
ϕ_q (°)	.000	-.036	-.024	-6.848	6.860
X	.960	1.005	.945	.813	1.212
ϵ	.904	.904	.906	.893	.915
$\lvert\vec{p}\,'\rvert$ (MeV/c)	968.000	968.308	981.127	924.453	1011.507
$\lvert\vec{p}_R\rvert$ (MeV/c)	275.851	295.734	274.963	231.995	359.477
θ_{pq} (°)	16.010	17.113	15.983	13.271	20.792
ϕ_x (°)	.000	175.856	173.175	.009	359.998
E_{miss} (MeV)	32.455	18.400	18.400	18.400	18.400
W (GeV)	15.316	15.303	15.313	15.271	15.336
θ_{CM} (°)	17.545	18.752	17.486	14.481	22.829

Table A.52: E_e = 2.445 GeV: $^1P_{3/2}$ state, Σ2 Kinematics, θ_{pq} = -16°.

Variable	Central	Average	Centroid	Minimum	Maximum
θ_e (°)	23.360	23.432	23.111	21.932	24.792
ω (MeV)	445.000	431.924	438.195	400.257	463.446
$\lvert\vec{q}\rvert$ (MeV/c)	999.838	999.384	989.906	942.459	1051.421
Q^2 ((GeV/c)^2)	.802	.813	.788	.704	.917
θ_q (°)	-52.480	-53.151	-52.659	-55.353	-50.741
ϕ_q (°)	.000	-.031	-.025	-6.848	6.860
X	.960	1.005	.960	.813	1.212
ϵ	.904	.904	.906	.893	.915
$\lvert\vec{p}\,'\rvert$ (MeV/c)	970.000	970.308	979.378	926.373	1013.611
$\lvert\vec{p}_R\rvert$ (MeV/c)	208.204	230.669	215.160	165.206	301.099
θ_{pq} (°)	12.010	13.237	12.421	9.282	17.319
ϕ_x (°)	.000	175.661	174.008	.017	359.992
E_{miss} (MeV)	32.187	18.400	18.400	18.400	18.400
W (GeV)	15.316	15.303	15.310	15.271	15.336
θ_{CM} (°)	13.169	14.514	13.601	10.132	19.011

Table A.53: E_e = 2.445 GeV: $^1P_{3/2}$ state, Σ2 Kinematics, θ_{pq} = -12°.

Variable	Central	Average	Centroid	Minimum	Maximum
θ_e (°)	23.360	23.433	23.135	21.932	24.792
ω (MeV)	445.000	431.996	437.860	400.448	463.778
$\vert\vec{q}\vert$ (MeV/c)	999.838	999.431	990.652	942.459	1051.421
Q^2 ((GeV/c)^2)	.802	.813	.790	.704	.917
θ_q (°)	-52.480	-53.147	-52.691	-55.353	-50.741
ϕ_q (°)	.000	-.034	-.031	-6.848	6.860
X	.960	1.004	.963	.813	1.212
ϵ	.904	.904	.906	.893	.915
$\vert\vec{p}\,'\vert$ (MeV/c)	971.000	971.384	979.812	927.352	1014.648
$\vert\vec{p}_R\vert$ (MeV/c)	157.452	183.055	167.692	116.243	259.643
θ_{pq} (°)	9.010	10.397	9.601	6.298	14.886
ϕ_x (°)	.000	175.995	174.668	.013	359.920
E_{miss} (MeV)	32.131	18.400	18.400	18.400	18.400
W (GeV)	15.316	15.303	15.310	15.271	15.336
θ_{CM} (°)	9.882	11.404	10.518	6.877	16.347

Table A.54: E_e = 2.445 GeV: $^1P_{3/2}$ state, Σ2 Kinematics, θ_{pq} = -9°.

Variable	Central	Average	Centroid	Minimum	Maximum
θ_e (°)	23.360	23.433	23.233	21.932	24.792
ω (MeV)	445.000	432.771	435.244	401.349	464.134
$\vert\vec{q}\vert$ (MeV/c)	999.838	999.613	993.347	942.459	1051.421
Q^2 ((GeV/c)^2)	.802	.812	.798	.703	.917
θ_q (°)	-52.480	-53.104	-52.879	-55.353	-50.640
ϕ_q (°)	.000	-.019	-.020	-6.848	6.860
X	.960	1.002	.978	.808	1.212
ϵ	.904	.904	.905	.893	.915
$\vert\vec{p}\,'\vert$ (MeV/c)	973.000	973.189	976.745	929.232	1016.781
$\vert\vec{p}_R\vert$ (MeV/c)	106.842	137.063	128.889	67.615	222.889
θ_{pq} (°)	6.010	7.631	7.244	3.237	12.696
ϕ_x (°)	.000	176.926	175.845	.047	359.978
E_{miss} (MeV)	31.170	18.400	18.400	18.400	18.400
W (GeV)	15.316	15.304	15.307	15.271	15.338
θ_{CM} (°)	6.593	8.372	7.941	3.533	13.946

Table A.55: E_e = 2.445 GeV: $^1P_{3/2}$ state, Σ2 Kinematics, θ_{pq} = -6°.

Variable	Central	Average	Centroid	Minimum	Maximum
θ_e ($^\circ$)	23.360	23.435	23.386	21.932	24.792
ω (MeV)	445.000	432.341	431.723	400.775	463.863
$\|\vec{q}\|$ (MeV/c)	999.838	999.568	997.802	942.459	1051.421
Q^2 ((GeV/c)^2)	.802	.813	.809	.704	.917
θ_q ($^\circ$)	-52.480	-53.128	-53.124	-55.353	-50.741
ϕ_q ($^\circ$)	.000	-.020	-.009	-6.848	6.860
X	.960	1.004	1.002	.813	1.212
ϵ	.904	.904	.905	.893	.915
$\|\vec{p}\,'\|$ (MeV/c)	973.000	973.225	972.296	929.247	1016.622
$\|\vec{p}_R\|$ (MeV/c)	26.838	75.502	85.194	1.484	177.873
θ_{pq} ($^\circ$)	.010	3.647	4.249	.047	10.100
ϕ_x ($^\circ$)	.000	178.164	178.875	.030	359.809
E_{miss} (MeV)	31.552	18.400	18.400	18.400	18.400
W (GeV)	15.316	15.304	15.303	15.271	15.337
θ_{CM} ($^\circ$)	.011	4.002	4.661	.052	11.085

Table A.56: E$_e$ = 2.445 GeV: ^{1}P$_{3/2}$ state, $\|$ Kinematics.

Variable	Central	Average	Centroid	Minimum	Maximum
θ_e ($^\circ$)	23.360	23.433	23.287	21.932	24.792
ω (MeV)	445.000	432.687	433.182	401.054	464.552
$\|\vec{q}\|$ (MeV/c)	999.838	999.592	994.713	942.459	1051.421
Q^2 ((GeV/c)^2)	.802	.812	.802	.703	.917
θ_q ($^\circ$)	-52.480	-53.108	-53.018	-55.353	-50.640
ϕ_q ($^\circ$)	.000	-.021	-.029	-6.848	6.860
X	.960	1.003	.989	.808	1.212
ϵ	.904	.904	.905	.893	.915
$\|\vec{p}\,'\|$ (MeV/c)	973.000	973.286	974.006	929.216	1016.783
$\|\vec{p}_R\|$ (MeV/c)	106.502	121.114	118.941	53.280	212.200
θ_{pq} ($^\circ$)	5.990	6.547	6.508	2.148	12.009
ϕ_x ($^\circ$)	180.000	179.630	179.510	104.992	253.463
E_{miss} (MeV)	31.173	18.400	18.400	18.400	18.400
W (GeV)	15.316	15.304	15.305	15.271	15.338
θ_{CM} ($^\circ$)	6.570	7.180	7.134	2.370	13.156

Table A.57: E$_e$ = 2.445 GeV: ^{1}P$_{3/2}$ state, Σ1 Kinematics, θ_{pq} = 6°.

Variable	Central	Average	Centroid	Minimum	Maximum
θ_e ($^\circ$)	23.360	23.433	23.262	21.932	24.792
ω (MeV)	445.000	431.711	428.276	399.963	463.815
$\|\vec{q}\|$ (MeV/c)	999.838	999.390	992.707	942.459	1051.421
Q^2 ((GeV/c)^2)	.802	.813	.802	.704	.917
θ_q ($^\circ$)	-52.480	-53.163	-53.291	-55.420	-50.741
ϕ_q ($^\circ$)	.000	-.038	-.039	-6.848	6.860
X	.960	1.005	1.000	.813	1.214
ϵ	.904	.904	.906	.893	.915
$\|\vec{p}\,'\|$ (MeV/c)	971.000	971.333	966.701	927.431	1014.662
$\|\vec{p}_R\|$ (MeV/c)	157.108	163.411	154.711	99.127	247.286
θ_{pq} ($^\circ$)	8.990	9.142	8.707	5.054	14.009
ϕ_x ($^\circ$)	180.000	179.587	179.535	119.669	237.981
E_{miss} (MeV)	32.135	18.400	18.400	18.400	18.400
W (GeV)	15.316	15.303	15.300	15.270	15.337
θ_{CM} ($^\circ$)	9.860	10.025	9.545	5.567	15.344

Table A.58: E$_e$ = 2.445 GeV: ^{1}P$_{3/2}$ state, Σ1 Kinematics, θ_{pq} = 9°.

Variable	Central	Average	Centroid	Minimum	Maximum
θ_e ($^\circ$)	23.360	23.433	23.264	21.932	24.792
ω (MeV)	445.000	431.639	426.735	399.649	463.815
$\|\vec{q}\|$ (MeV/c)	999.838	999.368	992.419	942.459	1051.421
Q^2 ((GeV/c)^2)	.802	.813	.803	.704	.917
θ_q ($^\circ$)	-52.480	-53.167	-53.378	-55.420	-50.741
ϕ_q ($^\circ$)	.000	-.041	-.043	-6.848	6.860
X	.960	1.006	1.005	.813	1.214
ϵ	.904	.904	.906	.893	.915
$\|\vec{p}\,'\|$ (MeV/c)	970.000	970.374	963.755	926.423	1013.625
$\|\vec{p}_R\|$ (MeV/c)	207.859	209.790	199.956	146.613	287.623
θ_{pq} ($^\circ$)	11.990	11.937	11.445	8.026	16.317
ϕ_x ($^\circ$)	180.000	179.667	179.598	130.532	228.283
E_{miss} (MeV)	32.193	18.400	18.400	18.400	18.400
W (GeV)	15.316	15.303	15.299	15.270	15.337
θ_{CM} ($^\circ$)	13.146	13.087	12.545	8.839	17.865

Table A.59: E$_e$ = 2.445 GeV: ^{1}P$_{3/2}$ state, Σ1 Kinematics, θ_{pq} = 12°.

Variable	Central	Average	Centroid	Minimum	Maximum
θ_e ($^\circ$)	23.360	23.430	23.238	21.932	24.792
ω (MeV)	445.000	431.224	421.341	399.042	463.815
$\lvert\vec{q}\rvert$ (MeV/c)	999.838	999.176	990.260	942.459	1051.421
Q^2 ((GeV/c)^2)	.802	.813	.803	.704	.917
θ_q ($^\circ$)	-52.480	-53.189	-53.673	-55.420	-50.741
ϕ_q ($^\circ$)	.000	-.032	-.021	-6.848	6.860
X	.960	1.006	1.018	.813	1.214
ϵ	.904	.904	.906	.893	.915
$\lvert\vec{p}\,'\rvert$ (MeV/c)	968.000	968.258	954.940	924.442	1011.430
$\lvert\vec{p}_R\rvert$ (MeV/c)	275.507	273.646	256.381	210.580	346.151
θ_{pq} ($^\circ$)	15.990	15.757	14.884	12.010	19.684
ϕ_x ($^\circ$)	180.000	179.816	179.835	140.614	219.150
E_{miss} (MeV)	32.462	18.400	18.400	18.400	18.400
W (GeV)	15.316	15.303	15.293	15.269	15.337
θ_{CM} ($^\circ$)	17.523	17.267	16.311	13.222	21.540

Table A.60: E_e = 2.445 GeV: $^1P_{3/2}$ state, Σ1 Kinematics, $\theta_{pq} = 16^\circ$.

Variable	Central	Average	Centroid	Minimum	Maximum
θ_e ($^\circ$)	23.360	23.432	23.231	21.932	24.792
ω (MeV)	445.000	431.857	419.952	399.649	464.552
$\lvert\vec{q}\rvert$ (MeV/c)	999.838	999.393	989.710	942.459	1051.421
Q^2 ((GeV/c)^2)	.802	.813	.804	.704	.917
θ_q ($^\circ$)	-52.480	-53.155	-53.749	-55.420	-50.712
ϕ_q ($^\circ$)	.000	-.035	-.042	-6.848	6.860
X	.960	1.005	1.021	.813	1.214
ϵ	.904	.904	.906	.893	.915
$\lvert\vec{p}\,'\rvert$ (MeV/c)	968.000	968.178	952.188	924.532	1011.486
$\lvert\vec{p}_R\rvert$ (MeV/c)	309.267	306.901	286.416	242.580	376.641
θ_{pq} ($^\circ$)	17.990	17.739	16.715	14.005	21.456
ϕ_x ($^\circ$)	180.000	179.807	179.744	144.326	215.714
E_{miss} (MeV)	31.756	18.400	18.400	18.400	18.400
W (GeV)	15.316	15.303	15.292	15.270	15.338
θ_{CM} ($^\circ$)	19.707	19.432	18.314	15.414	23.463

Table A.61: E_e = 2.445 GeV: $^1P_{3/2}$ state, Σ1 Kinematics, $\theta_{pq} = 18^\circ$.

Variable	Central	Average	Centroid	Minimum	Maximum
θ_e ($^\circ$)	23.360	23.431	23.220	21.932	24.792
ω (MeV)	445.000	431.497	418.464	399.383	464.109
$\|\vec{q}\|$ (MeV/c)	999.838	999.267	989.005	942.459	1051.421
Q^2 ((GeV/c)^2)	.802	.813	.803	.704	.917
θ_q ($^\circ$)	-52.480	-53.174	-53.829	-55.420	-50.741
ϕ_q ($^\circ$)	.000	-.032	-.013	-6.848	6.860
X	.960	1.006	1.025	.813	1.214
ϵ	.904	.904	.907	.893	.915
$\|\vec{p}\,'\|$ (MeV/c)	967.000	967.177	949.686	923.490	1010.438
$\|\vec{p}_R\|$ (MeV/c)	326.062	322.825	300.574	258.648	392.087
θ_{pq} ($^\circ$)	18.990	18.694	17.592	15.003	22.413
ϕ_x ($^\circ$)	180.000	179.852	179.930	145.937	214.209
E_{miss} (MeV)	32.093	18.400	18.400	18.400	18.400
W (GeV)	15.316	15.303	15.291	15.270	15.337
θ_{CM} ($^\circ$)	20.800	20.476	19.273	16.510	24.493

Table A.62: E_e = 2.445 GeV: $^1P_{3/2}$ state, Σ1 Kinematics, $\theta_{pq} = 19^\circ$.

Variable	Central	Average	Centroid	Minimum	Maximum
θ_e ($^\circ$)	23.360	23.432	23.224	21.932	24.792
ω (MeV)	445.000	431.900	418.914	399.632	464.552
$\|\vec{q}\|$ (MeV/c)	999.838	999.394	989.227	942.459	1051.421
Q^2 ((GeV/c)^2)	.802	.813	.803	.704	.917
θ_q ($^\circ$)	-52.480	-53.152	-53.804	-55.420	-50.712
ϕ_q ($^\circ$)	.000	-.040	-.040	-6.848	6.860
X	.960	1.005	1.024	.813	1.214
ϵ	.904	.904	.907	.893	.915
$\|\vec{p}\,'\|$ (MeV/c)	967.000	967.184	949.795	923.487	1010.504
$\|\vec{p}_R\|$ (MeV/c)	342.894	339.628	317.490	274.743	407.911
θ_{pq} ($^\circ$)	19.990	19.696	18.613	16.001	23.374
ϕ_x ($^\circ$)	180.000	179.814	179.794	147.409	212.825
E_{miss} (MeV)	31.691	18.400	18.400	18.400	18.400
W (GeV)	15.316	15.303	15.291	15.270	15.338
θ_{CM} ($^\circ$)	21.890	21.569	20.388	17.606	25.537

Table A.63: E_e = 2.445 GeV: $^1P_{3/2}$ state, Σ1 Kinematics, $\theta_{pq} = 20^\circ$.

Variable	Central	Average	Centroid	Minimum	Maximum
θ_e (°)	23.360	23.430	23.265	21.932	24.792
ω (MeV)	445.000	431.656	427.718	399.042	464.671
$\lvert\vec{q}\rvert$ (MeV/c)	999.838	999.271	992.690	942.459	1051.421
Q^2 ((GeV/c)^2)	.802	.812	.803	.704	.917
θ_q (°)	-52.480	-53.165	-53.313	-55.420	-50.712
ϕ_q (°)	.000	-.028	-.025	-6.848	6.860
X	.960	1.005	1.002	.813	1.214
ϵ	.904	.904	.906	.893	.915
$\lvert\vec{p}\,'\rvert$ (MeV/c)	960.000	960.012	954.876	916.806	1003.097
$\lvert\vec{p}_R\rvert$ (MeV/c)	508.533	502.236	495.173	435.335	571.414
θ_{pq} (°)	29.990	29.547	29.309	25.990	33.178
ϕ_x (°)	180.000	179.918	179.887	157.168	203.447
E_{miss} (MeV)	31.671	18.400	18.400	18.400	18.400
W (GeV)	15.316	15.303	15.300	15.270	15.338
θ_{CM} (°)	32.764	32.284	32.017	28.538	36.075

Table A.64: E_e = 2.445 GeV: $^1P_{3/2}$ state, Σ1 Kinematics, $\theta_{pq} = 30°$.

A.4 The $^1S_{1/2}$ state of ^{16}O

Variable	Central	Average	Centroid	Minimum	Maximum
θ_e (°)	100.760	100.753	100.721	99.331	102.192
ω (MeV)	445.000	444.959	446.466	427.010	462.997
$\lvert\vec{q}\rvert$ (MeV/c)	1000.116	1000.124	999.095	982.693	1018.341
Q^2 ((GeV/c)^2)	.802	.802	.799	.751	.854
θ_q (°)	-23.136	-23.126	-23.062	-24.282	-21.986
ϕ_q (°)	.000	-.003	-.006	-1.396	1.393
X	.961	.962	.954	.865	1.065
ϵ	.216	.216	.215	.204	.227
$\lvert\vec{p}\,'\rvert$ (MeV/c)	973.000	965.201	967.320	939.805	990.354
$\lvert\vec{p}_R\rvert$ (MeV/c)	27.117	50.315	47.262	4.102	100.982
θ_{pq} (°)	.016	1.824	1.756	.029	4.649
ϕ_x (°)	.000	180.808	181.243	.168	359.889
E_{miss} (MeV)	31.552	37.000	37.000	37.000	37.000
W (GeV)	15.316	15.316	15.318	15.297	15.336
θ_{CM} (°)	.018	2.002	1.927	.031	5.100

Table A.65: E_e = 0.845 GeV: $^1S_{1/2}$ state, $\parallel$ Kinematics.

Variable	Central	Average	Centroid	Minimum	Maximum
θ_e (°)	100.760	100.753	100.691	99.331	102.192
ω (MeV)	445.000	444.959	445.209	427.010	462.997
$\lvert\vec{q}\rvert$ (MeV/c)	1000.116	1000.124	999.622	982.693	1018.341
Q^2 ((GeV/c)^2)	.802	.802	.801	.751	.854
θ_q (°)	-23.136	-23.126	-23.129	-24.282	-21.986
ϕ_q (°)	.000	-.003	-.005	-1.396	1.393
X	.961	.962	.960	.865	1.065
ϵ	.216	.216	.216	.204	.227
$\lvert\vec{p}\,'\rvert$ (MeV/c)	973.000	964.675	965.055	939.335	989.827
$\lvert\vec{p}_R\rvert$ (MeV/c)	106.483	115.212	112.643	80.860	147.632
θ_{pq} (°)	5.984	6.260	6.121	3.656	8.535
ϕ_x (°)	180.000	180.183	180.166	136.617	222.818
E_{miss} (MeV)	31.173	37.000	37.000	37.000	37.000
W (GeV)	15.316	15.316	15.317	15.297	15.336
θ_{CM} (°)	6.564	6.869	6.716	4.019	9.351

Table A.66: $E_e = 0.845$ GeV: $^1S_{1/2}$ state, $\Sigma3$ Kinematics, $\theta_{pq} = 6°$.

Variable	Central	Average	Centroid	Minimum	Maximum
θ_e (°)	100.760	100.753	100.688	99.331	102.192
ω (MeV)	445.000	444.959	444.767	427.010	462.997
$\lvert\vec{q}\rvert$ (MeV/c)	1000.116	1000.124	999.852	982.693	1018.341
Q^2 ((GeV/c)^2)	.802	.802	.802	.751	.854
θ_q (°)	-23.136	-23.126	-23.150	-24.282	-21.986
ϕ_q (°)	.000	-.003	-.004	-1.396	1.393
X	.961	.962	.962	.865	1.065
ϵ	.216	.216	.216	.204	.227
$\lvert\vec{p}\,'\rvert$ (MeV/c)	971.000	964.018	963.797	938.658	989.204
$\lvert\vec{p}_R\rvert$ (MeV/c)	157.076	162.649	159.757	127.538	198.008
θ_{pq} (°)	8.984	9.172	9.002	6.654	11.440
ϕ_x (°)	180.000	180.130	180.112	148.878	210.913
E_{miss} (MeV)	32.136	37.000	37.000	37.000	37.000
W (GeV)	15.316	15.316	15.316	15.297	15.336
θ_{CM} (°)	9.853	10.063	9.876	7.314	12.528

Table A.67: $E_e = 0.845$ GeV: $^1S_{1/2}$ state, $\Sigma3$ Kinematics, $\theta_{pq} = 9°$.

Variable	Central	Average	Centroid	Minimum	Maximum
θ_e ($^\circ$)	100.760	100.753	100.658	99.331	102.192
ω (MeV)	445.000	444.959	443.912	427.010	462.997
$\lvert\vec{q}\rvert$ (MeV/c)	1000.116	1000.124	1000.152	982.693	1018.341
Q^2 ((GeV/c)^2)	.802	.802	.803	.751	.854
θ_q ($^\circ$)	-23.136	-23.126	-23.198	-24.282	-21.986
ϕ_q ($^\circ$)	.000	-.003	-.004	-1.396	1.393
X	.961	.962	.965	.865	1.065
ϵ	.216	.216	.216	.204	.227
$\lvert\vec{p}\,'\rvert$ (MeV/c)	970.000	963.101	961.749	937.721	988.329
$\lvert\vec{p}_R\rvert$ (MeV/c)	207.822	211.755	206.559	175.012	249.104
θ_{pq} ($^\circ$)	11.984	12.126	11.810	9.653	14.417
ϕ_x ($^\circ$)	180.000	180.100	180.060	155.695	204.393
E_{miss} (MeV)	32.193	37.000	37.000	37.000	37.000
W (GeV)	15.316	15.316	15.315	15.297	15.336
θ_{CM} ($^\circ$)	13.140	13.300	12.955	10.608	15.783

Table A.68: $E_e = 0.845$ GeV: $^1S_{1/2}$ state, $\Sigma 3$ Kinematics, $\theta_{pq} = 12^\circ$.

Variable	Central	Average	Centroid	Minimum	Maximum
θ_e ($^\circ$)	100.760	100.753	100.641	99.331	102.192
ω (MeV)	445.000	444.959	443.192	427.010	462.997
$\lvert\vec{q}\rvert$ (MeV/c)	1000.116	1000.124	1000.453	982.693	1018.341
Q^2 ((GeV/c)^2)	.802	.802	.804	.751	.854
θ_q ($^\circ$)	-23.136	-23.126	-23.236	-24.282	-21.986
ϕ_q ($^\circ$)	.000	-.003	-.003	-1.396	1.393
X	.961	.962	.968	.865	1.065
ϵ	.216	.216	.217	.204	.227
$\lvert\vec{p}\,'\rvert$ (MeV/c)	968.000	961.482	959.197	936.075	986.763
$\lvert\vec{p}_R\rvert$ (MeV/c)	275.472	278.054	271.377	239.492	317.028
θ_{pq} ($^\circ$)	15.984	16.091	15.687	13.653	18.397
ϕ_x ($^\circ$)	180.000	180.076	180.034	160.989	199.260
E_{miss} (MeV)	32.462	37.000	37.000	37.000	37.000
W (GeV)	15.316	15.316	15.315	15.297	15.336
θ_{CM} ($^\circ$)	17.517	17.640	17.201	14.997	20.128

Table A.69: $E_e = 0.845$ GeV: $^1S_{1/2}$ state, $\Sigma 3$ Kinematics, $\theta_{pq} = 16^\circ$.

Variable	Central	Average	Centroid	Minimum	Maximum
θ_e (°)	100.760	100.753	100.623	99.331	102.192
ω (MeV)	445.000	444.959	442.613	427.010	462.997
$\|\vec{q}\|$ (MeV/c)	1000.116	1000.124	1000.671	982.693	1018.341
Q^2 ((GeV/c)^2)	.802	.802	.805	.751	.854
θ_q (°)	-23.136	-23.126	-23.268	-24.282	-21.986
ϕ_q (°)	.000	-.003	-.002	-1.396	1.393
X	.961	.962	.971	.865	1.065
ϵ	.216	.216	.217	.204	.227
$\|\vec{p}\,'\|$ (MeV/c)	968.000	960.505	957.474	935.068	985.821
$\|\vec{p}_R\|$ (MeV/c)	309.234	311.278	303.197	272.060	350.827
θ_{pq} (°)	17.984	18.079	17.592	15.653	20.391
ϕ_x (°)	180.000	180.068	180.019	162.708	197.507
E_{miss} (MeV)	31.757	37.000	37.000	37.000	37.000
W (GeV)	15.316	15.316	15.314	15.297	15.336
θ_{CM} (°)	19.701	19.813	19.285	17.188	22.301

Table A.70: $E_e = 0.845$ GeV: $^1S_{1/2}$ state, $\Sigma 3$ Kinematics, $\theta_{pq} = 18°$.

Variable	Central	Average	Centroid	Minimum	Maximum
θ_e (°)	100.760	100.753	100.612	99.331	102.192
ω (MeV)	445.000	444.959	442.276	427.010	462.997
$\|\vec{q}\|$ (MeV/c)	1000.116	1000.124	1000.796	982.693	1018.341
Q^2 ((GeV/c)^2)	.802	.802	.806	.751	.854
θ_q (°)	-23.136	-23.126	-23.286	-24.282	-21.986
ϕ_q (°)	.000	-.003	-.002	-1.396	1.393
X	.961	.962	.972	.865	1.065
ϵ	.216	.216	.217	.204	.227
$\|\vec{p}\,'\|$ (MeV/c)	967.000	959.975	956.511	934.523	985.314
$\|\vec{p}_R\|$ (MeV/c)	326.030	327.878	318.983	288.386	367.675
θ_{pq} (°)	18.984	19.074	18.539	16.653	21.388
ϕ_x (°)	180.000	180.064	180.012	163.426	196.765
E_{miss} (MeV)	32.094	37.000	37.000	37.000	37.000
W (GeV)	15.316	15.316	15.314	15.297	15.336
θ_{CM} (°)	20.794	20.899	20.320	18.283	23.387

Table A.71: $E_e = 0.845$ GeV: $^1S_{1/2}$ state, $\Sigma 3$ Kinematics, $\theta_{pq} = 19°$.

Variable	Central	Average	Centroid	Minimum	Maximum
θ_e (°)	100.760	100.753	100.560	99.331	102.192
ω (MeV)	445.000	444.959	440.859	427.010	462.997
$\lvert\vec{q}\rvert$ (MeV/c)	1000.116	1000.124	1001.279	982.693	1018.341
Q^2 ((GeV/c)^2)	.802	.802	.808	.751	.854
θ_q (°)	-23.136	-23.126	-23.365	-24.282	-21.986
ϕ_q (°)	.000	-.003	0.000	-1.396	1.393
X	.961	.962	.978	.865	1.065
ϵ	.216	.216	.218	.204	.227
$\lvert\vec{p}\,'\rvert$ (MeV/c)	967.000	959.418	954.114	933.950	984.778
$\lvert\vec{p}_R\rvert$ (MeV/c)	342.863	344.462	331.769	304.723	384.485
θ_{pq} (°)	19.984	20.070	19.306	17.652	22.385
ϕ_x (°)	180.000	180.061	179.982	164.076	196.094
E_{miss} (MeV)	31.692	37.000	37.000	37.000	37.000
W (GeV)	15.316	15.316	15.312	15.297	15.336
θ_{CM} (°)	21.884	21.986	21.161	19.378	24.472

Table A.72: E$_e$ = 0.845 GeV: ^{1}S$_{1/2}$ state, Σ3 Kinematics, θ_{pq} = 20°.

Variable	Central	Average	Centroid	Minimum	Maximum
θ_e (°)	37.170	37.207	37.023	35.742	38.602
ω (MeV)	445.000	450.220	458.961	418.866	481.223
$\lvert\vec{q}\rvert$ (MeV/c)	1000.038	1001.561	998.807	968.091	1032.603
Q^2 ((GeV/c)^2)	.802	.800	.787	.723	.878
θ_q (°)	-46.468	-46.136	-45.615	-48.025	-44.183
ϕ_q (°)	.000	-.027	-.051	-4.111	4.100
X	.960	.949	.915	.803	1.115
ϵ	.780	.779	.779	.763	.796
$\lvert\vec{p}\,'\rvert$ (MeV/c)	970.000	970.356	982.801	926.394	1013.618
$\lvert\vec{p}_R\rvert$ (MeV/c)	208.387	209.513	195.089	153.689	268.973
θ_{pq} (°)	12.018	11.984	11.188	8.692	15.321
ϕ_x (°)	.000	180.111	181.849	.012	359.994
E_{miss} (MeV)	32.185	37.000	37.000	37.000	37.000
W (GeV)	15.316	15.322	15.330	15.289	15.354
θ_{CM} (°)	13.177	13.144	12.260	9.502	16.840

Table A.73: E$_e$ = 1.645 GeV: ^{1}S$_{1/2}$ state, Σ4 Kinematics, θ_{pq} = -12°.

Variable	Central	Average	Centroid	Minimum	Maximum
θ_e ($^\circ$)	37.170	37.208	37.061	35.742	38.602
ω (MeV)	445.000	450.281	456.344	418.866	481.435
$\|\vec{q}\|$ (MeV/c)	1000.038	1001.590	999.269	968.091	1032.603
Q^2 ((GeV/c)^2)	.802	.800	.790	.723	.878
θ_q ($^\circ$)	-46.468	-46.132	-45.769	-48.025	-44.183
ϕ_q ($^\circ$)	.000	-.029	-.049	-4.111	4.100
X	.960	.949	.925	.803	1.115
ϵ	.780	.779	.779	.763	.796
$\|\vec{p}\,'\|$ (MeV/c)	971.000	971.333	979.928	927.338	1014.683
$\|\vec{p}_R\|$ (MeV/c)	157.637	160.785	150.359	102.706	226.109
θ_{pq} ($^\circ$)	9.018	9.080	8.540	5.696	12.678
ϕ_x ($^\circ$)	.000	178.440	178.314	.003	359.998
E_{miss} (MeV)	32.129	37.000	37.000	37.000	37.000
W (GeV)	15.316	15.322	15.328	15.289	15.354
θ_{CM} ($^\circ$)	9.891	9.961	9.363	6.229	13.931

Table A.74: E$_e$ = 1.645 GeV: ^{1}S$_{1/2}$ state, Σ4 Kinematics, θ_{pq} = -9°.

Variable	Central	Average	Centroid	Minimum	Maximum
θ_e ($^\circ$)	37.170	37.207	37.081	35.742	38.602
ω (MeV)	445.000	451.080	453.332	419.552	482.513
$\|\vec{q}\|$ (MeV/c)	1000.038	1001.679	999.308	968.091	1032.603
Q^2 ((GeV/c)^2)	.802	.800	.793	.723	.878
θ_q ($^\circ$)	-46.468	-46.087	-45.944	-48.025	-44.122
ϕ_q ($^\circ$)	.000	-.019	-.042	-4.111	4.100
X	.960	.947	.934	.801	1.115
ϵ	.780	.779	.779	.762	.796
$\|\vec{p}\,'\|$ (MeV/c)	973.000	973.543	976.717	929.234	1016.774
$\|\vec{p}_R\|$ (MeV/c)	27.040	60.434	54.553	6.717	135.808
θ_{pq} ($^\circ$)	.018	2.632	2.421	.041	7.300
ϕ_x ($^\circ$)	.000	180.378	179.784	.160	359.956
E_{miss} (MeV)	31.552	37.000	37.000	37.000	37.000
W (GeV)	15.316	15.322	15.325	15.289	15.355
θ_{CM} ($^\circ$)	.020	2.887	2.655	.045	8.020

Table A.75: E$_e$ = 1.645 GeV: ^{1}S$_{1/2}$ state, $\|$ Kinematics.

Variable	Central	Average	Centroid	Minimum	Maximum
θ_e ($^\circ$)	37.170	37.207	37.089	35.742	38.602
ω (MeV)	445.000	450.534	446.705	418.632	482.441
$\lvert\vec{q}\rvert$ (MeV/c)	1000.038	1001.622	998.707	968.091	1032.603
Q^2 ((GeV/c)^2)	.802	.800	.798	.723	.878
θ_q ($^\circ$)	-46.468	-46.118	-46.323	-48.025	-44.122
ϕ_q ($^\circ$)	.000	-.026	-.036	-4.111	4.100
X	.960	.949	.954	.801	1.115
ϵ	.780	.779	.780	.763	.796
$\lvert\vec{p}\,'\rvert$ (MeV/c)	971.000	971.498	966.296	927.342	1014.693
$\lvert\vec{p}_R\rvert$ (MeV/c)	157.027	172.502	165.636	117.490	234.053
θ_{pq} ($^\circ$)	8.982	9.703	9.318	6.123	13.276
ϕ_x ($^\circ$)	180.000	180.045	179.878	133.758	225.837
E_{miss} (MeV)	32.136	37.000	37.000	37.000	37.000
W (GeV)	15.316	15.322	15.318	15.289	15.355
θ_{CM} ($^\circ$)	9.851	10.642	10.219	6.742	14.536

Table A.76: E_e = 1.645 GeV: $^1S_{1/2}$ state, $\Sigma 5$ Kinematics, $\theta_{pq} = 9^\circ$.

Variable	Central	Average	Centroid	Minimum	Maximum
θ_e ($^\circ$)	37.170	37.208	37.069	35.742	38.602
ω (MeV)	445.000	450.517	442.942	418.427	482.527
$\lvert\vec{q}\rvert$ (MeV/c)	1000.038	1001.631	997.848	968.091	1032.603
Q^2 ((GeV/c)^2)	.802	.800	.799	.723	.878
θ_q ($^\circ$)	-46.468	-46.119	-46.535	-48.068	-44.122
ϕ_q ($^\circ$)	.000	-.026	-.032	-4.111	4.100
X	.960	.949	.964	.801	1.116
ϵ	.780	.779	.781	.763	.796
$\lvert\vec{p}\,'\rvert$ (MeV/c)	970.000	970.521	960.247	926.370	1013.606
$\lvert\vec{p}_R\rvert$ (MeV/c)	207.774	221.109	208.893	163.450	282.005
θ_{pq} ($^\circ$)	11.982	12.614	11.927	9.121	16.023
ϕ_x ($^\circ$)	180.000	180.030	179.858	143.462	216.982
E_{miss} (MeV)	32.194	37.000	37.000	37.000	37.000
W (GeV)	15.316	15.322	15.314	15.288	15.355
θ_{CM} ($^\circ$)	13.138	13.829	13.080	10.041	17.537

Table A.77: E_e = 1.645 GeV: $^1S_{1/2}$ state, $\Sigma 5$ Kinematics, $\theta_{pq} = 12^\circ$.

Variable	Central	Average	Centroid	Minimum	Maximum
θ_e ($^\circ$)	23.360	23.426	22.820	21.943	24.792
ω (MeV)	445.000	450.390	462.237	419.166	482.174
$\|\vec{q}\|$ (MeV/c)	999.838	1003.595	986.314	946.441	1053.813
Q^2 ((GeV/c)^2)	.802	.805	.759	.697	.908
θ_q ($^\circ$)	-52.480	-52.122	-51.173	-54.385	-49.708
ϕ_q ($^\circ$)	.000	-.073	-.064	-6.847	6.812
X	.960	.954	.876	.774	1.150
ϵ	.904	.903	.905	.892	.914
$\|\vec{p}\,'\|$ (MeV/c)	967.000	966.851	984.272	923.505	1010.435
$\|\vec{p}_R\|$ (MeV/c)	343.237	345.223	317.009	281.682	413.056
θ_{pq} ($^\circ$)	20.010	20.002	18.464	16.186	23.494
ϕ_x ($^\circ$)	.000	174.588	175.651	.013	359.998
E_{miss} (MeV)	31.683	37.000	37.000	37.000	37.000
W (GeV)	15.316	15.322	15.335	15.289	15.354
θ_{CM} ($^\circ$)	21.913	21.912	20.183	17.640	25.848

Table A.78: E_e = 2.445 GeV: $^1S_{1/2}$ state, Σ2 Kinematics, θ_{pq} = -20°.

Variable	Central	Average	Centroid	Minimum	Maximum
θ_e ($^\circ$)	23.360	23.425	22.927	21.943	24.792
ω (MeV)	445.000	450.014	459.397	419.166	481.307
$\|\vec{q}\|$ (MeV/c)	999.838	1003.462	989.129	946.441	1053.813
Q^2 ((GeV/c)^2)	.802	.805	.768	.699	.908
θ_q ($^\circ$)	-52.480	-52.142	-51.384	-54.385	-49.813
ϕ_q ($^\circ$)	.000	-.054	-.039	-6.847	6.812
X	.960	.955	.892	.778	1.150
ϵ	.904	.903	.905	.892	.914
$\|\vec{p}\,'\|$ (MeV/c)	967.000	966.868	980.658	923.503	1010.504
$\|\vec{p}_R\|$ (MeV/c)	326.405	329.141	306.304	269.645	397.454
θ_{pq} ($^\circ$)	19.010	19.046	17.826	15.528	22.529
ϕ_x ($^\circ$)	.000	175.230	178.144	.012	359.994
E_{miss} (MeV)	32.085	37.000	37.000	37.000	37.000
W (GeV)	15.316	15.321	15.332	15.289	15.353
θ_{CM} ($^\circ$)	20.822	20.869	19.497	16.946	24.792

Table A.79: E_e = 2.445 GeV: $^1S_{1/2}$ state, Σ2 Kinematics, θ_{pq} = -19°.

Variable	Central	Average	Centroid	Minimum	Maximum
θ_e (°)	23.360	23.425	22.951	21.943	24.792
ω (MeV)	445.000	450.347	459.511	419.166	481.894
$\lvert\vec{q}\rvert$ (MeV/c)	999.838	1003.560	989.974	946.441	1053.813
Q^2 ((GeV/c)^2)	.802	.805	.769	.697	.908
θ_q (°)	-52.480	-52.124	-51.390	-54.385	-49.708
ϕ_q (°)	.000	-.069	-.070	-6.847	6.812
X	.960	.954	.893	.774	1.150
ϵ	.904	.903	.905	.892	.914
$\lvert\vec{p}\,'\rvert$ (MeV/c)	968.000	967.863	981.279	924.561	1011.441
$\lvert\vec{p}_R\rvert$ (MeV/c)	309.612	312.436	290.421	248.394	381.903
θ_{pq} (°)	18.010	18.046	16.870	14.188	21.567
ϕ_x (°)	.000	175.523	177.753	.028	359.987
E_{miss} (MeV)	31.749	37.000	37.000	37.000	37.000
W (GeV)	15.316	15.322	15.332	15.289	15.354
θ_{CM} (°)	19.730	19.777	18.456	15.467	23.739

Table A.80: E_e = 2.445 GeV: $^1S_{1/2}$ state, Σ2 Kinematics, θ_{pq} = -18°.

Variable	Central	Average	Centroid	Minimum	Maximum
θ_e (°)	23.360	23.425	23.000	21.943	24.792
ω (MeV)	445.000	449.725	458.047	418.756	480.938
$\lvert\vec{q}\rvert$ (MeV/c)	999.838	1003.405	991.208	946.441	1053.015
Q^2 ((GeV/c)^2)	.802	.805	.773	.699	.908
θ_q (°)	-52.480	-52.158	-51.496	-54.415	-49.813
ϕ_q (°)	.000	-.059	-.054	-6.847	6.812
X	.960	.956	.901	.778	1.150
ϵ	.904	.903	.905	.892	.914
$\lvert\vec{p}\,'\rvert$ (MeV/c)	968.000	967.944	980.075	924.498	1011.538
$\lvert\vec{p}_R\rvert$ (MeV/c)	275.851	280.246	260.008	219.147	351.015
θ_{pq} (°)	16.010	16.133	15.068	12.544	19.655
ϕ_x (°)	.000	175.115	178.435	.012	359.997
E_{miss} (MeV)	32.455	37.000	37.000	37.000	37.000
W (GeV)	15.316	15.321	15.330	15.289	15.353
θ_{CM} (°)	17.545	17.687	16.492	13.696	21.643

Table A.81: E_e = 2.445 GeV: $^1S_{1/2}$ state, Σ2 Kinematics, θ_{pq} = -16°.

Variable	Central	Average	Centroid	Minimum	Maximum
θ_e (°)	23.360	23.423	23.043	21.943	24.792
ω (MeV)	445.000	450.030	457.817	419.166	481.322
$\|\vec{q}\|$ (MeV/c)	999.838	1003.420	992.596	946.441	1053.813
Q^2 ((GeV/c)^2)	.802	.805	.776	.697	.908
θ_q (°)	-52.480	-52.140	-51.532	-54.415	-49.708
ϕ_q (°)	.000	-.059	-.072	-6.847	6.812
X	.960	.955	.905	.774	1.150
ϵ	.904	.903	.904	.892	.914
$\|\vec{p}\,'\|$ (MeV/c)	970.000	969.965	981.196	926.396	1013.610
$\|\vec{p}_R\|$ (MeV/c)	208.204	215.299	195.835	149.728	290.665
θ_{pq} (°)	12.010	12.265	11.259	8.199	16.239
ϕ_x (°)	.000	174.904	177.148	.028	359.987
E_{miss} (MeV)	32.187	37.000	37.000	37.000	37.000
W (GeV)	15.316	15.321	15.330	15.289	15.354
θ_{CM} (°)	13.169	13.454	12.332	8.943	17.822

Table A.82: E_e = 2.445 GeV: $^1S_{1/2}$ state, $\Sigma 2$ Kinematics, θ_{pq} = -12°.

Variable	Central	Average	Centroid	Minimum	Maximum
θ_e (°)	23.360	23.424	23.130	21.943	24.792
ω (MeV)	445.000	450.190	455.642	419.166	481.428
$\|\vec{q}\|$ (MeV/c)	999.838	1003.471	994.953	946.441	1053.813
Q^2 ((GeV/c)^2)	.802	.805	.783	.697	.908
θ_q (°)	-52.480	-52.132	-51.695	-54.415	-49.708
ϕ_q (°)	.000	-.064	-.075	-6.847	6.812
X	.960	.954	.917	.774	1.150
ϵ	.904	.903	.904	.892	.914
$\|\vec{p}\,'\|$ (MeV/c)	971.000	971.082	978.908	927.402	1014.622
$\|\vec{p}_R\|$ (MeV/c)	157.452	168.039	153.035	102.363	247.624
θ_{pq} (°)	9.010	9.439	8.697	5.212	13.950
ϕ_x (°)	.000	175.898	177.115	.013	359.958
E_{miss} (MeV)	32.131	37.000	37.000	37.000	37.000
W (GeV)	15.316	15.321	15.327	15.289	15.354
θ_{CM} (°)	9.882	10.357	9.532	5.686	15.315

Table A.83: E_e = 2.445 GeV: $^1S_{1/2}$ state, $\Sigma 2$ Kinematics, θ_{pq} = -9°.

Variable	Central	Average	Centroid	Minimum	Maximum
θ_e ($^\circ$)	23.360	23.429	23.137	21.943	24.792
ω (MeV)	445.000	451.005	456.310	420.070	482.967
$\lvert\vec{q}\rvert$ (MeV/c)	999.838	1003.854	995.362	946.441	1053.813
Q^2 ((GeV/c)^2)	.802	.805	.783	.697	.908
θ_q ($^\circ$)	-52.480	-52.089	-51.665	-54.385	-49.708
ϕ_q ($^\circ$)	.000	-.065	-.075	-6.847	6.812
X	.960	.953	.916	.774	1.150
ϵ	.904	.903	.904	.892	.914
$\lvert\vec{p}\,'\rvert$ (MeV/c)	973.000	972.850	980.423	929.226	1016.776
$\lvert\vec{p}_R\rvert$ (MeV/c)	106.842	123.499	106.712	49.443	210.864
θ_{pq} ($^\circ$)	6.010	6.735	5.913	2.196	11.976
ϕ_x ($^\circ$)	.000	176.795	177.913	.116	359.978
E_{miss} (MeV)	31.170	37.000	37.000	37.000	37.000
W (GeV)	15.316	15.322	15.328	15.289	15.355
θ_{CM} ($^\circ$)	6.593	7.392	6.483	2.399	13.152

Table A.84: E_e = 2.445 GeV: $^1S_{1/2}$ state, $\Sigma 2$ Kinematics, θ_{pq} = -6°.

Variable	Central	Average	Centroid	Minimum	Maximum
θ_e ($^\circ$)	23.360	23.425	23.196	21.943	24.792
ω (MeV)	445.000	450.731	452.387	419.554	482.967
$\lvert\vec{q}\rvert$ (MeV/c)	999.838	1003.670	996.327	946.441	1053.813
Q^2 ((GeV/c)^2)	.802	.804	.788	.697	.908
θ_q ($^\circ$)	-52.480	-52.103	-51.914	-54.415	-49.708
ϕ_q ($^\circ$)	.000	-.056	-.077	-6.847	6.812
X	.960	.953	.930	.774	1.150
ϵ	.904	.903	.904	.892	.914
$\lvert\vec{p}\,'\rvert$ (MeV/c)	973.000	972.929	975.335	929.231	1016.744
$\lvert\vec{p}_R\rvert$ (MeV/c)	26.838	76.548	63.826	6.063	174.589
θ_{pq} ($^\circ$)	.010	3.563	3.008	.047	9.827
ϕ_x ($^\circ$)	.000	177.531	177.739	.112	359.587
E_{miss} (MeV)	31.552	37.000	37.000	37.000	37.000
W (GeV)	15.316	15.322	15.324	15.289	15.355
θ_{CM} ($^\circ$)	.011	3.910	3.299	.052	10.773

Table A.85: E_e = 2.445 GeV: $^1S_{1/2}$ state, $\|$ Kinematics.

Variable	Central	Average	Centroid	Minimum	Maximum
θ_e ($^\circ$)	23.360	23.425	23.231	21.943	24.792
ω (MeV)	445.000	451.096	448.138	419.595	483.314
$\|\vec{q}\|$ (MeV/c)	999.838	1003.753	996.421	946.441	1053.813
Q^2 ((GeV/c)^2)	.802	.804	.792	.697	.908
θ_q ($^\circ$)	-52.480	-52.082	-52.168	-54.385	-49.708
ϕ_q ($^\circ$)	.000	-.051	-.069	-6.847	6.812
X	.960	.952	.944	.774	1.150
ϵ	.904	.903	.904	.892	.914
$\|\vec{p}\,'\|$ (MeV/c)	973.000	972.832	968.860	929.303	1016.770
$\|\vec{p}_R\|$ (MeV/c)	106.502	136.012	126.199	75.023	221.950
θ_{pq} ($^\circ$)	5.990	7.400	6.919	2.993	12.528
ϕ_x ($^\circ$)	180.000	179.487	179.144	113.263	247.953
E_{miss} (MeV)	31.173	37.000	37.000	37.000	37.000
W (GeV)	15.316	15.322	15.320	15.289	15.356
θ_{CM} ($^\circ$)	6.570	8.118	7.587	3.303	13.736

Table A.86: $E_e = 2.445$ GeV: $^1S_{1/2}$ state, $\Sigma 1$ Kinematics, $\theta_{pq} = 6^\circ$.

Variable	Central	Average	Centroid	Minimum	Maximum
θ_e ($^\circ$)	23.360	23.424	23.246	21.943	24.792
ω (MeV)	445.000	450.325	446.187	418.715	482.967
$\|\vec{q}\|$ (MeV/c)	999.838	1003.524	996.445	946.441	1053.813
Q^2 ((GeV/c)^2)	.802	.805	.794	.697	.908
θ_q ($^\circ$)	-52.480	-52.125	-52.282	-54.434	-49.708
ϕ_q ($^\circ$)	.000	-.061	-.081	-6.847	6.812
X	.960	.954	.950	.774	1.150
ϵ	.904	.903	.904	.892	.914
$\|\vec{p}\,'\|$ (MeV/c)	971.000	971.076	965.494	927.316	1014.639
$\|\vec{p}_R\|$ (MeV/c)	157.108	179.975	170.489	121.695	259.696
θ_{pq} ($^\circ$)	8.990	10.082	9.610	5.934	14.790
ϕ_x ($^\circ$)	180.000	179.594	179.222	126.762	235.507
E_{miss} (MeV)	32.135	37.000	37.000	37.000	37.000
W (GeV)	15.316	15.322	15.318	15.288	15.355
θ_{CM} ($^\circ$)	9.860	11.059	10.538	6.549	16.184

Table A.87: $E_e = 2.445$ GeV: $^1S_{1/2}$ state, $\Sigma 1$ Kinematics, $\theta_{pq} = 9^\circ$.

Variable	Central	Average	Centroid	Minimum	Maximum
θ_e ($^\circ$)	23.360	23.424	23.233	21.943	24.792
ω (MeV)	445.000	450.298	442.571	418.715	482.967
$\lvert\vec{q}\rvert$ (MeV/c)	999.838	1003.527	995.110	946.441	1053.813
Q^2 ((GeV/c)^2)	.802	.805	.795	.697	.908
θ_q ($^\circ$)	-52.480	-52.126	-52.480	-54.434	-49.708
ϕ_q ($^\circ$)	.000	-.058	-.071	-6.847	6.812
X	.960	.954	.958	.774	1.150
ϵ	.904	.903	.905	.892	.914
$\lvert\vec{p}\,'\rvert$ (MeV/c)	970.000	970.082	959.650	926.371	1013.648
$\lvert\vec{p}_R\rvert$ (MeV/c)	207.859	227.210	212.708	169.815	302.900
θ_{pq} ($^\circ$)	11.990	12.918	12.173	8.890	17.323
ϕ_x ($^\circ$)	180.000	179.746	179.294	136.397	226.281
E_{miss} (MeV)	32.193	37.000	37.000	37.000	37.000
W (GeV)	15.316	15.321	15.314	15.288	15.356
θ_{CM} ($^\circ$)	13.146	14.165	13.346	9.809	18.949

Table A.88: E$_e$ = 2.445 GeV: ^{1}S$_{1/2}$ state, Σ1 Kinematics, θ_{pq} = 12°.

Variable	Central	Average	Centroid	Minimum	Maximum
θ_e ($^\circ$)	23.360	23.426	23.228	21.943	24.792
ω (MeV)	445.000	450.037	439.677	418.160	482.967
$\lvert\vec{q}\rvert$ (MeV/c)	999.838	1003.516	994.206	946.441	1053.813
Q^2 ((GeV/c)^2)	.802	.805	.796	.697	.908
θ_q ($^\circ$)	-52.480	-52.141	-52.638	-54.434	-49.708
ϕ_q ($^\circ$)	.000	-.061	-.069	-6.847	6.812
X	.960	.955	.966	.774	1.150
ϵ	.904	.903	.905	.892	.914
$\lvert\vec{p}\,'\rvert$ (MeV/c)	968.000	968.056	954.126	924.453	1011.539
$\lvert\vec{p}_R\rvert$ (MeV/c)	275.507	291.663	273.731	233.668	365.191
θ_{pq} ($^\circ$)	15.990	16.766	15.871	12.861	20.927
ϕ_x ($^\circ$)	180.000	179.814	179.386	144.985	217.592
E_{miss} (MeV)	32.462	37.000	37.000	37.000	37.000
W (GeV)	15.316	15.321	15.311	15.288	15.356
θ_{CM} ($^\circ$)	17.523	18.375	17.395	14.185	22.856

Table A.89: E$_e$ = 2.445 GeV: ^{1}S$_{1/2}$ state, Σ1 Kinematics, θ_{pq} = 16°.

Variable	Central	Average	Centroid	Minimum	Maximum
θ_e (°)	23.360	23.424	23.209	21.943	24.792
ω (MeV)	445.000	450.807	438.159	418.715	483.371
$\vert\vec{q}\vert$ (MeV/c)	999.838	1003.665	993.200	946.441	1053.813
Q^2 ((GeV/c)^2)	.802	.804	.795	.697	.908
θ_q (°)	-52.480	-52.098	-52.715	-54.434	-49.708
ϕ_q (°)	.000	-.058	-.065	-6.847	6.812
X	.960	.953	.968	.774	1.150
ϵ	.904	.903	.905	.892	.914
$\vert\vec{p}\,'\vert$ (MeV/c)	968.000	968.102	951.148	924.468	1011.468
$\vert\vec{p}_R\vert$ (MeV/c)	309.267	325.084	303.539	266.783	397.460
θ_{pq} (°)	17.990	18.757	17.699	14.853	22.794
ϕ_x (°)	180.000	179.836	179.358	148.069	214.332
E_{miss} (MeV)	31.756	37.000	37.000	37.000	37.000
W (GeV)	15.316	15.322	15.310	15.288	15.356
θ_{CM} (°)	19.707	20.550	19.393	16.376	24.886

Table A.90: E$_e$ = 2.445 GeV: ^{1}S$_{1/2}$ state, Σ1 Kinematics, θ_{pq} = 18°.

Variable	Central	Average	Centroid	Minimum	Maximum
θ_e (°)	23.360	23.425	23.200	21.943	24.792
ω (MeV)	445.000	450.503	436.831	418.247	483.289
$\vert\vec{q}\vert$ (MeV/c)	999.838	1003.614	992.562	946.441	1053.813
Q^2 ((GeV/c)^2)	.802	.805	.795	.697	.908
θ_q (°)	-52.480	-52.115	-52.785	-54.434	-49.708
ϕ_q (°)	.000	-.062	-.068	-6.847	6.812
X	.960	.954	.971	.774	1.150
ϵ	.904	.903	.905	.892	.914
$\vert\vec{p}\,'\vert$ (MeV/c)	967.000	967.144	948.841	923.498	1010.501
$\vert\vec{p}_R\vert$ (MeV/c)	326.062	341.202	317.904	281.927	413.672
θ_{pq} (°)	18.990	19.723	18.586	15.849	23.736
ϕ_x (°)	180.000	179.844	179.352	149.414	212.905
E_{miss} (MeV)	32.093	37.000	37.000	37.000	37.000
W (GeV)	15.316	15.322	15.309	15.288	15.356
θ_{CM} (°)	20.800	21.604	20.364	17.472	25.909

Table A.91: E$_e$ = 2.445 GeV: ^{1}S$_{1/2}$ state, Σ1 Kinematics, θ_{pq} = 19°.

Variable	Central	Average	Centroid	Minimum	Maximum
θ_e ($^\circ$)	23.360	23.425	23.152	21.943	24.792
ω (MeV)	445.000	450.879	433.372	418.715	483.371
$\|\vec{q}\|$ (MeV/c)	999.838	1003.697	990.056	946.441	1053.813
Q^2 ((GeV/c)^2)	.802	.804	.793	.697	.908
θ_q ($^\circ$)	-52.480	-52.094	-52.960	-54.434	-49.708
ϕ_q ($^\circ$)	.000	-.055	-.020	-6.847	6.812
X	.960	.953	.976	.774	1.150
ϵ	.904	.903	.906	.892	.914
$\|\vec{p}\,'\|$ (MeV/c)	967.000	967.087	943.680	923.517	1010.490
$\|\vec{p}_R\|$ (MeV/c)	342.894	357.938	327.785	299.035	429.917
θ_{pq} ($^\circ$)	19.990	20.722	19.250	16.846	24.682
ϕ_x ($^\circ$)	180.000	179.860	179.328	150.647	211.593
E_{miss} (MeV)	31.691	37.000	37.000	37.000	37.000
W (GeV)	15.316	15.322	15.305	15.288	15.356
θ_{CM} ($^\circ$)	21.890	22.694	21.090	18.568	26.936

Table A.92: E_e = 2.445 GeV: $^1S_{1/2}$ state, Σ1 Kinematics, $\theta_{pq} = 20^\circ$.

Variable	Central	Average	Centroid	Minimum	Maximum
θ_e ($^\circ$)	23.360	23.424	23.183	21.943	24.792
ω (MeV)	445.000	450.999	437.103	418.247	484.229
$\|\vec{q}\|$ (MeV/c)	999.838	1003.690	992.043	946.441	1053.813
Q^2 ((GeV/c)^2)	.802	.804	.794	.697	.908
θ_q ($^\circ$)	-52.480	-52.087	-52.755	-54.434	-49.677
ϕ_q ($^\circ$)	.000	-.064	-.085	-6.847	6.812
X	.960	.952	.969	.774	1.150
ϵ	.904	.903	.905	.892	.914
$\|\vec{p}\,'\|$ (MeV/c)	960.000	960.103	941.869	916.883	1003.178
$\|\vec{p}_R\|$ (MeV/c)	508.533	521.149	497.426	457.276	592.370
θ_{pq} ($^\circ$)	29.990	30.608	29.610	26.825	34.306
ϕ_x ($^\circ$)	180.000	179.890	179.571	158.848	202.689
E_{miss} (MeV)	31.671	37.000	37.000	37.000	37.000
W (GeV)	15.316	15.322	15.309	15.288	15.357
θ_{CM} ($^\circ$)	32.764	33.442	32.359	29.503	37.342

Table A.93: E_e = 2.445 GeV: $^1S_{1/2}$ state, Σ1 Kinematics, $\theta_{pq} = 30^\circ$.

Appendix B

MCEEP spectra

The following figures illustrate the E_{miss} p_{miss} phase space to be probed by the experiment, both before and after matching in $\omega\vec{q}$ space.

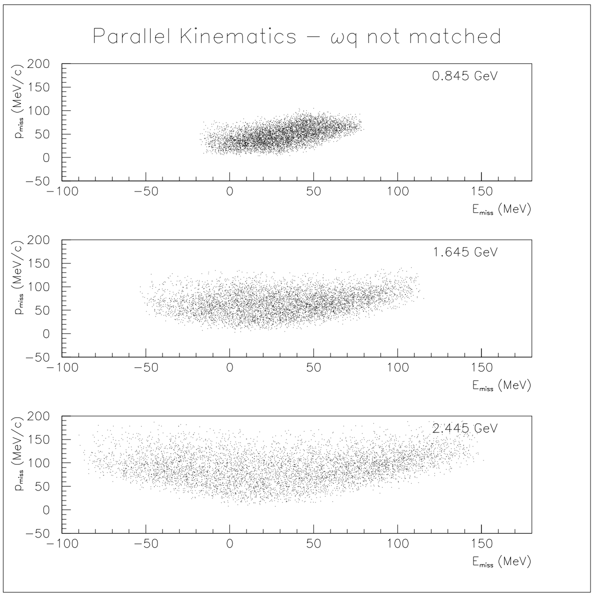

Figure B.1: $\theta_{pq} = 0°$, no $\omega\vec{q}$ matching.

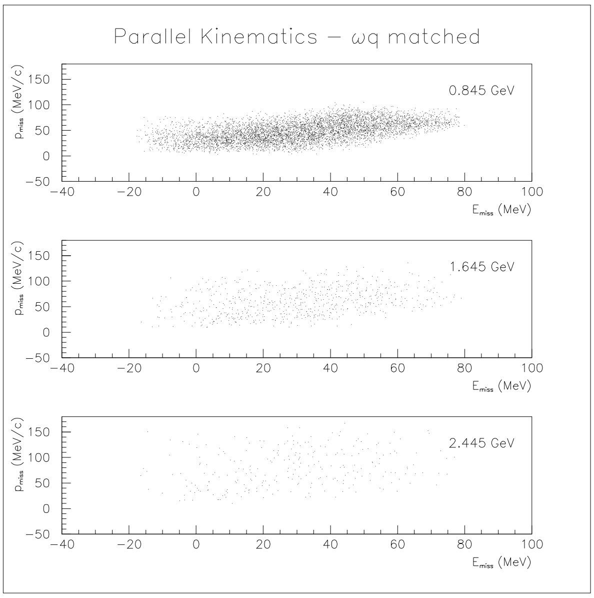

Figure B.2: $\theta_{pq} = 0°$, $\omega\vec{q}$ matching.

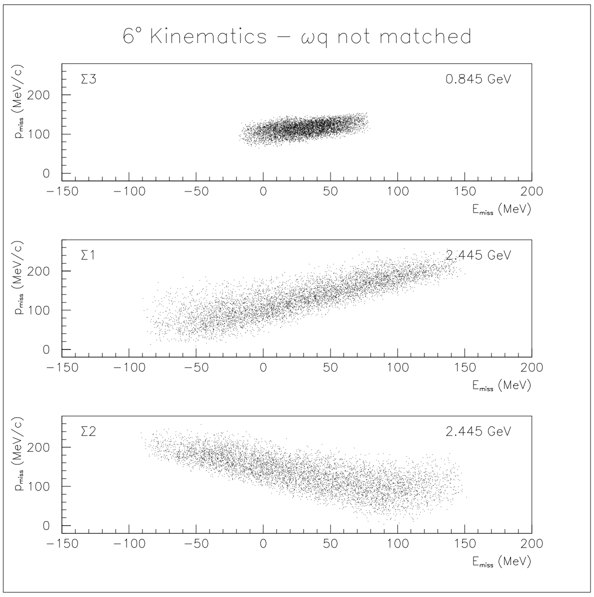

Figure B.3: $\theta_{pq} = 6°$, no $\omega\vec{q}$ matching.

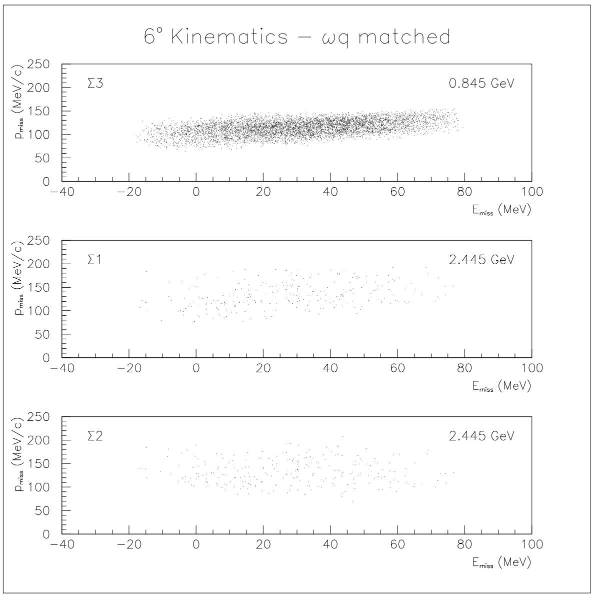

Figure B.4: $\theta_{pq} = 6°$, $\omega\vec{q}$ matching.

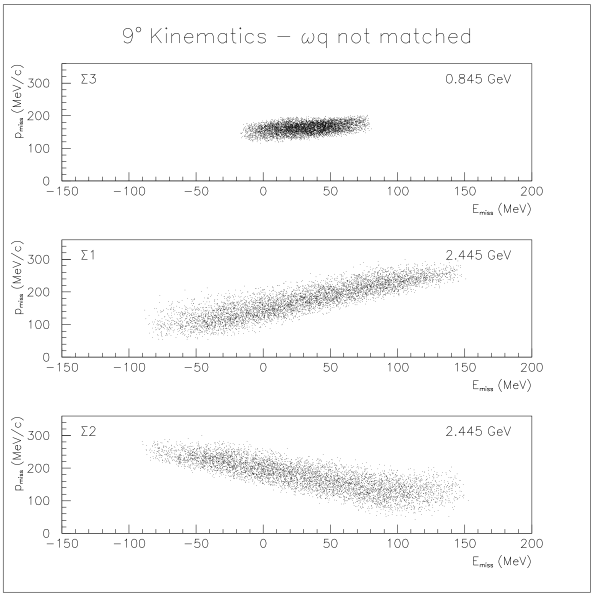

Figure B.5: $\theta_{pq} = 9°$, no $\omega\vec{q}$ matching.

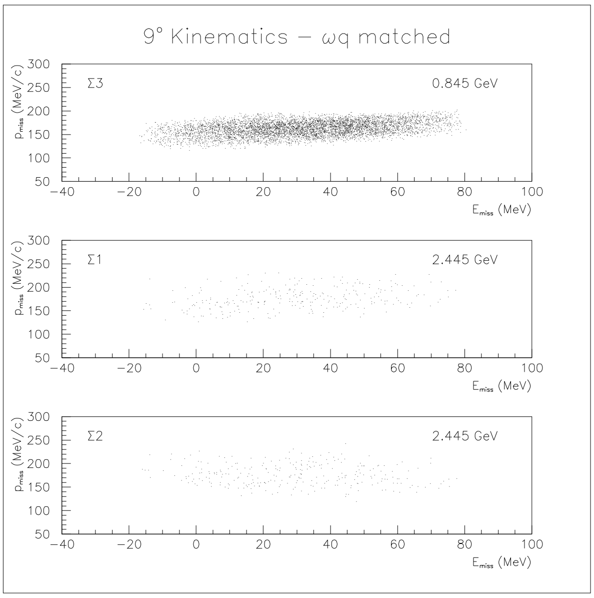

Figure B.6: $\theta_{pq} = 9°$, $\omega\vec{q}$ matching.

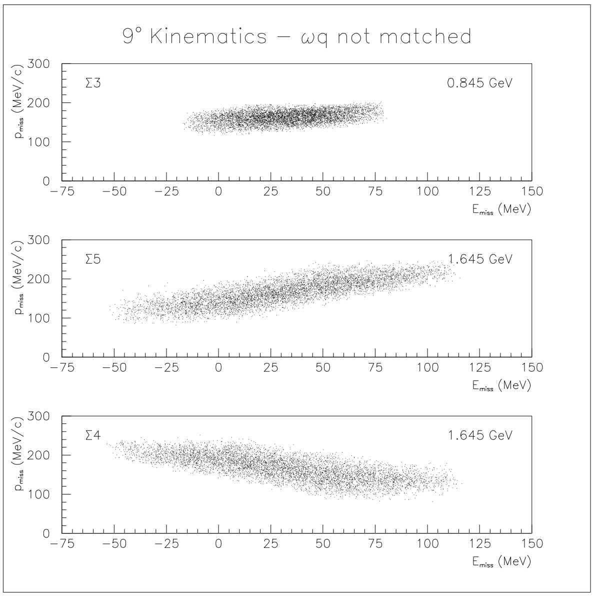

Figure B.7: $\theta_{pq} = 9°$, no $\omega\vec{q}$ matching.

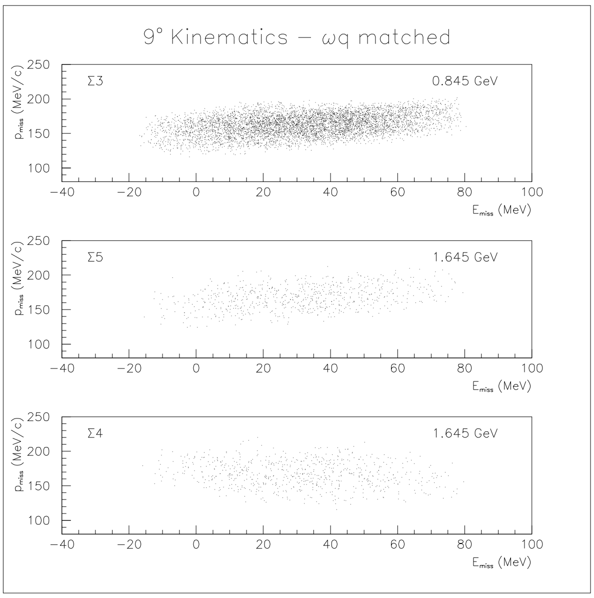

Figure B.8: $\theta_{pq} = 9°$, $\omega\vec{q}$ matching.

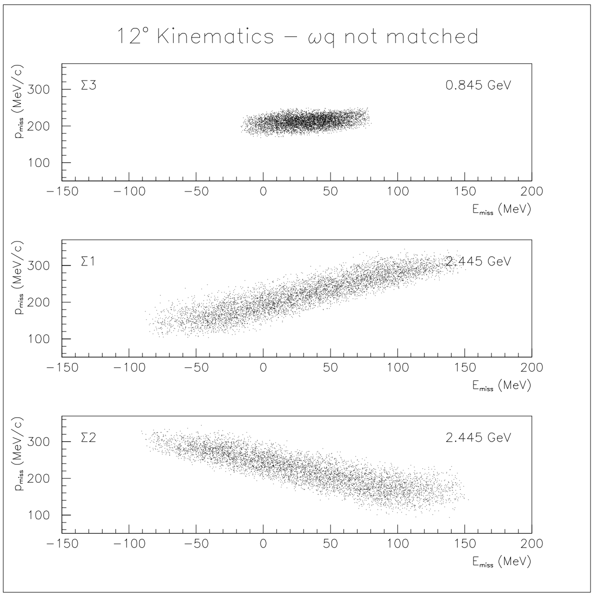

Figure B.9: $\theta_{pq} = 12°$, no $\omega\vec{q}$ matching.

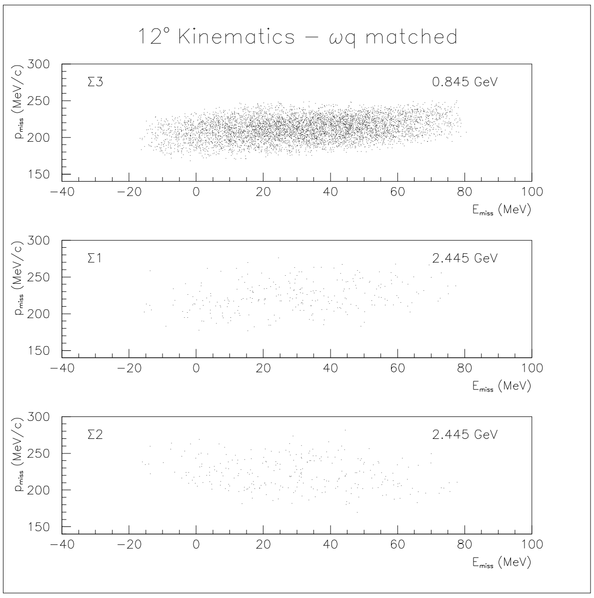

Figure B.10: $\theta_{pq} = 12°$, $\omega\vec{q}$ matching.

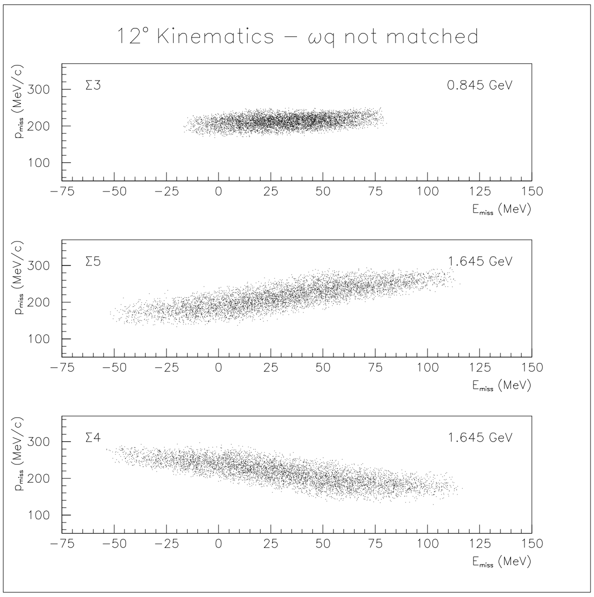

Figure B.11: $\theta_{pq} = 12°$, no $\omega\vec{q}$ matching

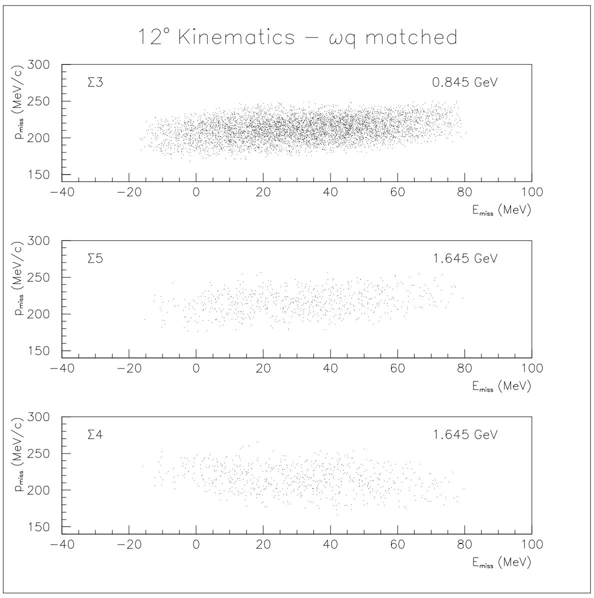

Figure B.12: $\theta_{pq} = 12°$, $\omega\vec{q}$ matching.

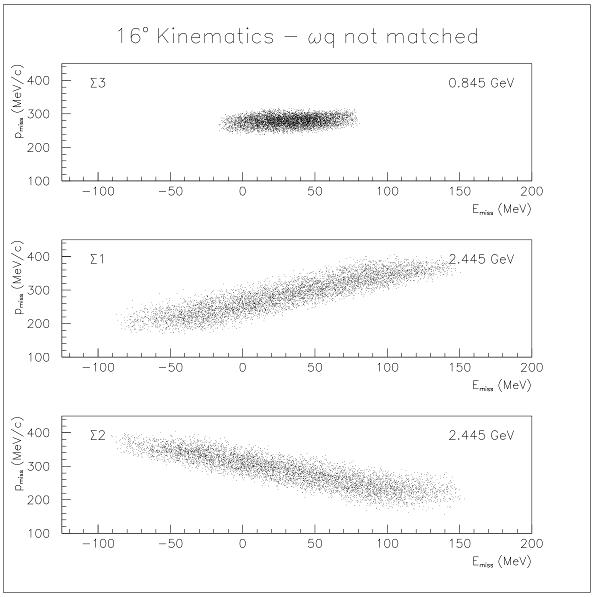

Figure B.13: $\theta_{pq} = 16°$, no $\omega\vec{q}$ matching.

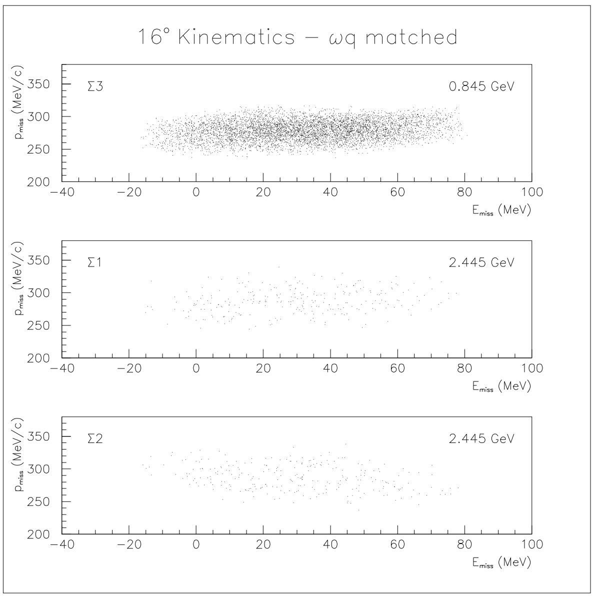

Figure B.14: $\theta_{pq} = 16°$, $\omega\vec{q}$ matching.

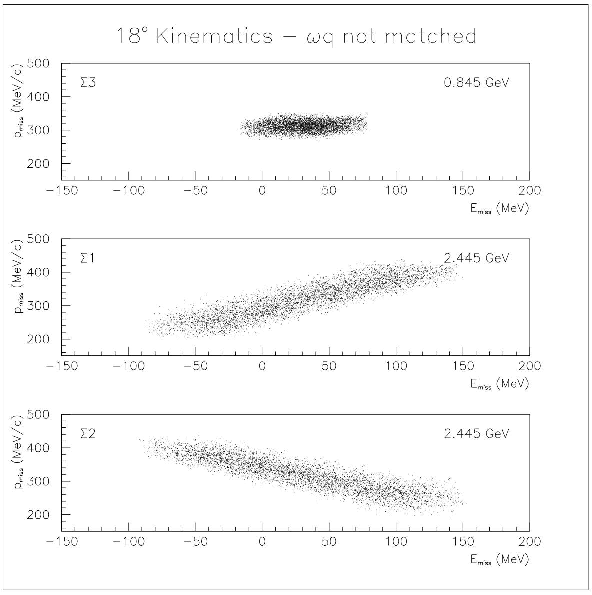

Figure B.15: $\theta_{pq} = 18°$, no $\omega\vec{q}$ matching.

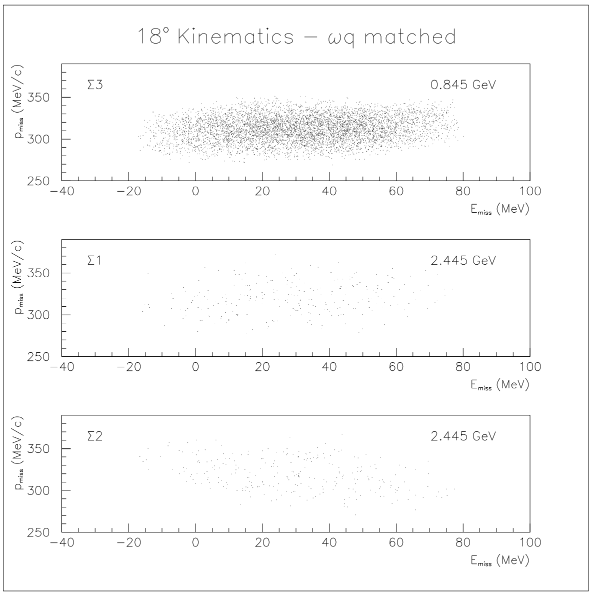

Figure B.16: $\theta_{pq} = 18°$, $\omega\vec{q}$ matching.

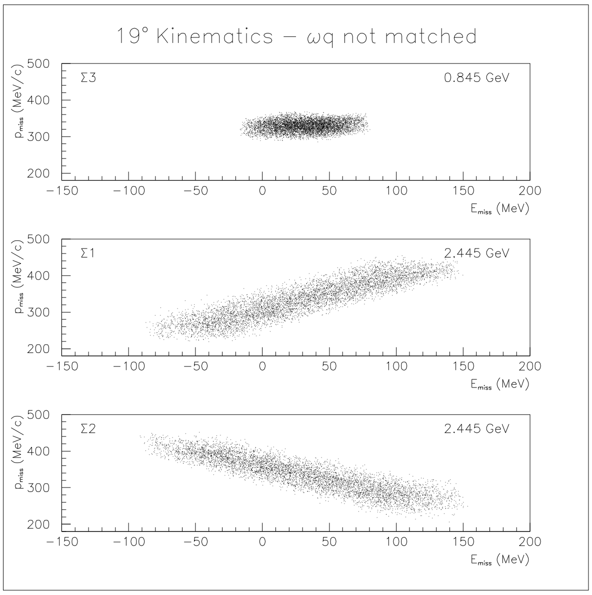

Figure B.17: $\theta_{pq} = 19°$, no $\omega\vec{q}$ matching.

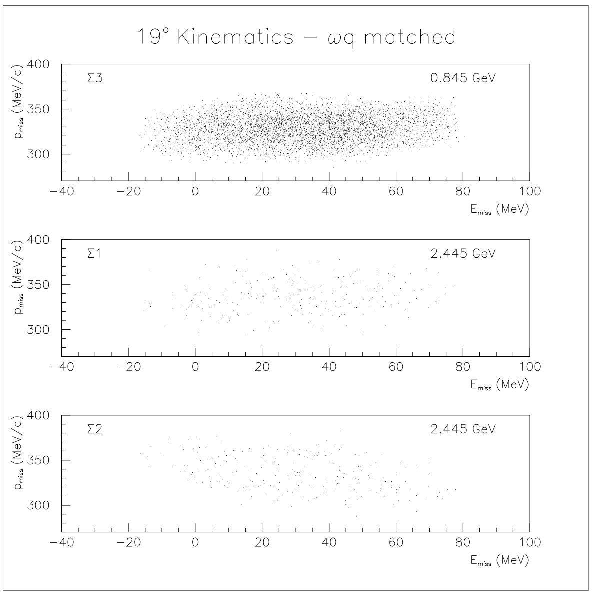

Figure B.18: $\theta_{pq} = 19°$, $\omega\vec{q}$ matching.

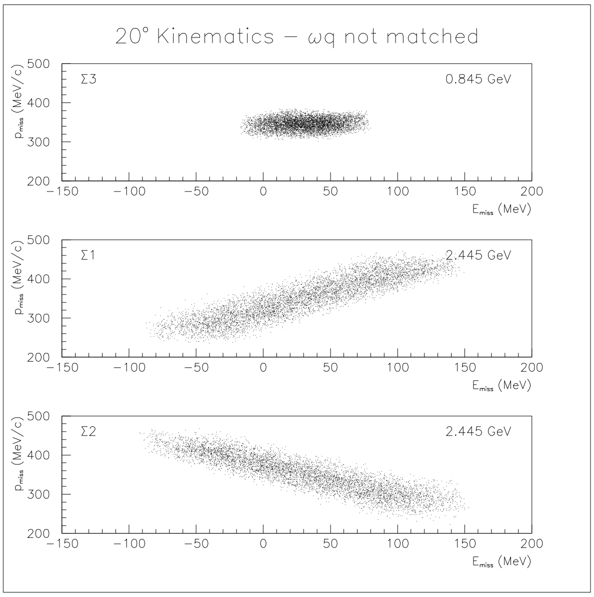

Figure B.19: $\theta_{pq} = 20°$, no $\omega\vec{q}$ matching.

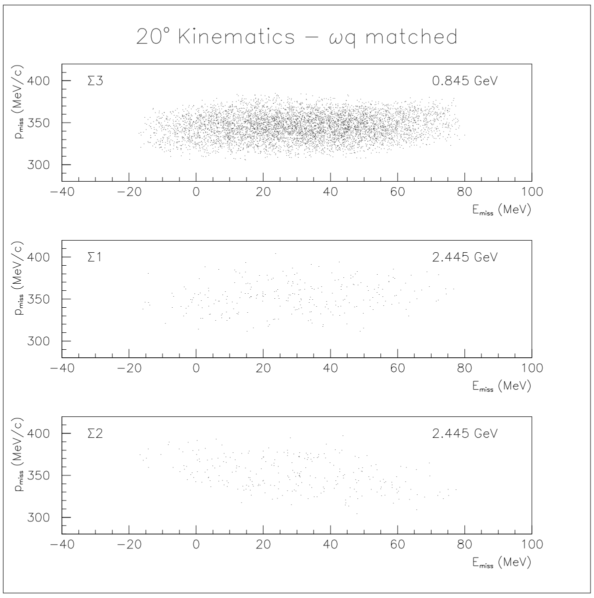

Figure B.20: $\theta_{pq} = 20°$, $\omega\vec{q}$ matching.

Appendix C

The Hall A Collaboration

American University
Bruce S. Flanders

California State University
Konrad Aniol
Martin Epstein
Demetrius J. Margaziotis

Clermont-Ferand
J. Berthot
Pierre-Yves Bertin
Vincent Breton
Helene Fonvielle
C. Jutier
G. Lavessiere
O. Ravel
Yves Roblin

DAPNIA
Jean Y. Mougey

Duke/TUNL
Calvin Howell

Florida International University
Werner Boeglin
Laird Kramer
Peter Markowitz
Brian Raue

Florida State University
A. J. Sarty

University of Georgia

F. Todd Baker
Jeff Templon

HARP-Grenoble
Serge Kox
Eric Voutier

Harvard
Richard Wilson

INFN, Bari
Raffaele de Leo

INFN, Lecce
Antonio Leone
Roberto Perrino

INFN, Roma
Evaristo Cisbani
Salvatore Frullani
Franco Garibaldi
Mauro Jodice
Guido Maria Urciuoli

Kent State
Bryon D. Anderson
Mohammad Khayat
Mark Manley
Gerassimos Petratos
Riad Suleiman
John Watson

University of Kentucky
Dan Dale
Brian C. Doyle
Ashot Gasparian
Tim Gorringe
Wolfgang Korsch
Valdis Zeps

University of Maryland
Betsy Beise
Herbert Breuer
C. C. (George) Chang
Nicholas S. Chant
Lars Ewell
Harry D. Holmgren
James J. Kelly
Philip G. Roos

MIT
William Bertozzi
Kevin Fissum
Juncai Gao
Shalev Gilad
Nilanga Liyanage
David Rowntree
S. van Verst
Jianguo Zhao
Zilu Zhou

University of New Hampshire
John Calarco
F.W. Hersman
Maurik Holtrop
Timothy Paul Smith

Norfolk State University
Mahbub Khandaker
Vina Punjabi

NCCU
Kim Elio Soldi
Branislav Vlahovic

ODU
Charles Hyde-Wright
Paul Ulmer
Larry Weinstein

Orsay
Louis Bimbot

Princeton
Gordon Cates
Krisna Kumar

University of Regina
Ed Brash
Garth M. Huber
G. J. Lolos
Amra Serdarevic-Offermann
Zisis Papandreou

Rutgers
Ron Gilman
Charles Glashausser

Sergey Malov
Justin Mcintyre
Ron Ransome
Paul M. Rutt

Saclay
Etienne Burtin
Christian Cavata
Jean-Eric Ducret
Bernard Frois
Nicole d'Hose
Sophie Kerhoas
Jacques Marroncle
Jacques Martino
Damien Neyret
Stephane Platchkov
Thierry Pussieux
Pascal Vernin

Syracuse
Richard S. Holmes
Paul Souder

Temple University
Leonard Auerbach
C. Jeffrey Martoff
Zein-Eddine Meziani

Jefferson Lab
Larry Cardman
J.P. Chen
Javier Gomez
Kees de Jager
John J. Lerose
Meihua Liang
Richard Madey
Bob Michaels
Sirish Nanda
Eddy Offerman
Arun Saha
Bogdan Wojtsekhowski

Tohoku University
Kouichi Kino
Kazushige Maeda
Teijiro Saito
Tatsuo Terasawa
H.Tsubota

Utrecht
Thomas S. Bauer

University of Virginia
Richard A. Lindgren
Robert Lourie
James S. McCarthy
Oscar A. Rondon-Aramayo

College of William and Mary
David Armstrong
Mike Finn
Keith Griffieon
Mark Jones
Charles F. Perdrisat
Gilles Quemener
Krishni Wijesooriya

Yamagata University
Seigo Kato
Hiroaki Ueno

Bibliography

[1] J.J. Kelly, Nucleon knockout by intermediate energy electrons, Advances in Nuclear Physics, edited by J.W. Negele and E. Vogt, Vol. 23, page 75, Plenum Press, 1996.

[2] J.W. van Orden, private communciation.

[3] F. Garibaldi, E. Cisbani, R. Crateri, S. Frullani, F. Ghio, F. Giuliani, M. Gricia, M. Iodice, M. Lucentini, L. Pierangeli, F. Santavenere, G.P. Capitani, E. De Sanctis, M. Bernheim, J.F. Danel, J.E. Ducret, L. Lakehal-Ayat, J.M. Le Goff, A. Magnon, C. Marchand, J. Morgenstern, P. Vernin, and A. Zghich, Nucl. Instrum. Methods **A314**, 1 (1992).

[4] K.I. Blomqvist, W.U. Boeglin, R. Böhm, M. Distler, R. Edelhoff, J. Friedrich, R. Geiges, M. Kahrau, M. Korn, H. Kramer, K.W. Krygier, V. Kunde, M. Kuss, J. Lác, A. Liesenfeld, K. Merle, R. Neuhausen, E.A.J.M. Offermann, Th. Pospischil, M. Potokar, A.W. Richter, A. Rokavec, G. Rosner, P. Sauer, S. Schardt, A. Serdarević, Th. Veit, B. Vodenik, A. Wagner, Th. Walcher and S. Wolf, Phys. Lett. **B344**, 85 (1995).

[5] C.M. Spaltro, H.P. Blok, E. Jans, L. Lapikás, M. van der Schaar, G. van der Steenhoven, and P.K.A. de Witt Huberts, Phys. Rev. **C48**, 2385 (1993).

[6] M. Leuschner, J.R. Calarco, F.W. Hersman, E. Jans, G.J. Kramer, L. Lapikás, G. van der Steenhoven, P.K.A. de Witt Huberts, H.P. Blok, N. Kalantar-Nayestanaki, and J. Friedrich, Phys. Rev. **C49**, 955 (1994).

[7] L. Chinitz, M. Bernheim, G.P. Capitani, A. Catarinella, J.F. Danel, E. De Sanctis, S. Frullani, F. Garibaldi, F. Ghio, M. Iodice, L. Lakehal-Ayat, J.M. LeGoff, J. LeRose, A. Magnon, C. Marchand, R. Minehart, J. Morgenstern, J. Mougey, S. Nanda, C. Perdrisat, R. Powers, V. Punjabi, A. Saha, P. Ulmer, and P. Vernin, Phys. Rev. Lett. **67**, 568 (1991).

[8] H. Müther and W.H. Dickhoff, Phys. Rev. **C49**, R17 (1994).

[9] S.C. Pieper, R.B. Wiringa, and V.R. Pandharipande, Phys. Rev. **C46**, 1741 (1992).

[10] I. Sick, S. Fantoni, A. Fabrocini and O. Benhar, Phys. Lett. **B323** 267 (1994).

[11] X. Ji and J. Engel, Phys. Rev. **C40**, R497 (1989).

[12] J.G. Zabolitzky and W. Ey, Phys. Lett. **76B**, 527 (1978).

[13] J.W. Van Orden, W. Truex, and M.K. Banerjee, Phys. Rev. **C21**, 2628 (1980).

[14] H. Müther, A. Polls, and W.H. Dickhoff, Phys. Rev. **C51**, 3040 (1995).

[15] V. Van der Sluys, J. Ryckebusch, M. Waroquier, Phys. Rev. **C51**, 2664 (1995).

[16] V. Van der Sluys, J. Ryckebusch, M. Waroquier, Phys. Rev. **C49**, 2695 (1994).